Università degli Studi di

Ferrara

DOTTORATO DI RICERCA IN
SCIENZE BIOMEDICHE E BIOTECNOLOGICHE

CICLO XXIX

COORDINATORE Prof. Paolo Pinton

Molecular basis and therapeutic strategies to rescue pre-mRNA splicing defects in Haemophilia A, Familial Dysautonomia and Spinal Muscular Atrophy

Settore Scientifico Disciplinare BIO/11

Dottorando
Dott. Donadon Irving

Tutore
Prof. Bernardi Francesco

Co-Tutori

Prof. Pinotti Mirko

Prof. Pagani Franco

Anni 2014/2016

DECLARATION

I, Irving Donadon, confirm that the work presented in this thesis is my own.
The PhD project was developed during the 2014-2016 academic years as follow:

- the *FVIII* and *IKBKAP* splicing analysis were performed at the University of Ferrara, in the laboratory of Biochemistry and Molecular Biology under the supervision of Prof. Mirko Pinotti and Prof. Francesco Bernardi;
- the rFVIII expression analysis were performed at the University of Surrey, in the laboratory of Molecular Medicine under the supervision of Prof. John McVey;
- the *in-vivo* analysis of ExSpeU1s activity in SMA mice was performed at the International Centre for Genetic Engineering and Biotechnology (ICGEB) of Trieste, in the Human Molecular Genetics (HMG) group under the supervision of Prof. Franco Pagani.

To Monika and Isabelle

Table of contents

ABSTRACT

Pre-mRNA splicing is an essential step of gene expression regulation, supervised by complex interactions between *cis*- and *trans*-acting factors that vary with species, cell-types and during development, which might dictate the synthesis of a multiplicity of different protein isoforms. Mutations or natural variations within both coding and non-coding sequences can affect this process with pathophysiological implications. Exon Specific U1 snRNAs (ExSpeU1s), modified U1 snRNAs that specifically bind to intronic sequences downstream affected exons, have been recently described as splicing-switching molecules able to revert pathological phenotypes [1].

In this thesis, in order to demonstrate the applicability of ExSpeU1s from the molecular characterization *in-vitro* to the evaluation of the efficacy *in-vivo*, I studied the mis-regulation of splicing in Hemophilia A, in Familial Dysautonomia, and in Spinal Muscular Atrophy.

Hemophilia A (HA) is a bleeding disorder due to the deficiency of the blood coagulation factor VIII (FVIII). Among the over 1300 point mutations found in HA, the c.6046C>T (p.R2016W) substitution represents the second most frequent mutation in Northern Italy. Through a hybrid minigene system and a lentiviral platform to express recombinant FVIII variants, I demonstrated that the c.6046C>T mutation impacts both the RNA and protein FVIII biology , respectively promoting skipping of exon 19 (≈30%) and reducing both the FVIII secretion (11.0±0.4%) and activity (6.0±2.9%). I characterized the presence of an exonic splicing regulatory element (ESRE) within the *F8* exon 19, identifying three missense mutations (c.6037G>A, p.G2013R; c.6053A>G, p.E2018G; c.6113A>G, p.N2038S) with differential impact on FVIII secretion/function and a severe impact on *F8* exon 19 splicing, inducing >60% of exon skipping. Combination of reduced protein secretion and activity with splicing alteration produced a gradient of FVIII deficiency, from mild to severe HA, even for mutations clustered in exon 19. Interestingly, I demonstrated that aberrant *F8* exon 19 splicing caused by

missense mutations can be improved by a modified U1 snRNA, promoting exon inclusion and increasing the amount of full length transcripts.

Familial Dysautonomia (FD), characterized by impairment of the autonomous nervous system, is mainly caused (>99% of cases) by the intronic mutation IVS20+6T>C in the *IKBKAP* gene that promotes skipping of exon 20 through a reduced affinity between the wild type U1 snRNA and the donor site. With minigene assays I developed several ExSpeU1s that, targeting the intronic region downstream of the exon 20 donor site, efficiently correct the aberrant *IKBKAP* splicing *in-vitro*. Here, I also demonstrated that ExSpeU1s promote exon 20 inclusion in an active manner and not through antisense mechanisms. Moreover, taking advantage of a lentiviral delivery in FD patients' fibroblasts, I demonstrated the *ex-vivo* efficacy of one ExSpeU1, providing a novel therapeutic opportunity to treat a disease for which there are no currently alternatives.

Spinal Muscular Atrophy (SMA) primarily affects α-motor neurons and is caused by mutations in the *Survival Motor Neuron 1* (*SMN1*) gene encoding the SMN protein. Interestingly on the same chromosome is located one or more copies of its paralog (*SMN2*) that however carries a synonymous mutation (c.840C>T) promoting skipping of *SMN2* exon 7, which reduces the SMN expression. In this thesis, I challenged the *in-vivo* efficacy of two already characterized ExSpeU1s for this disease [2]. Through an Adeno-associated virus 9, I intraperitoneally delivered these molecules in SMA animal models with a mild and a severe phenotype. In the mild SMA mouse the ExSpeU1s efficiently corrected the aberrant *SMN2* splicing and improved the phenotype that consist of a recover of the tail lenght. In the severe SMA mouse, that normally die at 10-12 days, I demonstrated that treatment with ExSpeU1 significantly extend the survival (40% of animals alive after 250 days).

Altogether these *in-vitro, ex-vivo* and *in-vivo* data provide novel insights into the potential of the RNA therapeutics based on modified U1 snRNAs and lay the foundation for further studies aimed at developing novel therapies for genetic disorders.

ABSTRACT ITALIANO

BASI MOLECOLARI E STRATEGIE TERAPEUTICHE PER CORREGGERE DIFETTI DI SPLICING DEL pre-mRNA IN EMOFILIA A, DISAUTONOMIA FAMILIARE ED ATROFIA MUSCOLARE SPINALE.

Lo splicing dei pre-mRNA è un punto essenziale della regolazione dell'espressione genica il quale, controllato da complesse interazioni tra elementi in *cis*- ed in *trans*- che variano con le specie, tipi cellulari e durante lo sviluppo, può comportare la produzione di un grandissima varietà di isoforme proteiche a partire da un unico trascritto.
Mutazioni o variazioni naturali all'interno delle sequenze codificanti e non-codificanti dei trascritti possono compromettere questo processo cellulare, con implicazione patologiche.
Exon specific U1 snRNAs (ExSpeU1s) sono molecole di U1 snRNAs modificate per riconoscere in modo specifico le sequenze introniche che si trovano a valle di esoni negativamente influenzati da mutazioni. Gli ExSpeU1s sono stati recentemente proposti come molecole in grado di modificare lo splicing aberrante, correggendo i fenotipi patologici [1].
In questa tesi, per dimostrare l'applicabilità degli ExSpeU1s partendo da una caratterizzazione molecolare *in-vitro* alla valutazione della loro efficacia *in-vivo*, ho studiato lo splicing aberrante in: emofilia A, Disautonomia familiare ed atrofia muscolare spinale.

L'emofilia A (HA) è una patologia della coagulazione causato da una deficienza del fattore della coagulazione VIII (FVIII). Tra le oltre 1300 mutazioni identificate in emofilia A, il cambio c.6046C>T (p.R2016W) rappresenta la seconda mutazione più frequente nel Nord Italia. Attraverso un sistema di minigeni ed una piattaforma lentivirale per l'espressione di FVIII ricombinante, ho dimostrato che la mutazione c.6046C>T ha un effetto sia a livello del processamento dell'RNA che su quello proteico del FVIII, rispettivamente inducendo un salto dell'esone 19 (≈30%) e

riducendo sia la secrezione (11.0±0.4%) che l'attività (6.0±2.9%) del FVIII. Qui, ho caratterizzato un elemento regolatorio di splicing esonico (ESRE) all'interno dell'esone 19 del *F8*, identificando tre mutazioni missenso (c.6037G>A, p.G2013R; c.6053A>G, p.E2018G; c.6113A>G, p.N2038S) con un diverso impatto sulla secrezione/attività del FVIII e con un severo effetto sullo splicing dell'esone 19, inducendo un salto dell'esone superiore al 60%. Una combinazione di ridotta secrezione ed attività proteica con un'alterazione dello splicing ha prodotto un gradiente di deficit del FVIII, da una forma moderata ad una severa di emofilia A, anche per mutazioni raggruppate nell'esone 19. Interessatemene, ho dimostrato che lo splicing aberrante dell'esone 19 causato da queste mutazioni missenso può essere corretto da uno U1 snRNA modificato, stimolando l'inclusione dell'esone ed aumentando la quantità di trascritti completi.

La Disautonomia familiare (FD) è una patologia caratterizzata da un difetto del sistema nervoso autonomo causato nella maggior parte dei casi (>99%) da una mutazione intronica (IVS20+6T>C) nel gene *IKBKAP* che induce un salto dell'esone 20 attraverso una riduzione dell'affinità tra lo U1 snRNA cellulare ed il sito donatore. Mediante l'uso di sistemi di minigeni, ho creato diversi ExSpeU1s che, riconoscendo la regione intronica a valle dell'esone 20, hanno efficientemente corretto lo splicing aberrante di *IKBKAP in-vitro*. Qui, ho inoltre dimostrato che questi ExSpeU1s promuovono una inclusione dell'esone 20 in modo attivo e non attraverso meccanismi antisenso. In aggiunta, sfruttando un sistema lentivirale per introdurre la molecola all'interno dei fibroblasti di pazienti FD, ho dimostrato l'efficacia di un ExSpeU1 in *ex-vivo*, fornendo una nuova opportunità terapeutica per il trattamento di questa patologia alla quale tuttora non esistono alternative.

L'atrofia muscolare spinale (SMA) è una patologia che colpisce principalmente gli α-motoneuroni ed è causata da mutazioni nel gene di *sopravvivenza dei motoneuroni 1* (*SMN1*) che codifica per la proteina SMN. Nello stesso cromosoma si trovano una o più copie del gene parologo (*SMN2*) che, tuttavia, contiene una mutazione sinonima (c.840C>T) che induce il salto dell'esone 7 di *SMN2*, riducendo l'espressione della proteina. In questa tesi, ho valutato l'efficacia *in-vivo* di due ExSpeU1s già caratterizzati per questa patologia [2]. Attraverso un virus adeno-associato 9, ho somministrato queste molecole per via intraperitoneale in modelli animali di SMA con fenotipo lieve e severo. Nel modello di topo SMA lieve, questi ExSpeU1s hanno efficientemente corretto lo splicing aberrante di *SMN2*, migliorando il fenotipo attraverso il recupero della lunghezza della coda. Nel modello di topo SMA severo, che normalmente muore dopo 10-12 giorni, ho dimostrato che il trattamento con ExSpeU1

estende significativamente la sopravvivenza con un 40% degli animali ancora vivi dopo 250 giorni.

Complessivamente, questi risultati ottenuti *in-vitro*, *ex-vivo* ed *in-vivo* forniscono nuove conoscenze riguardanti le potenzialità terapeutiche basate su molecole di U1 snRNA modificate e forniscono le basi per ulteriori studi volti allo sviluppo di nuove terapie per patologie genetiche.

Chapter 1

INTRODUCTION

1.1 Gene expression and RNA processing

DNA can be considered as a big cooking encyclopedia where all the recipes, known as genes, contain an encrypted formula for the production of specific molecules. Gene expression represents the biological process by which information from a gene is used for the synthesis of a functional gene product. Several high-fidelity copy machines, known as RNA polymerases, mediate this important process, called "transcription". The RNA polymerase II (RNA pol II), indeed, generates immature molecules, called pre-mRNAs, that must be properly processed to produce the mature mRNAs required for the protein biosynthesis [3].

Splicing is the cellular process responsible for decoding the pre-mRNA, producing a mature form of mRNA that will be used for the protein production. The encrypting code, by which pre-mRNAs are composed of, consists of two different parts, exons and introns. In order to produce mature mRNAs, which will successively undergo to some other post-transcriptional modifications before being translated into proteins, introns must be appropriately removed and exons joined together. This process is mediated by a macromolecular complex, whose activity must be extremely precise without altering the genetic information. This precision is supported by complex interactions between elements within the pre-mRNA sequence, *cis*-acting elements, and external factors that recognize these regions, *trans*-acting factors.

The fine mechanism of splicing is managed by a macromolecular complex known as spliceosome [4][5]. The native spliceosome machinery is composed of five small nuclear ribonucleoproteins (U1, U2, U4/U6, U5 snRNP) and more than 200 snRNP- and non-snRNP-associated proteins [6]. Studies of spliceosomes isolated from mammalian cell nuclei revealed that pre-mRNA molecules connect four active native spliceosomes together, creating a huge macromolecular complex of 21 MDa, thus called "supraspliceosome" [7]. These studies showed this homotetramer has a physical structure that allows to process pre-mRNA transcripts of different sizes and number of introns, indicating its universal nature. Furthermore, this homotetrameric configuration enables examination and allows rearrangement to select appropriate splice junctions through the complex interactions between *cis*- and *trans*-acting factors.

The proper pre-mRNA maturation is supported by the numerous elements involved into the splicing process [8]. Immature pre-mRNAs, indeed, are nucleotide sequences enriched of information that go beyond the relative simple coding sequence. This surplus is located on the sequence itself and is fundamental to drive a correct recognition of the exon-intron junctions, promoting a correct splicing. These on-sequence regions, called *cis*-acting elements, are principally divided into two categories: canonical and non-canonical sequences. The first ones are universal, conserved and essential sequences required for a proper splicing reaction, whereas the second ones are additional elements that vary between different transcripts and different regions of the transcript itself.
The canonical splicing signals recognized by the spliceosome to mediate the two trans-esterification reactions are:

- The **5' splice site (5' ss, or donor site):** a sequence located in the exon-intron junction at the 5' end of the intron and in most majority of cases consists of the GU dinucleotide, representing the first two nucleotides of the intron. The 5' ss motif consists of nine nucleotides spanning from position -3 to +6, where the GU dinucleotide is highly conserved and mutations of only one of these two nucleotides completely abolishes the splicing process [9].
- **The 3' splice site (3' ss, or acceptor site)**: a sequence located at the 3' end of the intron, which is characterized by a short YAG|G sequence, where the highly conserved AG represent the last two nucleotide of the intron.
- The **branch point site (BPS)**: a highly degenerated sequence, defined by the YNYURAC motif (R indicates purine; Y pyrimidine and N nucleotide), in which the

A is a universally conserved nucleotide that plays an essential role in the first step of trans-esterification reactions [10].

- **The polypyrimidine tract (PPT):** a sequence located between the BPS and the 3' splice site, which is composed of a stretch of pyrimidines, in particular uridines [11].

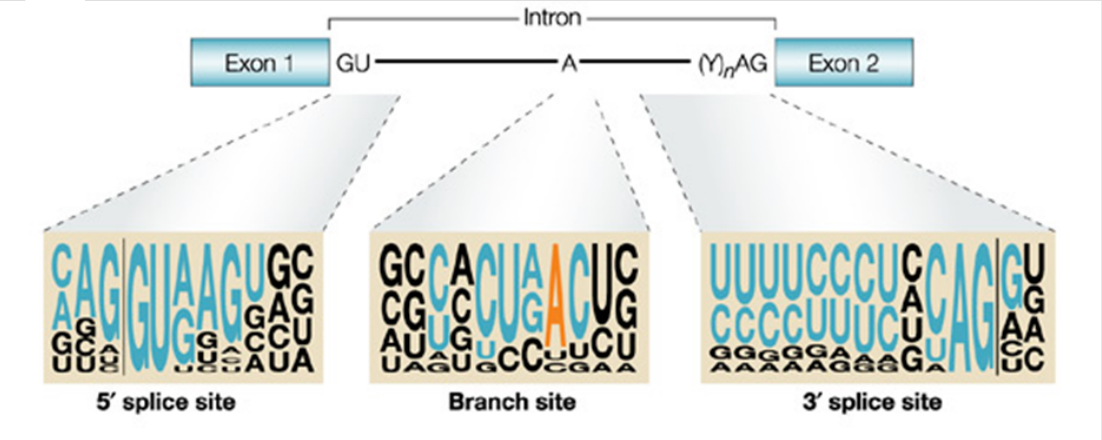

Figure 1.1 Overview of canonical *cis*-acting splicing signals.

Conserved motifs at or near the intron ends. The nearly invariant GU and AG dinucleotides at the intron ends, the polypyrimidine tract (Y)n preceding the 3' AG, and the A residue that serves as a branch point are shown in a two-exon pre-mRNA. The sequence motifs that surround these conserved nucleotides are shown below. For each sequence motif, the size of a nucleotide at a given position is proportional to the frequency of that nucleotide at that position in an alignment of conserved sequences from 1,683 human introns. Nucleotides that are part of the classical consensus motifs are shown in blue, except for the branch-point A, which is shown in orange. The vertical lines indicate the exon-intron boundaries.

These four elements are essential but not always sufficient for a proper exon-intron definition. In higher eukaryotes, indeed, the core splicing sequences often contain too little information to unambiguously define splice sites. For this reason, some other additional sequences are necessary for the correct exons' recognition. These less conserved *cis*-acting elements, called non-canonical splicing elements, are divided into two large families: enhancers and silencers. Both of these two families can be located within exons, exonic splicing enhancers (ESE) and exonic splicing silencers (ESS), and within introns, intronic splicing enhancers (ISE) and intronic splicing silencers (ISS) [12]. However, it might also happen that some sequences maintain a dual activity, thus working as enhancer or silencer, depending on the cellular context: the composite exonic regulatory elements of splicing (CERES) [13].

All these elements represent just a part of the complexity that regulates the splicing process. Indeed, another important part is given by all those molecules that recognize these *cis*-sequences through RNA:RNA, RNA:protein or protein:protein interactions. These elements are called *trans*-acting factors and, as well as the *cis*-acting elements, are divided into two groups: a group that recognizes the canonical splicing signals and a second one that binds to the non-canonical ones.

The splicing reaction starts with the first *trans*-acting factor that physically interacts with the donor site, the U1 snRNA. On the other hand, the recognition of the 3' splice site involves the binding of the U2AF65/35 heterodimer to the polypyrimidine tract and the conserved acceptor site, which facilitates the recruitment of the U2 snRNP to the branch site, involving base-pairing interactions between the U2 snRNA and nucleotides flanking the branch point adenosine [14].

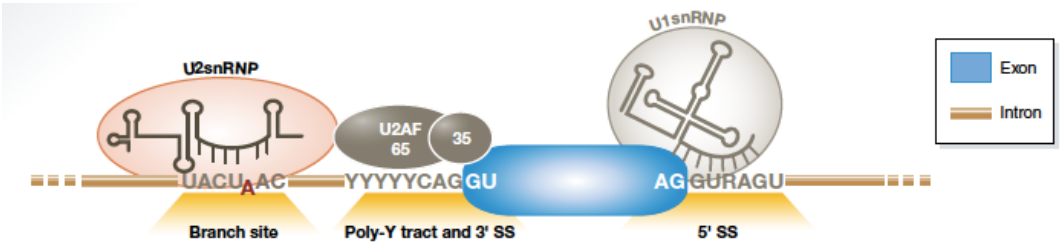

Figure 1.2 Exon recognition mediated by U1 and U snRNPs.

Splicing complex assembly is initiated by consensus sequence elements located at the exon (blue)/intron (brown) boundaries. Recognition of the 50 SS by U1 snRNP involves base-pairing interactions between the 50 end of U1 snRNA. Recognition of the 30 SS region involves binding of the U2AF65/35 heterodimer to the polypyrimidine tract (Poly-Y tract) and conserved 30 SS, which facilitates recruitment of U2 snRNP to the branch site, involving base-pairing interactions between U2 snRNA and nucleotides flanking the branch point adenosine.

More complicated is the nature of those *trans*-acting factors that recognize the non-canonical splicing elements. This group, indeed, can be distinguished on the basis of their biological function: enhancers when promoting exon inclusion, silencers when inhibiting the exon definition. In particular, these regulatory elements are largely represented by two families of RNA binding proteins: SR proteins (Serine-Arginine rich proteins) and hnRNP (heterogeneous nuclear ribonucleoproteins), which are fundamental in splicing due to their ability to recognize both enhancer and silencer regions.

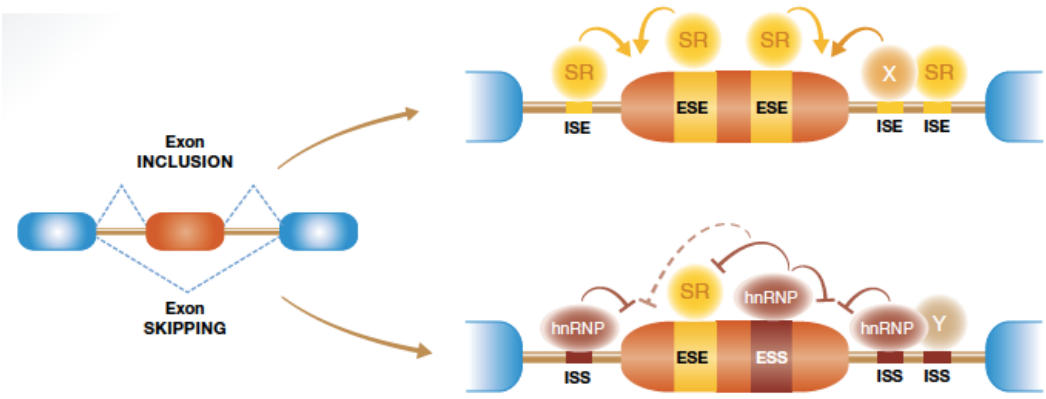

Figure 1.3 Role of *cis*- and *trans*-acting elements in exon definition.

Exon definition modulated by exonic and intronic sequence elements, which can promote (ESE & ISE, in orange) or suppress (ESS & ISS, in dark red) splice site recognition. A classic model involves recognition of splicing enhancers by proteins of the SR family and recognition of splicing silencers by hnRNP proteins. However, proteins of these and other families can promote or inhibit splicing depending upon the location of their binding sites relative to the splice sites and other regulatory sequences. A complex combinatorial interplay between regulatory elements and their cognate factors determines exon definition and regulation.

The **SR proteins** are a family of nuclear factors that have many important roles in the splicing of pre-mRNAs, functioning in both constitutive and alternative RNA splicing. They are generally known as positive regulators, by binding of exonic and intronic splicing enhancers (ESE, ISE) located within pre-mRNA sequences. These proteins are characterized by the presence of at least one RNA-binding domain (RBD) and by a distinctive serine/arginine rich region (RS domain) from which derives their "SR" name. The RS domain can be regulated through post-translational modifications as phosphorylations and dephosphorylations, influencing their subcellular localization and their ability to bind the RNA [15][16].

The reason for which they are recognized as positive factors is due to two non-exclusive models that explains their role into processing of pre-mRNA. The first model identify SR proteins as elements that recruit and stabilize U1-snRNP and U2AF binding to their respective splice regions through SR domain interactions. While, the second model proposes that SR proteins can antagonize the negative effect of a nearby silencer element [12].

On the other hand, the **hnRNP proteins**, are generally recognized as negative factors due to their binding to both exonic and intronic splicing silencers (ESS and ISS) of the nascent

pre-mRNA [12]. These proteins contains one or more RNA-binding domains associated with an auxiliary domain that is often involved in protein-protein interactions [17][18].

The hnRNP proteins remains associated with transcripts both during processing and during their export to the cytoplasm. Indeed, although many of them are localized in the nucleus, several hnRNPs moves between nucleus and cytoplasm, indicating that works also in nuclear export and in other cytoplasmatic processes [19].

Although the mechanisms of splicing silencing through hnRNPs interactions are still not fully understood, is thought that silencing can occurs by three different ways:

- By direct competition: a *cis*-acting element, characterized by enhancer and silencer overlap functions, could promote or inhibit splicing through a competition between positive factors, such as an SR protein, and negative factors, such as hnRNP. If the positive factor has higher affinity or higher concentration than the negative one, the exon is included; if vice versa, is excluded (Fig. 1.4 a).
- By exon looping: the presence of duplicate ISS in the introns that flank an alternative exon could promote exon looping through dimerization between bound protein, preventing exon recognition (Fig. 1.4 b).
- By multimerization: an alternative exon that present ESE and ESS at near regions could be silenced, and thus skipped, by the binding of hnRNPs which polymerize covering enhancer sequence and preventing the recognition mediated by SR protein (Fig. 1.4 c) [12].

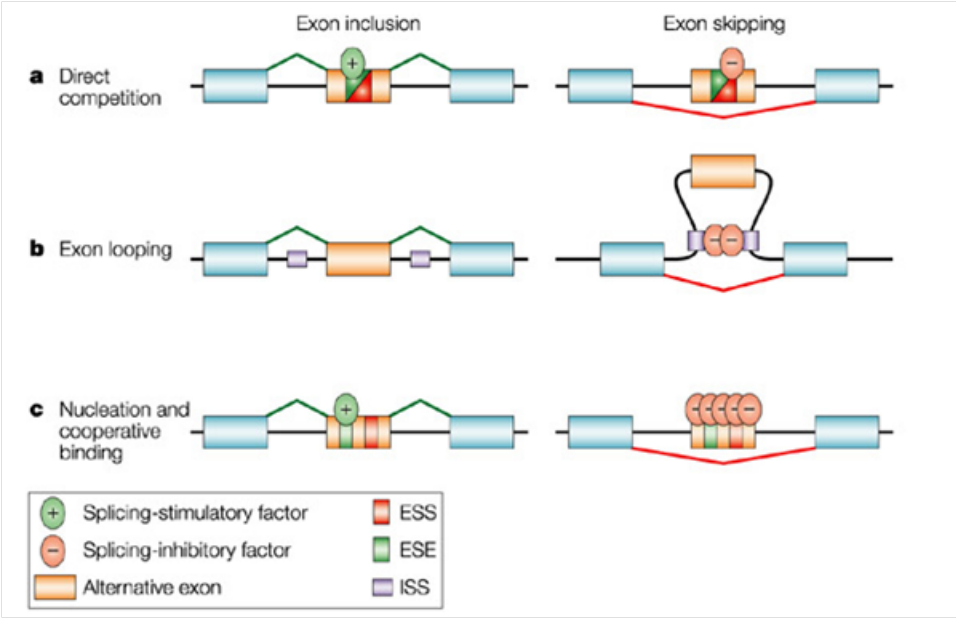

Figure 1.4 Models of splicing silencing.

Three different modes through which splicing silencers modulate splicing. [a] Silencing by direct competition. A splicing inhibitory factor (–) binds to an ESS. Because the ESS overlaps an ESE, bounded by a stimulatory factor (+), the binding of the positive and negative factors is mutually exclusive. [b] Silencing by exon looping. A splicing inhibitory factor binds to duplicate ISS. Dimerization of the bound protein brings the ISS elements and causes the exclusion of the alternative exon. [c] Silencing by nucleation and cooperative binding. An inhibitory factor initially binds to a high-affinity binding site in the ESS, and nucleates cooperative binding of additional inhibitory molecules, which polymerize along the exon, resulting in exon skipping.

1.2 The chemical reactions of splicing

The splicing process is characterized by two step reaction, in which *cis*- and *trans*- acting elements plays a key role for the maturation of pre-mRNAs (Fig.1.5.1). This mechanism start with the recognition of the 5' splice site through a Watson-Crick interaction with the snRNP U1 and the binding of the heterodimer U2AF$^{65/35}$ to the polypyrimidine tract, defining the 3' splice site (Fig. 1.5.2). This represent the Early complex (E) of the spliceosome in which is not request the hydrolysis of ATP. The binding of the snRNP U2 in an ATP-dependent manner to the branch point, through a base-pair interaction, represent the passage from complex E to complex A. This last complex is stabilized by the heteromeric complexes of U2 snRNP, called SF3a and SF3b [20].

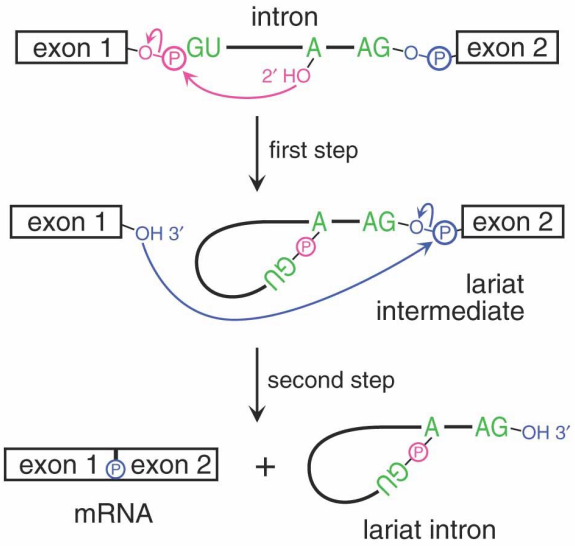

Figure 1.5.1 Splicing occurs in two trans-esterification reactions

Schematic representation of the precursor mRNA with essential signals for splicing reaction. Exons are white boxes, intron is a line. Position of the GU and AG dinucleotides at the 5' and 3'ss respectively and an A nucleotide at the branch site are indicated (green). The groups involved in the first reaction are highlighted in magenta, and those in the second, in blue. Phosphates are shown as circled P's

The complex A goes to complex B1 through the binding of U4/U6 snRNP to the U2 snRNP and the binding of U5 snRNP to exon flanking the 3' splice site, that successively moved on the U2 snRNP. Also this reaction require the hydrolysis of ATP [21][22].
In the complex B are present all the snRNPs, but are inactive. The activation of spliceosome require some conformational modifications that move the 5' splice site to the branch point, through interactions between U1 and U2 snRNPs. After this, the U1 and U4 snRNPs are release leading to complex B* (activated) with the formation of the catalytic center, in which U6 snRNP basepairs with the 5' splice site and also with U2 snRNP. The snRNP U2 remains basepaired with the branch site and U5 snRNP interacts with both exons through its loop. Thus, is formed the active complex C that catalyzes the first trans-esterification reaction: the 5' phosphate of the intron is attacked by the 2'-OH of the branch site Adenosine, causing cleavage 3', 5'- phosphodiester bond and formation of a 2', 5'- phosphodiester bond. This first reaction produce a lariat-like intermediate. Further rearrangements between U2, U6 and U5 snRNPs lead to the second trans-esterification reaction: the newly formed 3'-OH of exon 1 attacks the 5' phosphate of exon2, causing cleavage of a phosphodiester bond and formation of a new bond. After these two trans-esterification reactions, the two exons are ligated and the intron is removed as a lariat intermediate (Fig. 1.5.1). Then the lariat is linearized by the activity of debrenching enzyme and further degraded in exosomes. The snRNPs U2, U5 and U6 are released and are recycled for other rounds of splicing [23].

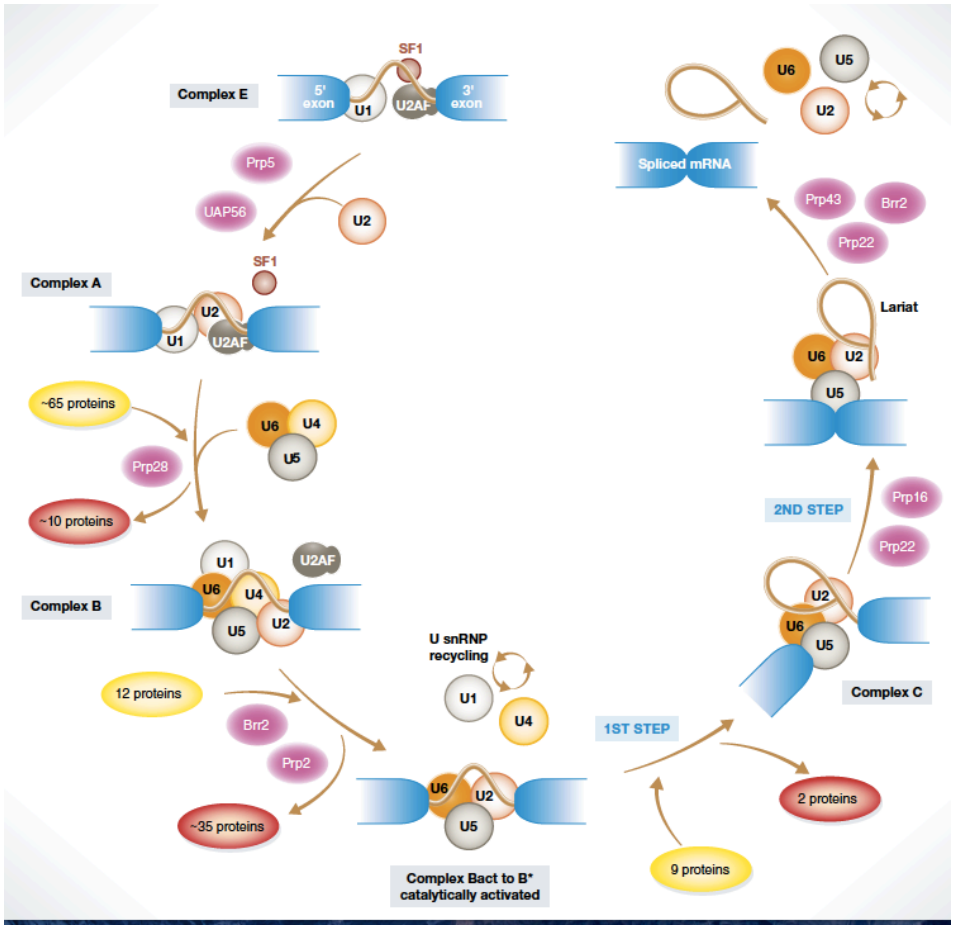

Figure 1.5.2 The assembly of the spliceosome.

The spliceosome assembles onto the pre-mRNA in a stepwise manner. Exons are noted by *boxes*, and introns by *lines*. Consensus nucleotides are indicated above the line. The complex E contains U1 snRNP bound to the 5' splice site, SF1 bound to the branch point, and $U2AF_{65}$ and $U2AF_{35}$ bound to the pyrimidine tract and 3' splice site AG, respectively (not showed in picture because are not U-snRNP). In the complex A, SF1 is replaced by U2 snRNP at the branch point. The U4/U6/U5 tri-snRNP then enters to form the B complex. Finally, a rearrangement occurs to form the catalytically active C complex, in which U2 and U6 interact, and U6 replaces U1 at the 5' splice site, promoting the two splicing reactions.

1.3 U1 snRNP

The *trans*-acting factors, involved into the recognition of *cis*-acting elements for a correct maturation of pre-mRNAs, are critical players in splicing reactions. In particular, Uridine-rich snRNPs, that compose the spliceosome machinery, are involved in the recognition of the canonical consensus signals to promote splicing processes. Among these, U1-snRNP represent the first important factor in splicing for its ability to identify the canonical 5'

splice site allowing the beginning of pre-mRNAs maturation. This capacity is due to its 5' single stand tail that interacts with the 5' splice site of pre-mRNAs by Watson-Crick base-pairing (Fig. 1.6) [24].

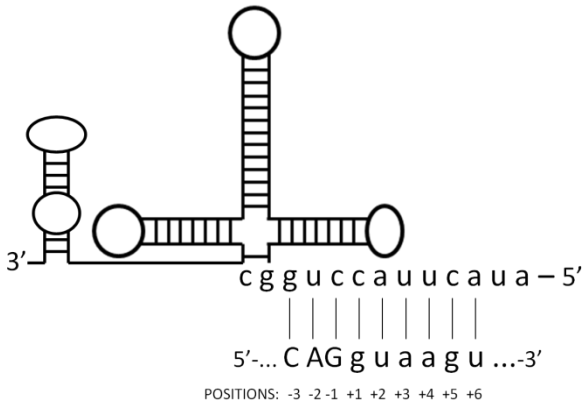

Figure 1.6 The mechanism of U1-snRNA binding to donor site.
In the picture are highlighted with vertical black lines the Watson-Crick interactions between the consensus sequence of 5' splice site and the 5'-tail of wild-type U1-snRNA.

In humans, U1-snRNP consists of a 164-nucleotide RNA molecule complexed with ten different proteins. Among these, seven are common to all other U snRNPs and represents the Sm proteins (B, D1, D2, D3, E, F and G), whereas three are specific to U1 snRNP (U1-70K, U1-A, U1-C) [24][25][26].

The secondary structure of U1-snRNA is characterized by four stem-loop regions (I, II, III, IV) and by two single-strand regions. One of these single-strand domain represent the 5' tail of U1-snRNA, which is responsible of interaction with the 5' ss of pre-mRNAs; whereas the other one represent the conserved Sm-binding site (sequence AAUUUGUGG), which is recognized in the cytoplasm by a heteroheptameric ring of Sm proteins [27][28].

Instead, the stem-loop regions are recognized by the other accessories proteins. In particular, U1-70K bind the first stem-loop (I), the U1-A bind the second stem-loop (II), while the U1-C protein is probably connected through a protein-protein interaction (Fig. 1.7).

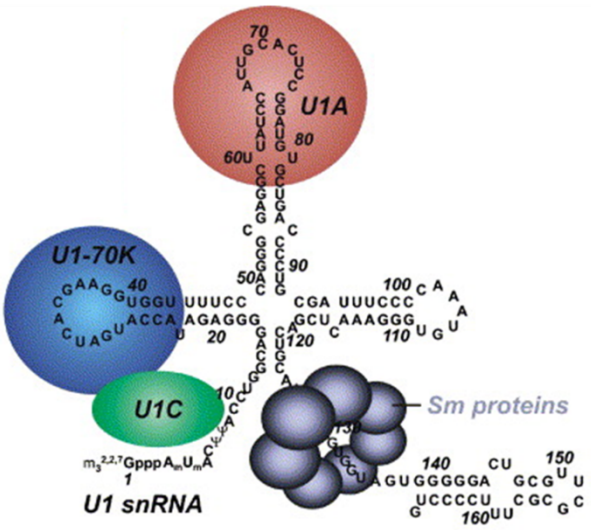

Figure 1.7 Schematic structure of U1-snRNP.

The secondary structure of U1-snRNA shown four stem-loops and two single strand regions. The accessory protein U1-70K bind the stem-loop I (blue circle), U1-A bind the stem-loop II (red circle) and U1-C bind through protein-protein interaction (green circle). The Sm binding site, one of the single strand regions, is bound by Sm proteins through a heteroheptameric ring (grey circles), whereas the other single strand region is represented by the characteristic 5'-tail tri-methylated (Figure adapted from D. Hof *et al.*, 2005).

1.4 U1 gene

The human U1 snRNA gene (*RNU1*) is encoded by clustered repeat units of 45 kb located on the short arm of chromosome 1, *1p36* [29]. However, in literature are reported many different U1 snRNA pseudogenes which are classified into three different classes and could generate functional variants of snRNAs [30].

The canonical U1 snRNA gene is characterized by the presence of two essential promoter elements, the distal sequence element (DSE) and the proximal sequence element (PSE), which the last one is recognized by the snRNA gene-specific factor PTF/PBP/SNAPc (Fig. 1.8) [31].

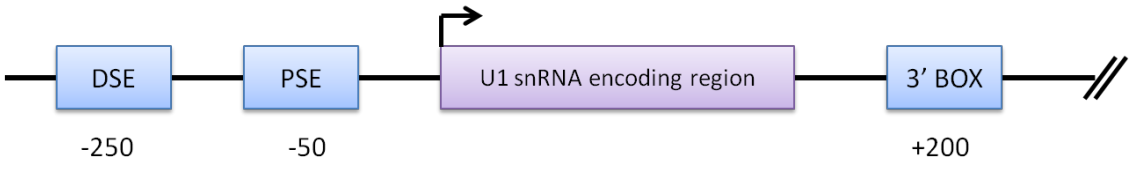

Figure 1.8 The structure of human U1-snRNA gene transcribed by Pol II.

The diagram shows the DSE and PSE *cis*-acting promoter elements and the 3' box *cis*-acting RNA-processing element of pol II-transcribed U1-snRNA gene boxed, with their position relative to the transcription start site noted below. The start site of transcription is marked with an arrow above the line.

The arrival of TATA-box binding protein (TBP) and several transcription factors (TFIIA, TFIIB, TFIIE and TFIIF) stimulate the transcription by RNA polymerase II to yield short non-polyadenylated 3'-elongated pre-snRNAs, which are maturated into the cytoplasm [32]. Proper 3' end formation of pre-U1 snRNA is an important step for the stability of snRNAs in the nucleus, in addition to transport through the nuclear membrane [33]. The 3' end formation requires the presence of a conserved element known as 3'-box, a *cis*-acting element located 9-19 nucleotides downstream of the 3' end of the RNA-encoding region, and phosphorylation of the carbossi-terminal domain (CTD) of Pol II [33][31][34]. A correct assemblage into the large export complex also requires the presence of a monomethyl guanosine cap structure (7mGpppG), which is recognized by the cap-binding complex (CBC) (Fig. 1.9) [35].

In the cytoplasm, these snRNAs dissociates from the export complex, associates with the Sm proteins and undergoes to hypermethylation of the 7mG cap to 2,2,7-trimethylguanosine (TMG) and to a specific exonucleolytic cleavage of the 3' end extensions. Successively, the mature snRNAs are re-imported into the nucleus through an import complex made of snurportin-1 (SPN1) and importin β , where they will mediate the splicing process [36].

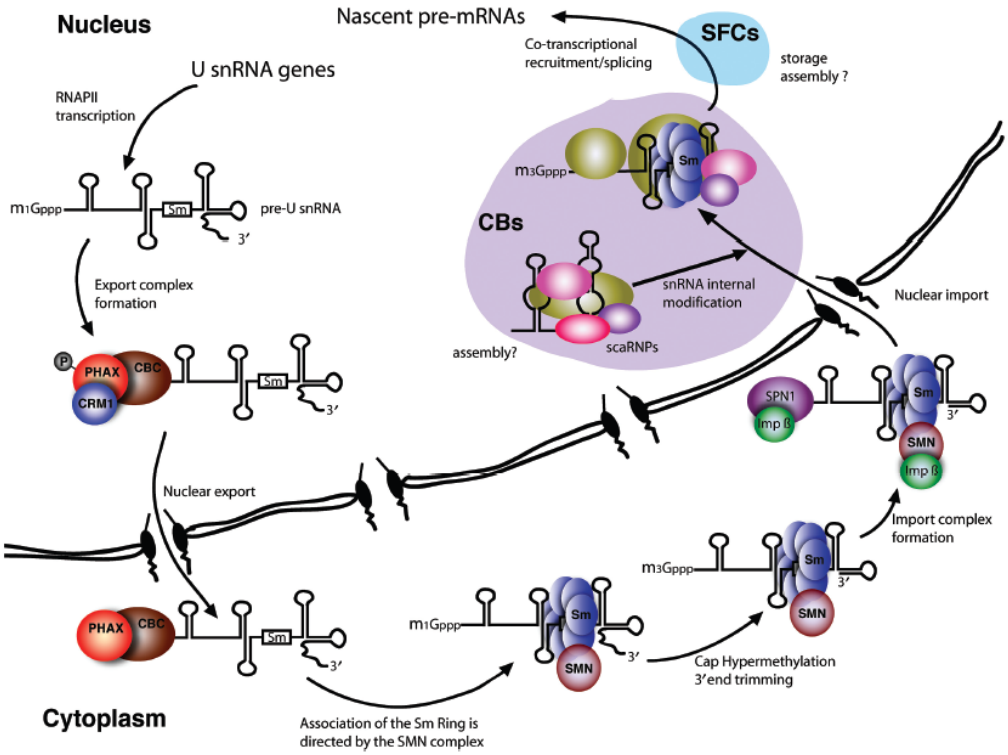

Figure 1.9 The Sm snRNP assembly and maturation pathway.

The U2 snRNA was used here as a representative member of the Sm snRNAs. In the nucleus, a non-polyadenylated 3'-elongated pre-U-snRNA is transcribed by RNA Pol II. This immature transcript is then monomethylated and assembled into a large export complex. In the cytoplasm, the transcript dissociate from export proteins and associate with Sm proteins. This new complex is further processed by 3'-end cleavage and tri-methylation of 5'. The mature snRNA is assembled into the import complex, which mediate the transport from cytoplasm to nucleus, where can exert their activity as snRNP.

1.4 Alternative Splicing

Alternative splicing (AS) is one of the most important mechanism of cells that increases the coding capability of genes, generating structural and functional different protein isoforms [37]. In fact, as described above, mammalian genes are transcribed by the RNA-pol II as immature molecules that need to be processed in order to produce uninterrupted mRNAs. The regulatory splicing elements within the nucleotide sequences are fundamental players that regulate the maturation of the pre-mRNAs. Indeed, these *cis*-acting elements can be differentially recognized, in physiological contexts, by a differential expression of specific *trans*-acting factors, leading to the production of thousand of

different mRNAs that will consequently generate different protein isoforms. One of the greatest examples of this spectacular mechanism is the *Drosophila melanogaster* gene *Down syndrome cell adhesion molecule (Dscam)*, which can generate 38,016 different mRNA isoforms, a number far in excess of the total number of gene in the organism (~14,500) [38].

Recent studies indicate that at least 95% of human genes are alternatively spliced, demonstrating that RNA molecules aren't simple passive intermediate in gene expression, increasing significantly the complexity of the already tough world of gene expression [39][40].

Several types of alternative transcripts are made by the differential usage of regulatory elements, which involves different modules as alternative 5' splice sites, alternative 3' splice sites, mutually exclusive exons, alternative promoters, alternative poly(A) sites and intron retention (Fig. 1.10) [41].

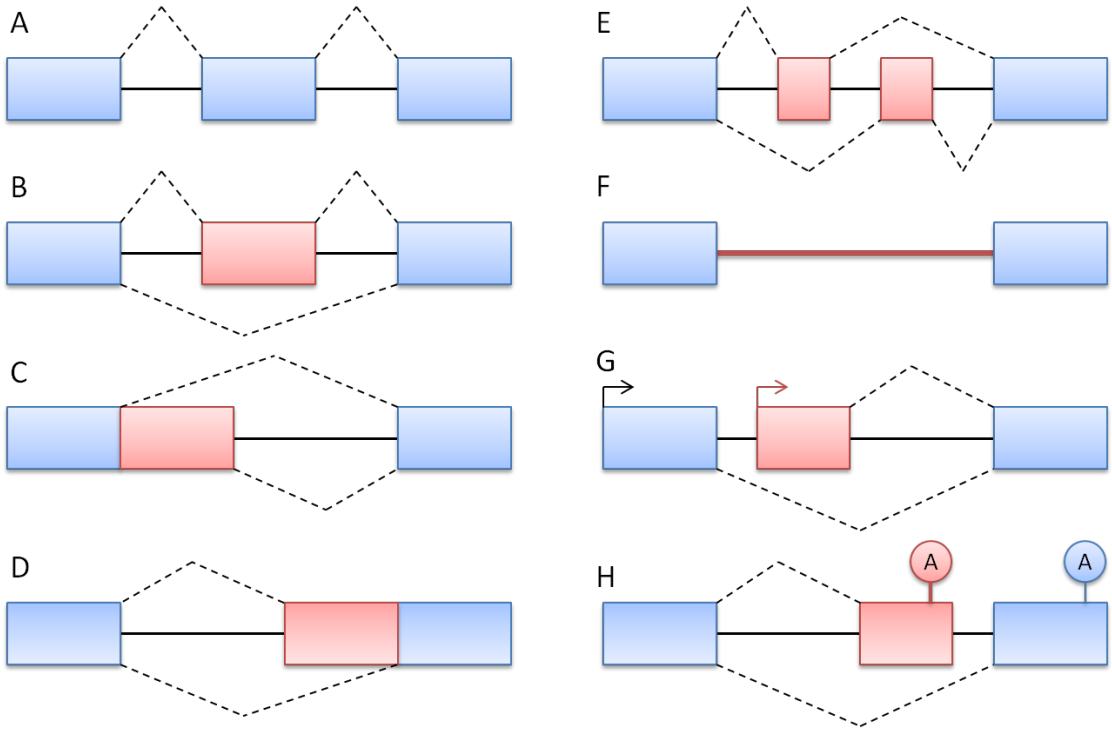

Figure 1.10 Patterns of alternative splicing.

Alternative splicing patterns increase mRNA diversity. Through alternative use of exons, introns, promoters and polyadenylation sites, alternative splicing acts to greatly increase the diversity of mRNA transcripts. **A**. Constitutive exon; **B**. Alternative exon; **C**. Alternative 5' splice site; **D**. alternative 3' splice site; **E**. Mutually exclusive exon; **F**. Intron retention; **G**. Alternative promoter; **H**. Alternative polyadenylation site.

Therefore, the number of potential mRNA isoforms that can be generated from one gene increases with the number of modules present in the sequence. In the example of *Dscam*, in fact, the 38,016 isoforms are produces by a gene containing 95 cassette exons, which are spliced in a mutually exclusive manner [38].

It is also known that most genes are alternatively spliced in both spatially and temporally manner. This results in the expression of different splice variants in different tissues, in different cells of the same tissue, in the same tissue at different stage of development, or in response to external stimuli.

The regulation of alternative splicing is very complex to be generalized, because it requires an accurate coordination of both *cis*- and *trans*-acting factors that can change on the basis of the considered gene. Moreover, splicing of each pre-mRNAs is frequently controlled by combinatorial or competitive effects of both activators and inhibitors. In human cells, in fact, there are several *trans*-acting elements, such as NOVA1, NOVA2, FOX1, FOX2, which have been shown to act as either repressors or activators depending on the location of their binding site [42][43][44][45]. For example, NOVA1 binds to an ISE in *GABRG2* (GABA A receptor, γ2) pre-mRNA and promotes inclusion of exon 9 [46], but it binds to the ESS in the alternative exon 4 of its own pre-mRNA and prevents exon 4 from being included [42].

Therefore, the final outcome depends on a spatial-temporal regulation of the expressed gene, which can generate a multitude of different molecules with different biological properties [47].

1.5 Splicing mutations and disease

Mis-regulation of splicing has been long known to be related to an increasing number of diseases, including genetic pathologies, neurodegenerative disorders and cancer. Aberrant splicing may result from mutations that impair *cis*-acting elements as well as mutations that affect *trans*-acting factors required for the proper splicing regulation. These mutations can directly cause the pathological condition or contribute to the susceptibility or severity of diseases [48].

Although the frequency of splicing mutations varies considerably between individual genes, it is considered that approximately 50% of pathogenic mutations cause disease through the defect they introduce in the splicing mechanism [49].

These mutations can affect splicing in different ways:

- disrupting a conserved canonical splice sites, directly interfering with the binding of U-snRNP (Fig. 1.11a);
- disrupting a splicing enhancer (ESE and ISE), preventing the binding of positive regulators (Fig. 1.11a);
- disrupting a splicing silencer (ESS and ISS), preventing the binding of negative regulators (Fig. 1.11a);
- disrupting an RNA secondary structure and, thus, preventing the recognition mediated by specific *trans*-acting factors (Fig. 1.11c);
- altering the expression of specific *trans*-acting factors (Fig. 1.11b).

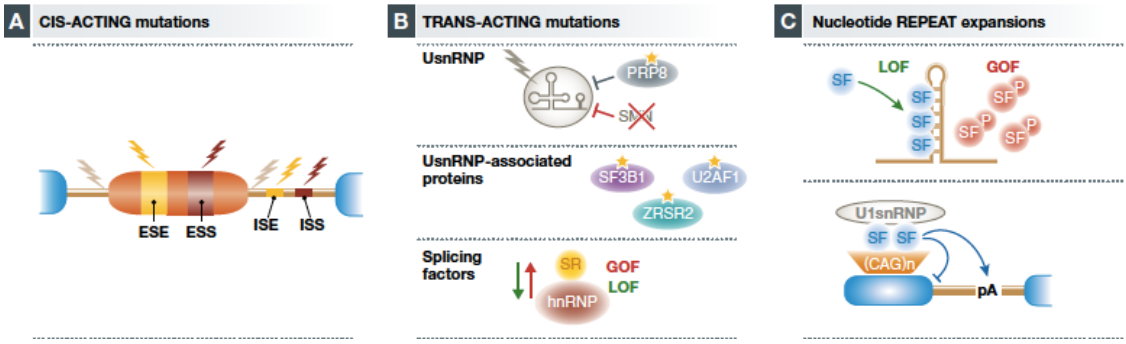

Figure 1.11 Molecular targets of splicing-causing mutations.

Schematic representation of mutations affecting cis-acting elements (A), trans-acting factors (B), and RNA secondary structure (C). [50]

The first important step of splicing is the recognition of the 5' splice site though a Watson-Crick interaction between the 5' binding tail of the U1 snRNA and the consensus sequence of the donor site. Aberrant splicing can occur when mutations affect the donor site, reducing the communication with the U1 snRNA. Indeed, most of the splice site mutations associated to pathological conditions affect the dinucleotide GU of the donor site as well as the dinucleotide AG of the acceptor site. Mutations at other positions of the 5' and 3' splice site can promote aberrant splicing by reducing the exon definition or activating a cryptic splice site [51].

Point mutations can also affect the regulatory splicing elements within the transcript [50]. One common example is given by the synonymous substitution in the exon 7 of the *survival of motor neuron 2* gene (*SMN2*), which significantly induces exon skipping, leading to the Spinal Muscular Atrophy (SMA) disease. Although the mutation does not alter the coding sequence, the C>T substitution affects a key exonic regulatory element, inducing an aberrant splicing that significantly compromises the protein outcome. The biochemical mechanism by which *SMN2* splicing is altered can be explained by a two non-exclusive models, either through gain of an ESS or loss of an ESE. In the ESS-gain model, the mutation creates an ESS binding site for hnRNPA1 which functions as a splicing repressor, whereas in the ESE-loss model, the mutation disrupts an ESE that is bound by the SR protein SF2/ASF [52][53].

Point mutations can also affects *trans*-acting factors, causing more severe or lethal conditions [50]. In fact, while disease-causing mutations that act in *cis* affect splicing of a single gene, mutations that affect components of the splicing machinery have a wide-spread effect, involving the processing of multiple genes. The relative scarcity of examples for severe loss-of-function mutations in *trans*-acting factors may be an indication that mutations with widespread consequences are lethal during embryonic development or in individual cells.

Recently, several evidences highlighted that also missense mutations are playing an important role in splicing [54]. Missense mutations indeed, even though are likely to impair the protein bio-functionality, can affect specific exonic splicing regulatory elements, inducing an aberrant splicing that will significantly reduce the protein outcome.
Therefore, it is of crucial importance to study the effect of each specific mutation in order to understand the molecular mechanisms underlying the pathology and, thus, provide the knowledge for the development of disease-tailored therapeutic strategies [48].

1.6 Hemophilia A (HA)

Haemophilia A (HA) is a life-threatening disease caused by a dysfunction in the blood coagulation pathway due to the loss of the coagulation factor VIII (FVIII). HA is inherited

as an X-linked disorder with an incidence of 1 in 5000 live births, representing the most common hereditary coagulation disease [55]. Due to its inheritance, HA affects the male population, whereas the female one usually acts as carrier. Haemophilia A is clinically indistinguishable from haemophilia B (HB), which is due to the loss of the coagulation factor IX (FIX) and affects about 1 in 25,000 newborns. Thus, in order to distinguish HA from HB, it is necessary to establish the etiology using a coagulation-factor assay [56]. Normal plasma levels of FVIII are usually between 50% and 150%. Depending on the percentage of clinically active FVIII, HA severity is divided into severe (<1% activity), moderate (1-5%) and mild (5-40%) [57][58]. Severe haemophilic patients are usually diagnosed during the first two years of life and they are characterized by frequent and spontaneous bleeding episodes that occur mostly into the joints and muscles. Moderate HA patients display less frequent bleeding episodes and are usually diagnosed before age of five to six years. Mild HA patients do not show spontaneous bleeding episodes, which usually occur after trauma or surgery. Tin this case, the bleeding frequency is reduced to once a year to once every ten years, and thus the diagnosis is determined later in life.
Treatments for haemophilia A displayed a lot of changes in the past decades due also to the improvements of the modern medicine. Early treatments were based on whole blood or plasma transfusions which, most of the times, were not sufficient to obtain a proper haemostasis. In the 1970s, a solution was introduced by plasma-derived FVIII (pdFVIII) concentrates, preventing and controlling bleeding episodes through their delivery by intravenous injections [59][60]. Although these strategies boosted up the life's expectancy of HA patients, the usage of blood products increased also the risk of viral infection such as HIV, Hepatitis B and C. Virucidal treatments were adopted to overcome the indirect transmission of these viruses, eliminating the risk of HIV infection since 1985 and of hepatitis since 1990. Another answer has been given by a new type of treatment with the introduction of recombinant FVIII (rFVIII) concentrates into the market since 1990 [61]. Despite these advances, however, the prophylactic treatment has its limitations, considering that a high proportion of patients also develop antibody inhibitors against FVIII. Nowadays, gene therapy represents the new frontier for the treatment of HA, overcoming the issues raised by today's treatment including the development of inhibitors, high costs, and frequency of injections [56].

The human FVIII gene is located on the long arm of the X chromosome and is composed of 26 exons and introns, with a total length of 186 kb. The 9 kb coding sequence produces a full-length glycoprotein of 2,332 amino acids (330 kDa) that is characterized by six

structural domains and three acidic subdomains, organized in a heavy chain (A1-a1-A2-a2-B) and a light chain (a3-A3-C1-C2) [61]. Every domain plays a physiological role throughout the life cycle of FVIII. The A domains of FVIII share approximately 40% amino acid identity with each other and to the A domain of FV [62]. Also the C domains share almost the same percentage of homology with each other and the FV [63]. An exception is the B domain, which does not have any similarity with other proteins, including the B domain of FV. This domain is encoded by a wide uninterrupted exon 14, which does not seem to be necessary for FVIII clotting activity but is important for internal processing of FVIII protein [64].

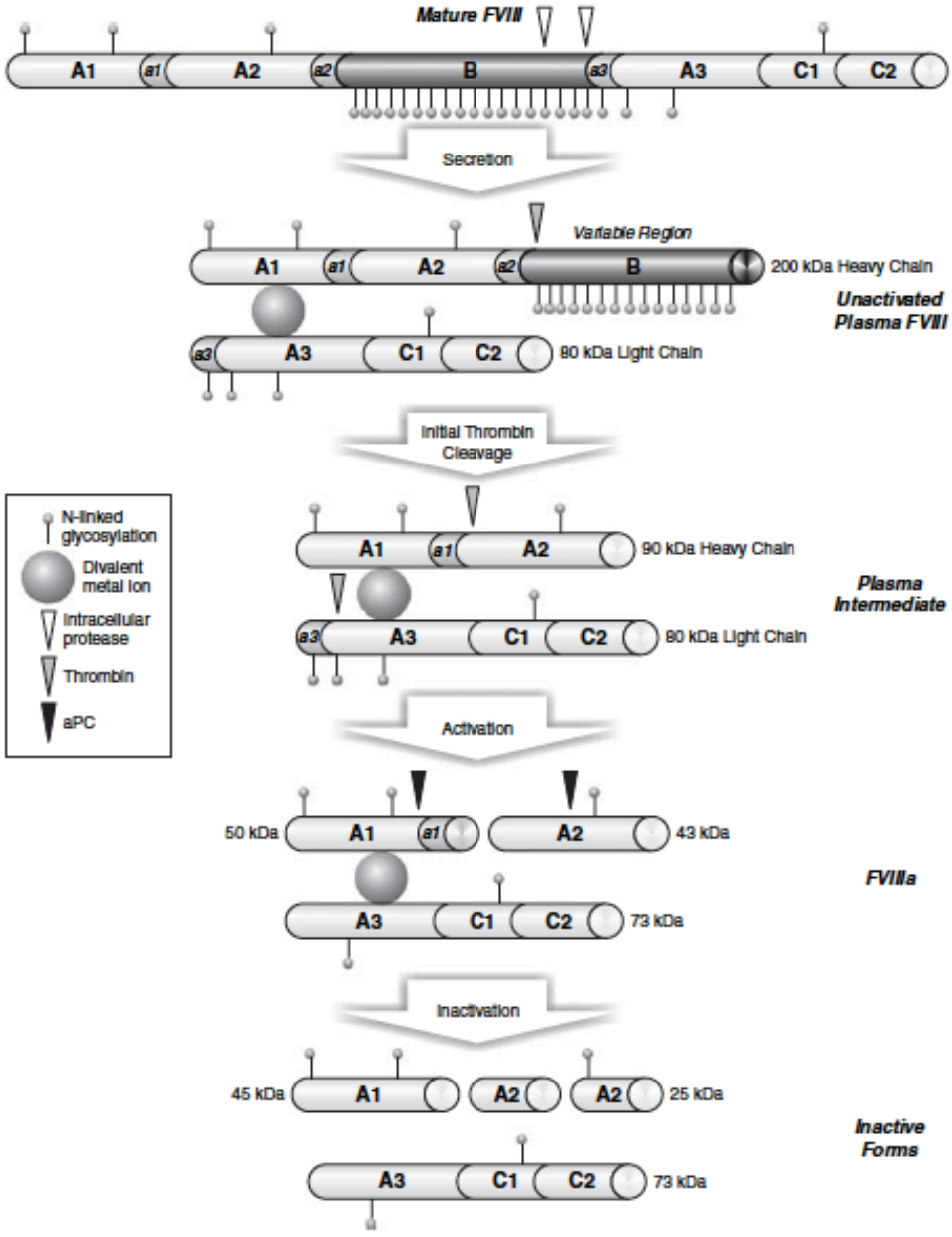

Figure 1.12 Domain structure and processing of FVIII.

Sinusoidal endothelial and Kupffer cells in the liver are the major site of FVIII expression [65][66]. Although FVIII has a high structural instability and the expression system is very inefficient, physiological levels are obtained in normal conditions [67][68]. However, mutations that affect the *F8* gene can affect its production on several levels, reducing the final yield and leading to the pathological condition. The genetic defects resulting in HA include deletions, exon and intron inversions, nonsense and missense mutations [69][70]. While the association of the so-called "null mutations" with severe forms is well-established, that of missense mutations, frequent in HA and largely predominant in the other coagulation factor deficiencies, with the phenotype is elusive. Missense mutations, by introducing amino acid substitutions, are candidate to affect protein biosynthesis and/or function [54]. However, they might affect the splicing regulatory network and impair splicing, an emerging mechanism whose pathophysiological impact is still poorly investigated [48]. The interplay between these mechanisms might concur to FVIII levels and to HA severity.

One example is given by the second most frequent HA mutation in the Northern Italian population, the c.6046C>T substitution [71]. This missense mutation causes the substitution of an arginine into tryptophan in the A3 domain of FVIII (Arg2016Trp), thus impairing the protein biology. Furthermore, in HA patients carrying the c.6046C>T substitution, it has been observed the presence of *F8* transcripts lacking of the exon 19, suggesting a role in the mRNA splicing [72]. This effect on pre-mRNA processing could explain the phenotypic variability registered in patients, which displayed FVIII:c levels ranging from <1% (severe) to 4% (moderate) and with different degrees of hemorrhagic severity, but the molecular mechanism remains still unknown [71].

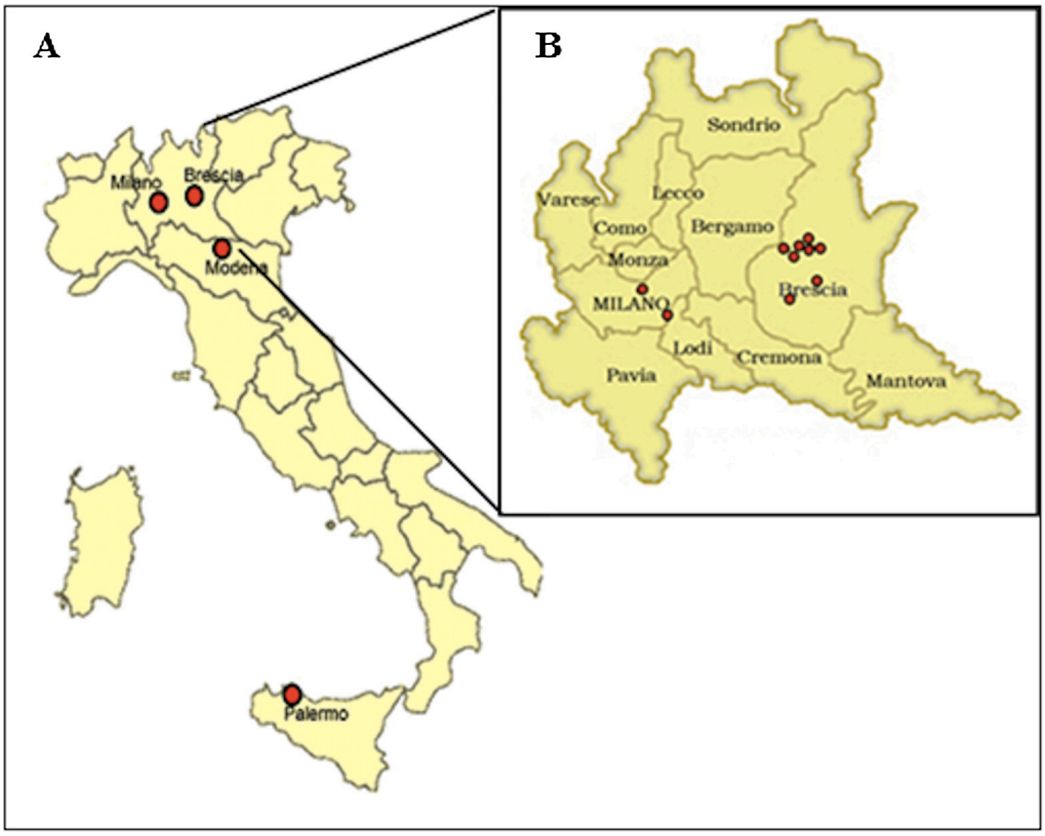

Figure 1.13 Geographic distribution of patients carrying the mutation c.6046C>T in Italy.

1.7 Familial dysautonomia (FD)

Familial dysautonomia (FD), or Riley-Day syndrome (OMIM #223900) belongs to rare neurodevelopmental disorders termed hereditary sensory and autonomic neuropathies (HSAN III) [73][74][75]. FD is characterized by incomplete neuronal development and progressive neuronal degeneration with a marked decrease in unmyelinated fibers, in the innervation of target tissues and in dorsal-root ganglia cells [76][74]. This is consistent with postural hypotension and exaggerated responses to sympathomimetic/parasympathomimetic agents. FD features also involve many other systems, with gastrointestinal dysfunction, cardiovascular instability, recurrent pneumonia, decreased sensitivity to pain/temperature, vomiting crisis, and defective lacrimation [77][73]. Currently, ~54% of patients are over 15 years and a newborn has a 50% probability of reaching 40 years.

FD is recognized as a life-threatening disorder with high mortality rate and there is no cure but only treatments to control symptoms.

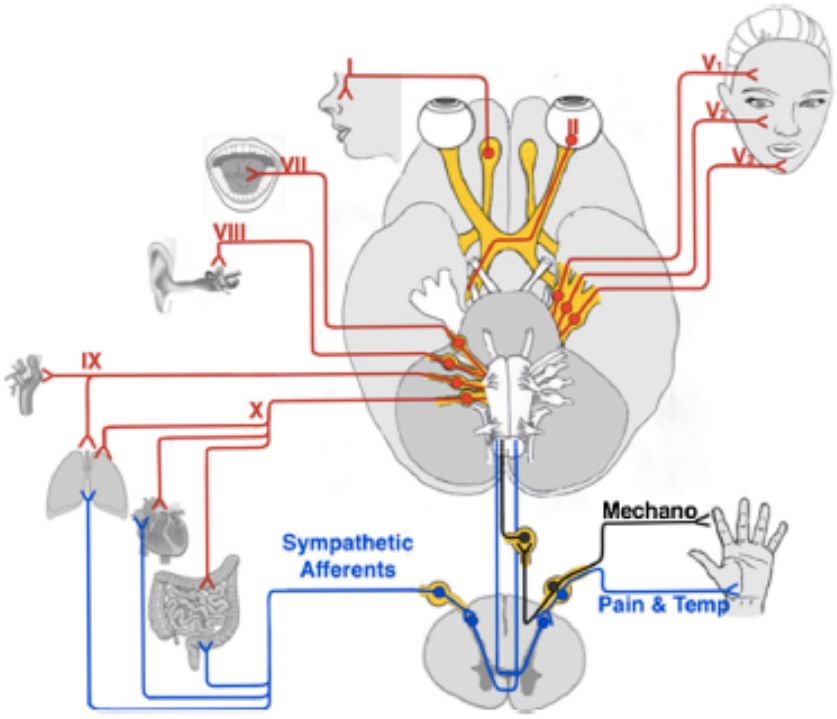

Figure 1.14. Affected pathways in FD.

The congenital deficiency in IKAP affects the development of mostly sensory (afferent) neurons. Cranial afferent nerves (shown in red) with cell bodies outside the CNS are widely affected. Involvement of the olfactory cranial nerve (I) results in hyposmia. Progressive involvement of the optic nerve (II) causes visual field defects and poor red/green color discrimination and eventual blindness. Severe involvement of the sensory branches of the trigeminal nerve (V) results in corneal insensitivity and dryness, hypoesthesia of the face and repeated trauma; and manifests electrophysiologically with an absence of the blink and jaw jerk reflexes. Involvement of the sensory branch of the facial nerve (VII) results in a dulled sense of taste. Involvement of the vestibulocochlear nerve (VIII) result in abnormal position sense and likely contributes to gait ataxia. Hearing abnormalities have never been assessed. Glossopharyngeal and vagal nerve (IX and X) involvement dominate the clinical picture as it results in afferent baroreflex failure with uncontrolled swings in blood pressure. Involvement of the glossopharyngeal nerve causes blunted chemoreflex responses to hypoxia and loss of protective airway reflexes including the gag response. Lack of vagal afferent information from the viscera contributes to widespread organ dysfunction. Spinal afferents shown in the bottom half are also severely affected. Sympathetic afferents (shown in blue) with cell bodies in the dorsal root ganglia are impaired and many mechanical, thermal, chemical, metabolic inputs from the viscera are lacking. Large diameter primary afferents (shown in black) with cell bodies in the dorsal root ganglia are also affected. This results in proprioceptive abnormalities and contributes to the characteristic gait ataxia of FD.

FD is an autosomal recessive disorder caused by mutations in the *IKBKAP* gene, spanning 68 kb on chromosome 9q31 and comprising 37 exons [78][79]. The mRNA (~5kb) encodes for the IKAP protein (1332 aa; 150 kDa), a component of the elongator complex (ELP1), known as ikappaB kinase (IKK) complex-associated protein (IKAP) [80][81][82].

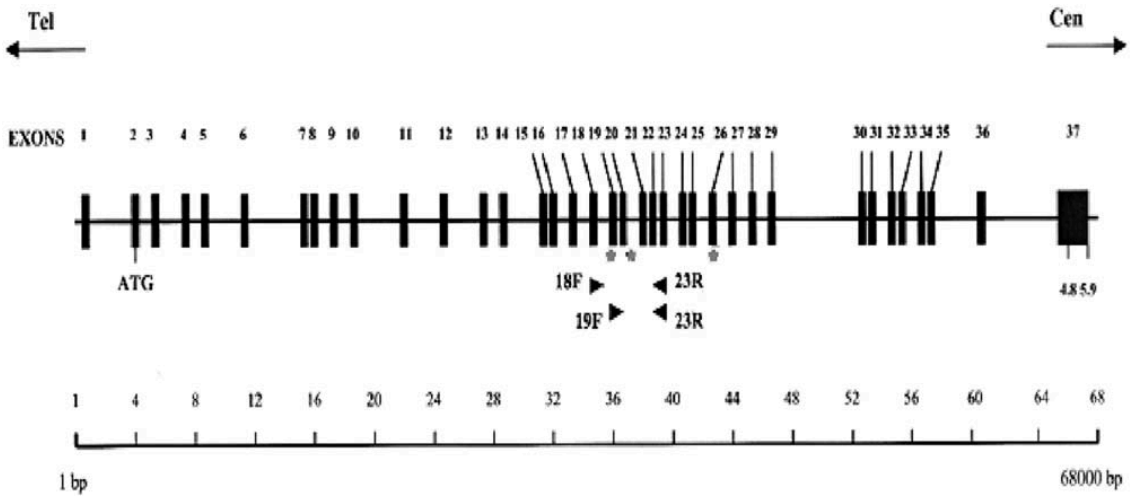

Figure 1.15 The IKBKAP gene and location of the three FD mutations.

Genomic structure of IKBKAP, showing orientation and placement of the 37 exons within a 68-kb genomic region of chromosome 9q31. The asterisks (*) indicate the location of the three mutations identified.

Besides being part of the ELP and involved in the RNA pol II elongation, IKAP participates in the cytoplasm in processes such as cell migration, JNK signaling, exocytosis and t-RNA modification [83]. IKAP has been implicated in the remodeling of actin cytoskeletal organization, necessary for neuron differentiation, migration and target tissue innervation [84][85][86]. I*n vivo* studies highlighted that IKAP loss leads to neuronal cell death due to failed tissue innervation rather that abnormal neuronal migration [87][88]. However, the IKAP functional alteration explaining FD features has not been clarified. On the other hand, it is clear that FD patients have reduced IKAP amounts, particularly in central/peripheral nervous system [79], which would explain the neurodegerative disease features.

FD is a rare disease but common in the Ashkenazi Jewish population (1 in 3,700) with a carrier frequency of 1 in 27, and 1 in 18 in those of polish descent [89]. The most common IKBKAP mutation is the c.2204+6T>C (IVS20+6T>C). Importantly, all FD patients possess at least one copy of the IVS20+6T>C mutation, with 99.5% of homozygotes and only five compound heterozygotes with the R696P or P914L missense mutations [79][90]. Studies in patients' cells showed that this mutation, occurring at the 5' donor splice site (5'ss) of intron 20 (IVS20), promotes exon 20 skipping and leads to a frame-shifted mRNA, together with residual levels of the normal transcript. Interestingly, for unknown mechanisms, the aberrant splicing pattern and the normal/mutant transcript ratio are tissue-specific, with the lowest value in neuronal tissues where the IKAP expression is very low [79].

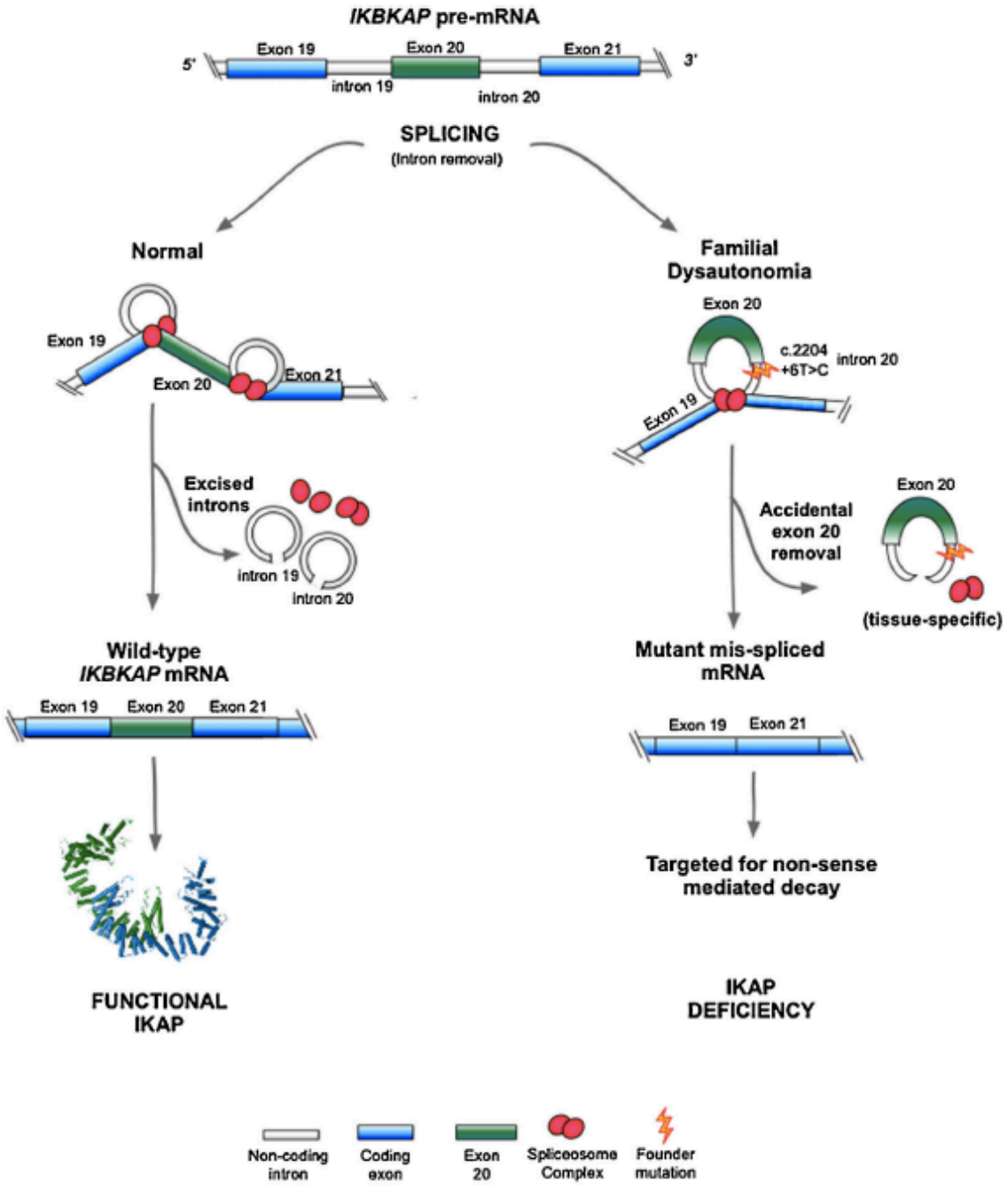

Figure 1.16 Pre-mRNA splicing of the IKBKAP gene.

The pre-messenger RNA is shown on top with exon 20 flanked by introns 19 and 20. Under normal circumstances (left) the 50 and 30 splice sites of intronic sequences are recognized by the small nuclear ribonucleoproteins (snRNPs), then looped and excised by spliceosomes. The flanking exons are assembled together into a mature mRNA coding sequence that is translated into functional IKAP. In FD (right), the founder mutation at base pair 6 of intron 20 prevents recognition of the intronic splicing junctions flanking exon 20. The splicesomes accidentally catalyze a reaction that joins together exons 19 and 21–"skipping" exon 20 from the mature mRNA coding sequence. This mutant mRNA is targeted for non-sense mediated decay. Patients with FD retain the ability to produce some wild-type (normal) mRNA transcripts, and thus

have a deficiency in IKAP, and not complete absence of functional protein product. This incorrect splicing of the IKBKAP gene occurs in a tissue specific manner. Most affected is neuronal tissue, which produces primarily mutant mRNA and almost no functional protein product. Adapted from [91] and [92].

FD is a recessive disorder, with asymptomatic IVS20+6T>C heterozygotes. On the other hand, the disease severity is highly variable both between and within families [77], a finding that might depend on the differences in the extent of exon 20 skipping between patients either in the specific tissues or at specific developmental stage [79]. The residual levels of IKAP expression (exon 20 inclusion) are much lower in neurons (~5% of normal) than in the not/less affected tissues (>20%)

Consistently, studies with transgenic ikbkap$^{\Delta 20/flox}$ mice indicated that a very small increase of IKAP expression (5-10% of wt) greatly diminishes the FD severity and DRG neuronal deficit, and increase the life-span [93]. This finding is further strengthened by the phenotype amelioration in TgFD9 ikbkap$^{\Delta 20/flox}$ mice harboring a mutated human FD transgene expressing low hIKAP levels [94].

Altogether these data suggest that even a partial rescue of exon 20 above 20% in FD tissues would have a therapeutic meaning, particularly in CNS and PNS.

Moreover, FD is characterized by both developmental impairment and progressive neurodegeneration, with most of dorsal root ganglia lost postnatally [95]. This supports the relevance of treating patients early in life. However, adult treatment would prevent further degeneration of sympathetic neurons.

Whereas the size of IKBKAP gene and the lack of sufficient information regarding its regulation complicates a replacement gene therapy approach, the genetic/molecular features of FD render it an ideal target for RNA-based strategies aimed at promoting exon 20 inclusion. Importantly, splicing modulation would maintain the physiologic *IKBKAP* gene regulation within cells.

A number of compounds have been tested to this purpose. Among them, the plant cytokines kinetin, which can be orally administered, rescued IKBKAP splicing in FD cells (fibroblasts and lymphoblast) [79][96], FD-iPSCs derived cells [97], FD mouse model [98], in FD heterozygotes and FD patients [99]. All patients with FD increased the amount of normal wild-type IKBKAP mRNA produced in white blood cells after taking kinetin. At baseline, the mean percentage exon inclusion (i.e., the percentage of correctly spliced IKBKAP mRNA) was 54 ±10%. This increased to 57±10% after receiving kinetin for 8 days and increased further to 71±9% after receiving kinetin for 28 days (p=0.002, Figure

2). There was no relationship between the kinetin dosages and peak concentration levels achieved or the effect on wild-type IKBKAP mRNA production.
However, kinetin, whose mechanism of action in unclear, was also shown to modify splicing of other genes [98].
IKBKAP splicing correction was also demonstrated in patients' cells through the glycoside digoxin, whose mechanism appear to be related to the splicing factor SRSF3 [100].
Phosphatidylserine (PS), a FDA-approved food supplement, was also active in FD cellular and mouse models where it increased FD transcription rather than splicing [101][102]. Although without evident side-effects in mice, PS seems to modify the expression of several other genes, and particularly those involved in cell-cycle regulation.
RECTAS (rectifier of aberrant splicing) is the last FDA-approved compound that has been shown to improve IKBKAP splicing in FD patients' cells at lower doses than kinetin [103]. Again, the mechanism is poorly known and RECTAS seems to stimulate alternative splicing of other genes.

Notwithstanding their activity, none of these compounds appear to be IKBKAP specific, thus holding the great risk of off-targets, a crucial issue particularly in case of prolonged treatments. Consequently, there is a strong request for splicing-correction approaches specifically designed on the IKBKAP exon 20 features.

1.8 Spinal Muscular Atrophy (SMA)

Spinal muscular atrophy (OMIM #253300, #253550, and #253400) is an inherited neuromuscular disease characterized by progressive muscle weakness resulting from degeneration of lower motor neurons (α-MNs) in the spinal cord and muscle atrophy. SMA is the primary genetic cause of infantile mortality, affecting approximately 1 in 6000-1 in 10,000 newborns, and a carrier frequency of 1:40 to 1:60 [104][105]. Patients with SMA are classified into 5 clinical subtypes (SMA type 0-IV) based on the age of onset, motor function achievement and age at death. SMA type 0 is the most severe form, which is characterized by a neonatal onset, reduced movements *in utero* and a premature death few months after birth [106]. SMA type I is the most common form, with onset

before the age of six months, inability to sit unsupported and a survival up to two years of age [107][106]. Patients with SMA type II are affected before 18 months of age, are able to sit upright without supports but are unable to walk independently. Patients with SMA type III show the first symptoms after the age of two years, maintain the ability to stand unsupported and live a normal lifespan. SMA type IV has an onset in the second or third decade of life, with a mild to moderate muscle weakness and without respiratory deficiencies [106]. To date, there are no effective treatments available to cure patients with SMA and medications remain limited to symptomatic and supportive care.

	OMIM number	Age at onset	Highest function achieved	Natural age of death
Type I (severe, Werdnig-Hoffmann disease)	253300	0–6 months	Never sit	<2 years
Type II (intermediate)	253550	7–18 months	Sit, never stand	>2 years
Type III (mild, Kugelberg-Welander disease)	253400	>18 months	Stand and walk	Adult
Type IV (adult)	271150	Second or third decade	Walk during adulthood	Adult

OMIM=Online Mendelian Inheritance in Man.

Table 1: Classification criteria for spinal muscular atrophy

Figure 1.17 Clinical classification of types of spinal muscular atrophy..

SMA is caused by homozygous deletion or mutation of the telomeric *survival motor neuron 1* (*SMN1*) gene, which results into the loss of SMN protein, leading to motor neuron degeneration. The SMN protein is a polypeptide of 294 amino acids with a molecular weight of 38 kDa. This protein is ubiquitously expressed and is highly conserved across species. Several studies showed that SMN plays a crucial role in the biogenesis of the small nuclear ribonucleoproteins (snRNPs), driving the assembly of the characteristic heteroheptameric Sm ring on snRNAs, which is an essential and obligated step of this biogenesis pathway. Thus, SMN deficiency causes alterations in snRNA levels, leading to a widespread defect in splicing.

Clinical variability results from the expression of a highly homologous centromeric copy of *SMN1*, called *survival motor neuron 2* (*SMN2*), that is located on the same 5q13 chromosome [108]. The paralogous *SMN2* gene differs from *SMN1* by a single synonymous C to T substitution in exon 7 (c.840C>T), which disrupts an exonic splicing enhancer and concomitantly creates an exonic splicing silencer [109][110][111]. This single nucleotide change potently affects *SMN* splicing, resulting into an aberrant skipping of exon 7 [109]. This exon is highly regulated and contains the translation termination signal for all full-length products, whereas the translational termination of the exon-

skipped transcript is at the 5' end of exon 8. The Δ7 mRNA encodes an unstable and not functional truncated SMN protein that is rapidly degraded [112][111]. However, the *SMN2* gene retains a minimal production of the full length SMN protein due to the 10-15% of transcripts that include exon 7. Importantly, multiple copies of *SMN2* can be present in the human genome and a higher *SMN2* copy number inversely correlates with disease severity [113]. Therefore, SMA is the result of a deficiency of functional SMN that is due to i) the loss of *SMN1* and ii) the aberrant processing of the paralogous *SMN2* gene.

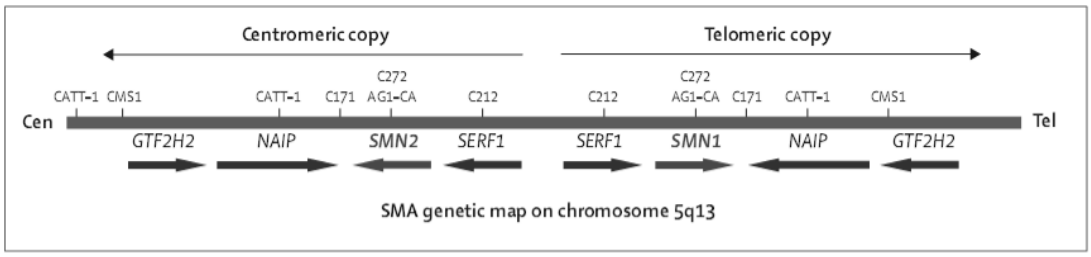

Fig. 1.18 Schematic localization of *SMN1* and *SMN2* genes.

Since the coding sequences of *SMN1* and *SMN2* are identical except for the single C>T substitution, it is clear that these two genes are highly regulated. Particularly, the region of exon 7 is characterized by the presence of several splicing regulatory elements that play a key role deciding the transcript's faith [53][114][115]. Within the exon 7 there are three important elements: an exonic splicing enhancer (ESE) bound by Tra2-β1, which itself acts as recruiter of other additional regulatory factors (like SRp30c, hnRNP-Q, hnRNP-G and RBMY) [116][117][118][119]; a stem-loop structure with inhibitory properties located at the exon 7-intron 7 junction that hinders U1 binding to the 5'ss; and an ESE located at the beginning of exon 7, which converts to an exonic splicing silencer (ESS) when the transition C>T occurs [52][111]. Indeed, in *SMN1* this elements is bound by SF2/ASF, promoting the inclusion of the exon; on the contrary, in *SMN2* it is recognized by hnRNP-A1, which stimulates the exclusion of the exon [120][121]. Additionally, other *cis*-acting elements are placed on the flanking intronic sequences, increasing the regulation of this specific region [122]. Intronic splicing silencers are located both in the intron 6 (-75 to -89), called element 1 (E1), and in the intron 7 (+10 to +24), named N1 [123][124]. It is known that both elements exerts a negative effect on the inclusion of exon 7, but the precise mode of inhibition is still unknown. Finally, another silencer was found with a +100A>G transition in SMN2 intron 7, creating a binding site for hnRNP-A1 and enhancing the repression stimulated by the +6 C>T change. All together, these information provide a knowledge that can be used to develop innovative approaches aimed at correcting the exon 7 splicing defect.

The main pathological feature of SMA is a specific loss of motor neurons in the ventral horn of the spinal cord [125]. For this reason, SMA has traditionally been classified as a pure disease of lower motor neurons caused by reduced levels of SMN, which remain the main target for a therapeutic strategy. However, numerous recent studies challenge this hypothesis, supporting the idea that SMA may actually be a multi-systemic disorder [126][127]. Although the majority of evidences are given by experiments in SMA animal models (less human tissues are available for research purposes), several studies showed an involvement of tissues far from the neuronal population, such as heart and liver [128][129][130][131][132][133]. These studies displayed that a splicing *SMN2* correction in these tissues positively restores the animal survival, whereas the effect limited to the brain and spinal cord does not improve the animals' destiny [126]. Therefore, whether SMA is the result of low SMN levels in multi-tissues or a consequence of the motor neurons deficit due to low SMN levels, it is still unclear. The loss of motor neurons, indeed, affects the physiological development of neuromuscular junctions (NMJ), those elements necessary for a correct communication between the central nervous system (CNS) and peripheral tissues. Thus, the impairment of this network might negatively influence the homeostasis of other non-neuronal tissues, exacerbating the disease [134].

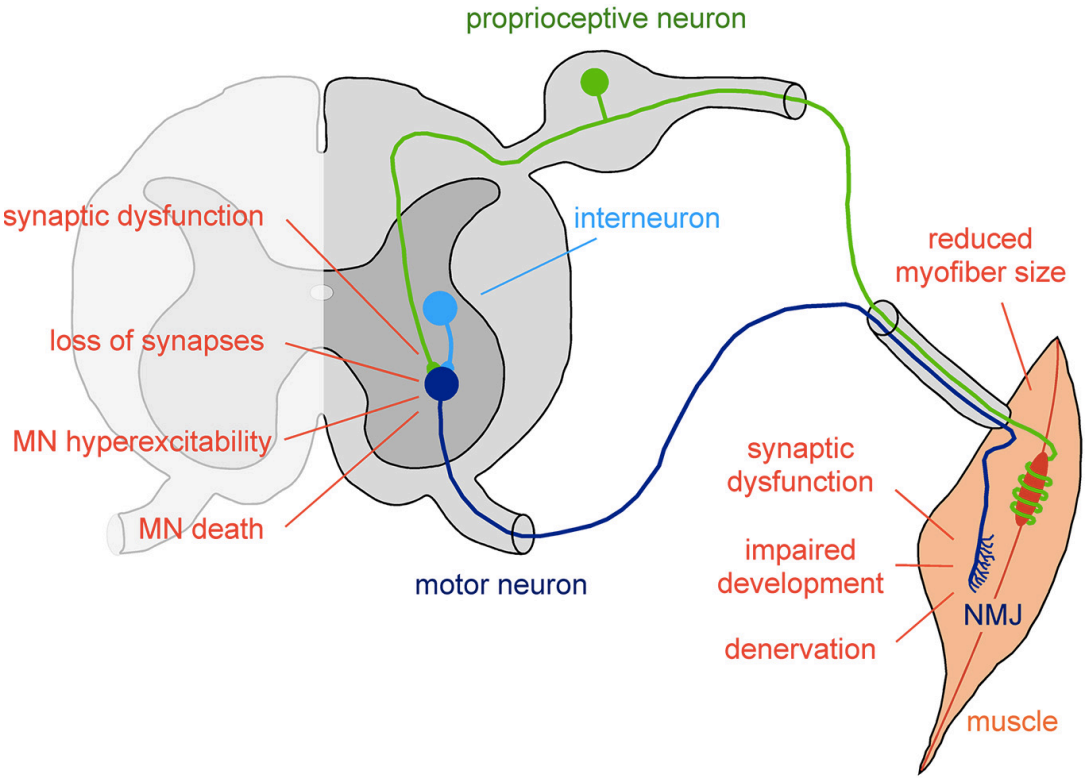

Figure 1.19 Schematic representation of the key morphological and functional abnormalities induced by SMN deficiency in the motor system of SMA mouse models.

Multiple aspects of the motor system are disrupted in SMA. For simplicity, only the excitatory premotor neurons of the motor circuit affected by the disease are depicted. Motor neurons (dark blue) in the ventral horn of the spinal cord receive excitatory synaptic inputs from proprioceptive neurons residing in the dorsal root ganglion (green) and local interneurons (light blue). Upon sufficient excitatory drive to generate action potentials, motor neurons innervating skeletal muscle induce muscle contraction through cholinergic neurotransmission at the NMJ. The specific deficits within the SMA motor system are indicated and are described in detail in the text.

The mechanism through low levels of SMN lead to the death of spinal motor neurons is still unknown. Several theories have been proposed to explain the specific role of SMN in the survival of MNs: i) SMN affects splicing of essential transcripts for the motor neurons integrity and differentiation [135][136][137]; ii) MNs require a higher amount of SMN than other tissues; iii) SMN fulfills a specific role in axonal transport and neuronal development that is independent of its role in snRNP biogenesis [138][139][140][141]. Nonetheless, it remains unclear which specific molecular pathway involved in SMA pathogenesis is particularly affected by low levels of SMN. Because the disease is not restricted to motor neurons, SMA is likely caused by disruption of multiple pathways across the entire motor circuit and other tissues.

To date, there are no effective treatments for SMA and patients' medications are limited solely on the amelioration of symptomatology. Thus, taking advantage of the current knowledge, the most promising therapeutic strategy consists of the restoration of SMN expression [142]. This result can be achieved in several ways, including enhancing *SMN2* promoter activation [143][144][145], stimulating exon 7 inclusion [146][147] [148][149][150][2] and introducing an exogenous *SMN1* cDNA [151][152][153][154]. Basic research and preclinical studies in animal models have displayed the efficacy of these approaches, leading to several ongoing clinical trials [155][142].

The c.840C>T substitution is a synonymous mutation that affects the processing of *SMN2* pre-mRNA. Since the coding sequence does not change, one potential strategy consists on correcting the splicing defect, promoting somehow the inclusion of exon 7. Several approaches have been developed so far, one of those is represented by antisense oligonucleotides (ASO) that bind to the inhibitory sequences, blocking the binding of negative factors [146][148][147]. A number of different ASO chemistries, delivery methods and doses have been tested, and the best is currently under investigation with a phase III clinical study [156]. This strategy targets the intronic splicing silencer N1, blocking the binding of hnRNP-A1 and promoting a strong splicing correction in vivo.

Experiments in the animal model, indeed, displayed a great impact on the animal survival, extending the lifespan beyond 250 days in comparison to the limited 10 days of untreated mice [126]. Although the influence on total transcriptome hasn't been evaluated yet, the ASO treatment has shown good safety and tolerability profiles in open-label phase 2 clinical trial after intratechal delivery in type I and II SMA infants. New updates are waited by next year, but to date this strategy remains the best opportunity to actually treat SMA.

Another advanced technology is represented by the delivery of *SMN1* through the self-complementary adeno-associated 9 virus (scAAV9), referred as "chariSMA" [157]. This strategy doesn't aim at correcting splicing but takes advantage of the relative small size of *SMN1* cDNA to deliver the entire correct coding sequence. Both systemic and intracerebroventricular injections of scAAV9-SMN showed efficient transduction of motor neurons in both mice and non-human primates (NHP), correcting SMA phenotype and improving the animals' survival [158][159]. Evaluation of safety and efficacy is currently conducted in a phase I clinical trial, representing the first gene therapy clinical trial.

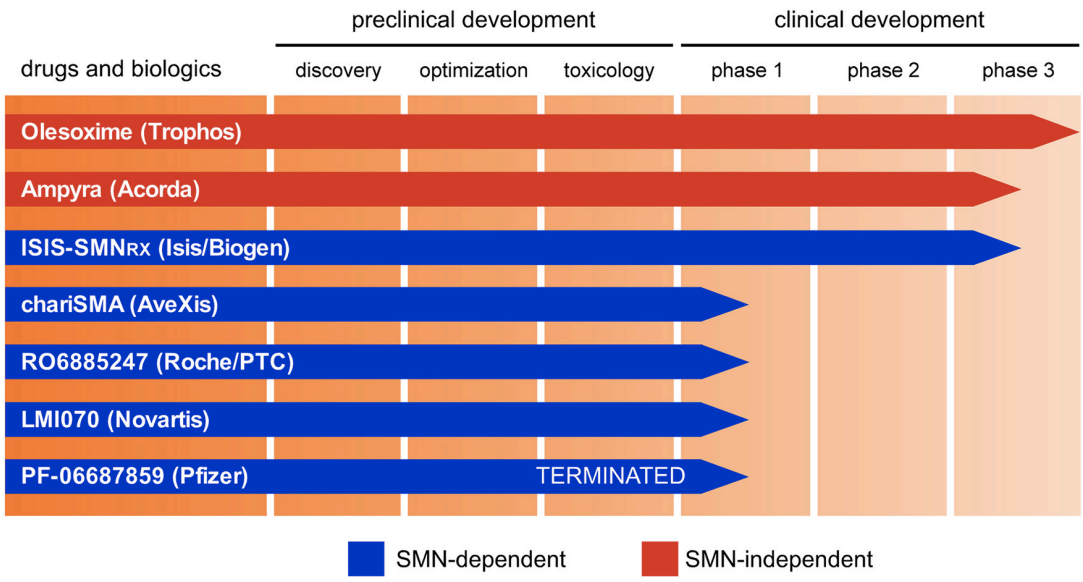

Figure 1.20 Candidate SMA therapeutics and their progress through the clinical development pipeline.

The chart summarizes the current status of the most advanced programs in SMA therapeutic development based on publicly available information. Small molecules and biologics listed with blue bars aim to increase the functional levels of SMN, and those denoted with red bars act by improving motor system function through SMN-independent mechanisms.

1.9 ExSpeU1s as novel therapeutic strategy to rescue exon skipping defects

Exon skipping is one of the major splicing defects that impairs the pre-mRNA processing, leading to a pathological phenotype [39][48]. This aberrant splicing is caused by mutations that affect the exon definition by disrupting the physiological communication between the spliceosome and the pre-mRNA. In general, mutations can i) affect the donor site, reducing the complementarity between the 5' splice site and the U1 snRNA, ii) affect an important splicing regulatory element, modifying the exon recognition, iii) affect a *trans*-acting element, altering its abundance and compromising its activity [50].

The exon definition is a fundamental step of splicing that is initiated by the U1 snRNP, which binds to the 5' splice site recruiting other splicing factors necessary for the pre-mRNA processing [24]. This important molecule communicate with the donor site via a physical Watson-Crick interaction between its 5' binding tail and nine nucleotides of the 5' splice site. These interactions are not always perfect and, usually, the presence of some mismatches are tolerated without compromising the pre-mRNA processing. However, both intronic and exonic mutations can affect this interaction, causing exon skipping and leading to a pathological condition.

An innovative therapeutic approach has been proposed by our laboratory to correct the exon skipping defects, developing modified U1 snRNAs that specifically bind to intronic sequences downstream the effected exons, the Exon-Specific U1 snRNAs (ExSpeU1s) [1][160]. These molecules consist of modified U1 snRNAs' tails in order to recognize the less-conserved intronic sequences in proximity of altered exons. This property significantly increases the specificity of ExSpeU1s, targeting the aberrant exons and consistently reducing the potential off-targets.

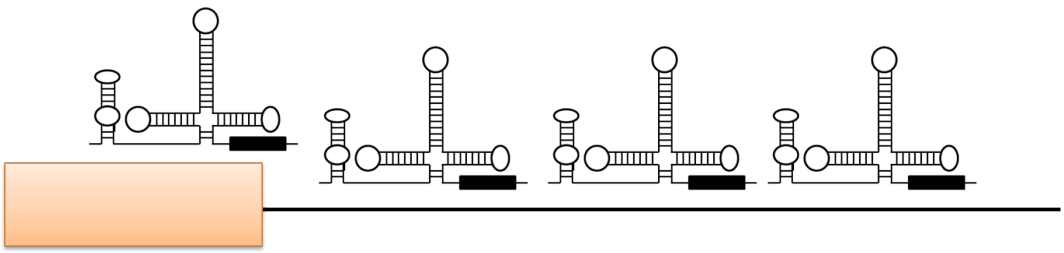

Figure 1.21 Therapeutic approach with ExSpeU1.

Schematic representation of ExSpeU1s binding to downstream intronic regions. Pink box represent the exon, while black line represent the flanking intron. At the top of sequence are reported four U1-snRNAs. The

secondary structure of U1-snRNA presents a small black box, indicating the complementary tail responsible of Watson-Crick interactions with the sequence.

The ExSpeU1s' activity has been showed both *in-vitro* and *in-vivo* for Haemophilia B (F9), Spinal Muscular Atrophy (SMA), Cystic Fibrosis (CF) and Netherton syndrome (NS). In particular, the splicing correction mediated by ExSpeU1s has been demonstrated for i) mutations that affect the donor sites (*F9* exon 5 and *CFTR* exon 12), ii) mutations at the polypyrimidine tract (*F9* exon 5) and iii) mutations that impair splicing regulatory elements (*CFTR* exon 12, *SMN2* exon 7, *SPINK5* exon 11) [1][161][150][162][2]. The experiments conducted in these pathological contexts demonstrated the efficacy of ExSpeU1s at correcting the aberrant exon skipping events, providing a therapeutic alternative for these disease.

One of the most important aspects of ExSpeU1s is the binding to intronic sequences that significantly reduces the number of off-targets. Indeed, most of the splicing-switching molecules and general drugs have a wide-spread effect with a significant number of off-targets which, in some cases, might worsen the pathological condition. On the contrary, ExSpeU1s are thought to specifically restore the aberrant splicing, correcting the disease's phenotype and limiting the number of side-effects. Recently, it has been demonstrated that ExSpeU1s have a minimal genome-wide effect in a mouse model constitutively expressing one of these molecules for the splicing correction of the aberrant *SMN2*, providing evidence of this important feature [2]. In addition, the specificity of ExSpeU1s can be implemented by increasing the 5' binding tail, in order to increase the Waston-Crick interaction with the intronic sequences, and, therefore, significantly reduce the probability to recognize improper regions.

Furthermore, in comparison with classical gene therapies, the ExSpeU1s' strategy provides a additional advantages. The correction of splicing defects, in fact, allow the maintenance of a physiological regulation of gene expression in its chromosomal context through its endogenous regulatory factors. This approach could be helpful in mutations that affects several proteins that requires an expression in a specific stage of differentiation. Moreover, the short length of the ExSpeU1s cassette (about 500 bp) can also be useful in gene therapy of splicing mutations in large genes, such as *IKBKAP* and *F8*, whose full-length transcripts can represent a limiting step for their insertion in viral vectors such as AAV. Another advantage regard dominant-negative mutations, where the replacement therapy is not possible. Indeed, ExSpeU1s can restore the negative effect, correcting splicing defects and reducing the amount of the mutated toxic protein.

Therefore, we support the ExSpeU1 as a therapeutic strategy aimed at correcting several splicing defects caused by different type of mutations, recovering the biosynthesis and the function of specific proteins, and reducing the number of off-targets.

Chapter 2

AIM OF THE THESIS

A goal of human genetics studies is to determine the precise mechanisms by which genetic variation produces phenotypic differences that affect human health. Growing evidences are supporting the idea that genetic variants play a key role in RNA processing, altering the information in *cis* and leading to pathological conditions [48]. Furthermore, recent studies showed that missense mutations, that primarily affect the protein structure, can affect the pre-mRNA processing as well [54]. Thus, understanding the molecular mechanisms underlying genetic diseases can help to develop new tailored therapeutic strategies, such as the ExSpeU1s. Our laboratory, indeed, recently demonstrated the potential of these modified U1 snRNAs as molecular system aimed at correcting splicing defects [1][150][162]. These molecules are designed to specifically target the not conserved intronic downstream regions nearby affected exons, promoting their recognition and, thus, improving the aberrant processing.

In this thesis, I'm going to show how this useful and innovative strategy can be applied from the basis, identifying mutations that influence splicing and creating modified U1 snRNAs that correct these defects, to an *ex-vivo* correction, using lentiviral particles expressing the most active ExSpeU1, and finally, to the application *in-vivo* through AAV9 delivery.

Therefore, the aim of this thesis consists of:

- to explore the effect of missense mutations on pre-mRNA processing and protein function using as model the *FVIII* gene;
- to develop novel therapeutic strategies based on modified U1 snRNAs to rescue aberrant splicing *in-vitro* and *ex-vivo*;
- to evaluate the *in-vivo* efficacy of ExSpeU1s by AAV9 delivery.

Chapter 3

MATERIAL AND METHODS

3.1 Chemical reagents

General chemical were purchased from Sigma Chemical Co., Merck, Gibco BRL, Boehringer Mannheim, Invitrogen, Fluka and Quiagen.

3.2 Standard solutions

All solutions are identified in the text except for the following:

- 1X TE: 10 mM Tris-HCl (pH 7.4), 1mM EDTA (pH 7.4)
- 1X PBS: 137 mM NaCl, 2.7mM KCl, 10mM Na_2HPO_4, 1.8mM KH_2PO_4, pH 7.4
- 10X TBE: 108g/l Tris-HCl, 55g/l Boric acid, 9.5g/l EDTA
- 6X DNA sample buffer: 0.25 % w/v bromophenol blue, 0.25% w/v xylene cyanol FF, 30% v/v glycerol in H_2O.

3.3 Synthetic oligonucleotides

Synthetic oligonucleotides were purchased from Integrated DNA Technologies (IDT).

3.4 Bacterial culture

The *E. coli* K_{12} strain DH5α was transformed with the plasmid described in this study and used for their amplification. Plasmid were maintained in the short term as single colonies on agar plates at 4°C. Bacteria were amplified by an overnight incubation in Luria-Bertani medium (per litre: 10g Difco Bactotryptone, 5g Oxoid yeast extract, 10g NaCl, pH 7.5). Bacterial growth media were sterilized before use by autoclaving. Then ampicillin (Sigma-Aldrich) was added to the media at a final concentration of 200µg/ml.

3.5 Preparation of bacterial competent cells

Bacterial competent cells were prepared following the method described by Chung and Niemela. *E. coli* strains were grown overnight in 10 ml of LB at 37°C. The following day, 150ml of fresh LB were added and the cells were grown in the shaker at room temperature until the OD_{600} was 0.3-0.4. Then the cells were placed in ice and centrifuged at 4°C and 1000g for 10 minutes. The pellet was resuspended in 1/10ml of the initial volume of cold 1X TSS solution (10% w/v PEG 4000, 5% v/v DMSO, 35mM $MgCl_2$, pH 6.5 in LB medium). The cells were aliquoted, rapidly frozen in liquid nitrogen and stored at -80°C. Competence was determined by transformation with 0.1ng of pUC19 control DNA plasmid and was deemed satisfactory if this procedure resulted in more than 100 colonies.

3.6 Transformation of bacteria

Transformation of ligation reactions were performed using half of the initial reaction volume (10µl). Transformation of clone was carried out using 1ng of the DNA plasmid. The DNA was incubated with 60µl of competent cells for 30 minutes on ice, followed by a heat shock at 42°C for 45 seconds and finally the cells were placed again on ice for 10

minutes and then spread onto agarose plates containing the appropriate antibiotic concentration (100μg/ml of ampicillin).
When DNA inserts were cloned into β-galactosidase-based plasmid, 30 μl of X-Gal (4% v/v in dimethylformamide) were spread onto the surface of the agarose before plating to facilitate screening of positive clones (white colonies) through identification of β-galactosidase activity (blue colonies).

3.7 DNA preparation

3.7.1 Small scale preparation of DNA plasmid from bacterial cultures

Single bacterial colony was picked and transferred into 6ml of LB medium containing the ampicillin in a loosely capped 15ml tube. The culture was incubated overnight at 37°C in a shaking incubator. The Wizard Plus SV Minipreps DNA Purification System (Promega) was used according to the manufacturer's instructions in order to obtain small amounts of pure plasmidic DNA. The final pellet was resuspended in 100μl of Nuclease-Free water. The DNA was stored at -20°C. Routinely 3μl of such DNA preparation were taken for the restriction enzyme digestion and 20μl were taken for sequence analysis (Macrogen).

3.7.2 Large scale preparation of DNA plasmid from bacterial cultures

For large-scale preparation (MIDIprep and MAXIprep) of DNA plasmid was used the JETSTAR Plasmid Purification Kit (Genomed) according to the manufacturer's instructions. In order to get a good amount of plasmid, we used a 50ml and 500ml of overnight bacterial culture using LB medium, respectively.

3.8 Enzymatic modification of DNA

3.8.1 Restriction enzymes

Restriction enzymes were from New England Biolabs Inc. (NEB). All buffers were also supplied by the same company and were used according with the manufacturer's instructions. In alternative, we also used different concentrations of 10X OPA buffer (100mM Tris-acetate (pH 7.5), 100mM magnesium acetate, 500mM potassium acetate).
For analytical digests 200-300ng of DNA were digested in a volume of 20µl containing the appropriate units of the restriction enzyme per µg DNA. The digest was incubated 2-3 hours at the optimal temperature required by the enzyme used.
Preparative digestions of vectors and inserts were made of 3-5µg DNA using the appropriate conditions needed by the restriction enzyme in 50µl reaction volume.

3.8.2 DNA Polymerase I, Large (Klenow) Fragment T4 Polynucleotide Kinase

These enzymes, provided from New England Biolabs Inc., were used to treat PCR products for blunt-end ligation during construction of recombinant plasmids.
The large fragment of DNA Polymerase I (Klenow) is a proteolytic product of E. Coli DNA Pol I, which retains polymerization and 3'→5' exonuclease activity, but has lost 5'→3' exonuclease activity. This was useful for digesting a specific residues added by *Taq* DNA Polymerase at the 3' terminus to create a compatible end for digestion. Briefly, the DNA was dissolved in 1X NEBuffer 2 and supplemented with 33µM dTNPs. Then, 1 unit of Klenow per µg was added and the mixture (final volume 20µl) was incubated for 10 minutes at RT. The reaction was inactivated by heating at 70°C for 20 minutes.
T4 Polynucleotide Kinase catalyzes the transfer and exchange of phospate from ATP to the 5'-hydroxyl terminus of double- and single-stranded DNA and RNA. It was useful for the addition of 5'-phosphate to PCR products to allow subsequent ligation. The proper units of Kinase, 1X of its reaction buffer (70mM Tris-HCl, 10mM $MgCl_2$, 5mM Dithiothreitol, pH 7.6) and ATP (10mM) were added to the DNA and incubated at 37°C for 30 minutes. The enzyme was inactivated by incubation at 65°C for 20 minutes.

3.8.3 T4 DNA ligase

T4 DNA ligase catalyzes the joining of two strands of DNA between the 5'-phosphate and the 3'-hydroxyl groups of adjacent nucleotides in either a cohesive-ended or blunt-ended configuration. 20ng of linearized vector were ligated with a 5-10 fold molar excess of insert in a total volume of 20µl containing 1X ligase buffer and 1 unit of enzyme. Reaction was carried out at RT for 3 hours.

3.8.4 Calf Intestinal Alkaline-Phosphatase (CIP)

Calf intestinal phosphatase (CIP), provided from New England Biolabs Inc., catalyzes the removal of 5' phosphate groups from DNA and RNA. Since CIP-treated fragments lack the 5' phosphoryl termini required by ligases, they cannot self-ligate. This property can be used to decrease the vector background in cloning strategies. The standard reaction was carried out in a final volume of 50µl using 0.5U of enzyme per 1µg DNA at 37°C for 30 minutes. The enzyme was then inactivated by incubation at 85°C for 15 minutes.

3.9 Agarose gel electrophoresis of nucleic acids

DNA sample were size fractionated by electrophoresis in agarose gels ranging in concentration from 0.8% w/v (large fragments) to 2% w/v (small fragments). The gels contained ethidium bromide (0.5µg/ml) and 1X TBE solution. Horizontal gels were used for fast analysis of DNA restriction enzyme digests, estimation of DNA concentration, or DNA fragment separation prior to elution from the gel.
A fast analysis of RNA samples was obtained by running samples on 0.8% agarose gels.

The gels were electrophoresed at 50-90mA in 1X TBE running buffer for a time depending on the expected fragment length and gel concentration. Sample was visualized by UV transillumination and the result recorded by digital photography.

3.10 Elution and purification of DNA fragments from agarose gels

The following protocol was applied for purification of both vectors and inserts of DNA for cloning strategies. The DNA samples were electrophoresed onto an agarose gel as previously described. The DNA was visualized with UV light and the DNA fragments of interest was excised from the gel and the QIAquick Gel Extraction Kit (Qiagen) was used for extraction according to manufacturer's instruction. 50µl of DNA was obtained: the amount of recovered DNA was estimated by UV fluorescence of intercalated ethidium bromide in agarose gel electrophoresis.

3.11 Amplification of selected DNA fragments

The polymerase chain reaction (PCR) was performed using plasmid DNA as template and following the basic protocol of Roche or NEB Taq DNA polymerase. The volume of the reaction was 50µl and comprised: 1X Taq buffer, dNTPs mix (100µM each), oligonucleotide primers (100nM each), Taq DNA polymerase (2.5U) and 0.1ng of plasmid DNA.

The synthetic DNA oligonucleotides used for PCR amplification were purchased from Sigma-Aldrich and from Integrated DNA Technologies.

The standard amplification conditions were the following: 94°C for 5' (initial denaturation), 94°C for 30'' (denaturation), 56°C for 30'' (annealing), 72°C for 30'' (extension) and 72°C for 10' (final extension) for 30 cycles. PCRs were optimized to be in the exponential phase of amplification and products were fractionated on agarose gels. The PCR reactions were performed on a Gene Amp PCR System (Applied Biosystem).

3.12 Sequence analysis for cloning purpose

Sequence analysis of plasmid DNA were performed in Macrogen Europe (Amsterdam, Netherlands), using 20µl of DNA samples (100ng/µl) in 1.5ml tubes.
The result of sequencing were analyzed using the FinchTV program and SerialCloner 2.5.

3.13 Hybrid minigene constructs

Transient transfection of hybrid minigenes is a commonly used *in vitro* technique to identify the different features of exon regulation during the splicing process. Hybrid minigenes are useful construct tools to study *cis*- and *trans*-acting elements that influence splicing process, to understand the cell-specific splicing pattern, to identify exonic and intronic elements that enhance or silence splicing and to determine whether a specific mutation can compromise the splicing and to establish the role of the splice sites in the exon recognition.
A minigene, as its name indicates, is a simplified version of a gene and usually contains a genomic region from the gene of interest and the part of interest with its flanking genomic sequences. The genomic segment is generated by PCR amplification directly from target DNA as template and the oligonucleotides used has to contain the restriction enzyme sites at their ends that match restriction sites in the recipient plasmid.
This system, after transient transfection and RNA analysis, allows us to study the splicing outcome.

3.13.1 pTB-F8 minigenes

The pTB-Nde plasmid is a hybrid minigene vector that contains the SV40 promoter, the α-globin reporter gene and a polyadenilation signal. The reporter gene is composed of the exons 1, 2 and 3 of the α-globin gene, in which the exon 3 is divided by the insertion of the

exon 7 and 9 of the fibronectin gene, interposed by an intronic sequence carrying a NdeI restriction site. This NdeI site was used to clone the sequence of interest to validate in the splicing assay. In the context of the F8 minigene, I inserted the genomic region spanning from intron 18 to intron 19 of the *F8* gene. The FVIII cassette, amplified by PCR, consists of the 117 bp exon 19 surrounded by the last part of intron 18 (343 bp) and the 5' part of the intron 19 (332 bp). The wild type sequence was then confirmed by direct sequencing and, successively, used to create the FVIII variants by site-specific mutagenesis (XL-quick change mutagenesis, Agilent). The list of primers used to created the F8 minigenes is reported below:

oligo name	**sequence 5' -> 3'**
F8 int18 NdeI DIR	TACATATGgagtccacatctggccaatg
F8 int19 NdeI REV	TACATATGtctaagttatctggtaact
5ss HC F8ex19 DIR	TCTGGTGTACAGCAcaggtaagtAGCAATGTGGGCA
5ss HC F8ex19 REV	TGCCCACATTGCTacttacctgTGCTGTACACCAGA
6037G>A dir	TTACCATCCAAAGCTAGAATTTGGCGGGTGG
6037G>A rev	CCACCCGCCAAATTCTAGCTTTGGATGGTAA
6045G>C dir	CAAAGCTGGAATTTGCCGGGTGGAATGCCTT
6045G>C rev	AAGGCATTCCACCCGGCAAATTCCAGCTTTG
6046C>T dir	CAAAGCTGGAATTTGGtGGGTGGAATGCCTTAT
6046C>T rev	ATAAGGCATTCCACCCaCCAAATTCCAGCTTTG
6047G>C dir	AAGCTGGAATTTGGCCGGTGGAATGCCTTAT
6047G>C rev	ATAAGGCATTCCACCGGCCAAATTCCAGCTT
6049G>A dir	GCTGGAATTTGGCGGATGGAATGCCTTATTG
6049G>A rev	CAATAAGGCATTCCATCCGCCAAATTCCAGC
6053A>G dir	GAATTTGGCGGGTGGGATGCCTTATTGGCGA
6053A>G rev	TCGCCAATAAGGCATCCCACCCGCCAAATTC
6104T>C dir	GCACACTTTTTCTGGCGTACAGCAATAGTGA
6104T>C rev	TCACTATTGCTGTACGCCAGAAAAAGTGTGC
6113A>G dir	TTCTGGTGTACAGCAGTAGTGAGTAGCAATG
6113A>G rev	CATTGCTACTCACTACTGCTGTACACCAGAA

3.13.2 pTB-IKBKAP minigenes

The above described pTB-Nde vector was used as backbone to insert the genomic IKBKAP region spanning from intron 18 to intron 22 in the NdeI restriction site. The wild type sequence was confirmed by direct sequencing and, successively, used to insert the intronic mutation in position +6 of the intron 20. The list of primers used to create these minigenes is reported below.

oligo name	sequence 5' -> 3'
IKAP IVS18 NdeI dir	aatcatatggccaacttattttctttgcttcc
IKAP IVS22 NdeI rev	aat catatgatatataggttgcttactggac
IKAP IVS20+6T>C dir	TGGACAAGTAAGCGCCATTGTACTGTTTGC
IKAP IVS20+6T>C rev	GCAAACAGTACAATGGCGCTTACTTGTCCA

3.13.3 pFLARE-IKBKAP minigenes

pFLARE is a versatile Two-Colour reporter system suitable for high throughput screening of alternative splicing with:

- a broad dynamic range, allowing measurement of small changes in exon inclusion;
- a reporter system that can distinguish changes in alternative splicing patterns from changes in transcription and translation and from general inhibition of splicing;
- a system that can accommodate a variety of test exon from different genes.

This vector consist of ORFs for destabilized GFP and RFP expressed from a single promoter as a bicistronic transcript. The start codon of the GFP ORF is split by an alternative exon cassette with its flanking introns. If the alternative exons is included, the start codon of the GFP ORF is formed and GFP is expressed from the mature transcript. In this case, the translation of RFP is repressed because eukaryotic ribosomes initiate poorly at downstream ORFs. However, when the alternative exon is skipped in the mRNA, the GFP ORF loses its start codon and is not translated. The initiating ribosomes will scan for the first available ATG codon of the downstream RFP ORF. Thus, two mRNAs are produced from this minigene, depending on the splicing of the alternative cassette. These mRNA express GFP when the exon is included and RFP

when the exon is skipped. Therefore the GFP/RFP ratio will reflect the level of exon inclusion. The multi cloning site to insert the sequence of interest is located upstream the coding sequence of the GFP. The genomic *IKBKAP* region from intron 19 to intron 20 was inserted within this restriction site and confirmed by direct sequencing. The wild type sequence was then mutagenized by site-specific mutagenesis, introducing the Familial dysautonomia intronic mutation. The set of primers used to create the pFLARE-IKBKAP minigenes are reported below.

oligo name	sequence 5' -> 3'
IKAP IVS19 EcoRI-NdeI dir	aatgaattccatatgtgaaagtcaagataaatatagag
IKAP IVS20 BamHI-NdeI rev	aaaggatcccatatgtcacgattctttctgctaggaa
IKAP IVS20+6T>C dir	TGGACAAGTAAGCGCCATTGTACTGTTTGC
IKAP IVS20+6T>C rev	GCAAACAGTACAATGGCGCTTACTTGTCCA

3.14 recombinant coFVIII variants

pLNT/SFFV-SQ FVIII (co) has been previously described by Ward et al. [163], which contains a codon optimized FVIII cDNA sequence. In order to do not introduce any aspecific mutation, I subcloned a 1796 bp region from the original backbone gently provided by Prof. John McVey containing the exon 19 into the pGEM-T easy vector (Promega, TA cloning). This cassette has been PCR amplified using 10515 and 12278 primers. The obtained pGEM-FVIII wt has been mutagenized to produce the FVIII missense variants using the XL mutagenesis kit (Agilent). The FVIII delta19 was created through overlapping PCR using the previous primers with the coFVIII delta19 primers (see table below). Successively, all the sequences have been digested with MluI and SbfI restriction sites and ligated into the opened pLNT/SFFV-SQ FVIII (co) plasmid. Each variant has been confirmed by sequencing analysis. The list of primers used to create the rFVIII variants is reported below.

oligo name	sequence 5' -> 3'
rFVIII delta 19 dir	TGTACCCCGAGTGCCAGACCCCACTGGGCATG

rFVIII delta 19 rev	GGTCTGGCACTCGGGGTACAGGTTGTACAGGG
rFVIII 6037G>A dir	CTGCCCAGCAAGGCCCGCATCTGGCGGGTGG
rFVIII 6037G>A rev	CCACCCGCCAGATGCGGGCCTTGCTGGGCAG
rFVIII 6046C>T dir	AAGGCCGGCATCTGGTGGGTGGAGTGTCTGA
rFVIII 6046C>T rev	TCAGACACTCCACCCACCAGATGCCGGCCTT
rFVIII 6053A>G dir	GCATCTGGCGGGTGGGGTGTCTGATCGGCGA
rFVIII 6053A>G rev	TCGCCGATCAGACACCCCACCCGCCAGATGC
rFVIII 6113A>G dir	TTTCTGGTGTACAGCAGCAAGTGCCAGACCCC
rFVIII 6113A>G rev	GGGGTCTGGCACTTGCTGCTGTACACCAGAAA
rFVIII 10515 dir	CCATCGAACCCCGGAGCTTC
rFVIII 12278 rev	GACCTGAGGCCGCCAGGC

3.15 Expression vector for generation of U1-snRNAs

The vector used for the production of U1-snRNAs is the pSP64, which is a standard cloning vector. The wild-type U1-snRNA gene was cloned in *BamHI* restriction site and the region between *BglII* and *BclI* sites encoding for the 5'-tail complementary to 5'-ss was replaced with specific annealed DNA oligonucleotides (Fig. 3.1). The sequences of each oligo used for creation of modified-U1 is reported below.

oligo name	sequence 5' -> 3'
U1 F8ex19 HC dir	gatctcataACTCACTATgcaggggagataccat
U1 F8ex19 HC rev	gatcatggtatctcccctgcATAGTGAGTtatga
U1 IKAP sh2 dir	gatctcataTGGCGCTTAgcaggggagataccat
U1 IKAP sh2 rev	gatcatggtatctcccctgcTAAGCGCCAtatga
U1 IKAP sh4 dir	gatctcataAATGGCGCTgcaggggagataccat
U1 IKAP sh4 rev	gatcatggtatctcccctgcAGCGCCATTtatga
U1 IKAP sh5 dir	gatctcataAGTACAATGGCGCgcaggggagataccat
U1 IKAP sh5 rev	gatcatggtatctcccctgcGCGCCATTGTACTtatga
U1 IKAP sh10 dir	gatctcataGCAAACAGTACAATgcaggggagataccat
U1 IKAP sh10 rev	gatcatggtatctcccctgcATTGTACTGTTTGCtatga
U1 IKAP sh12 dir	gatctcataTCGCAAACAGTACAgcaggggagataccat
U1 IKAP sh12 rev	gatcatggtatctcccctgcTGTACTGTTTGCGAtatga
U1 IKAP sh15 dir	gatctcataGCAAACAGTgcaggggagataccat
U1 IKAP sh15 rev	gatcatggtatctcccctgcACTGTTTGCtatga
U1 IKAP sh19 dir	gatctcataCTAGTCGCAAACgcaggggagataccat
U1 IKAP sh19 rev	gatcatggtatctcccctgcGTTTGCGACTAGtatga
U1 IKAP sh33 dir	gatctcataATCACAAGCgcaggggagataccat
U1 IKAP sh33 rev	gatcatggtatctcccctgcGCTTGTGATtatga

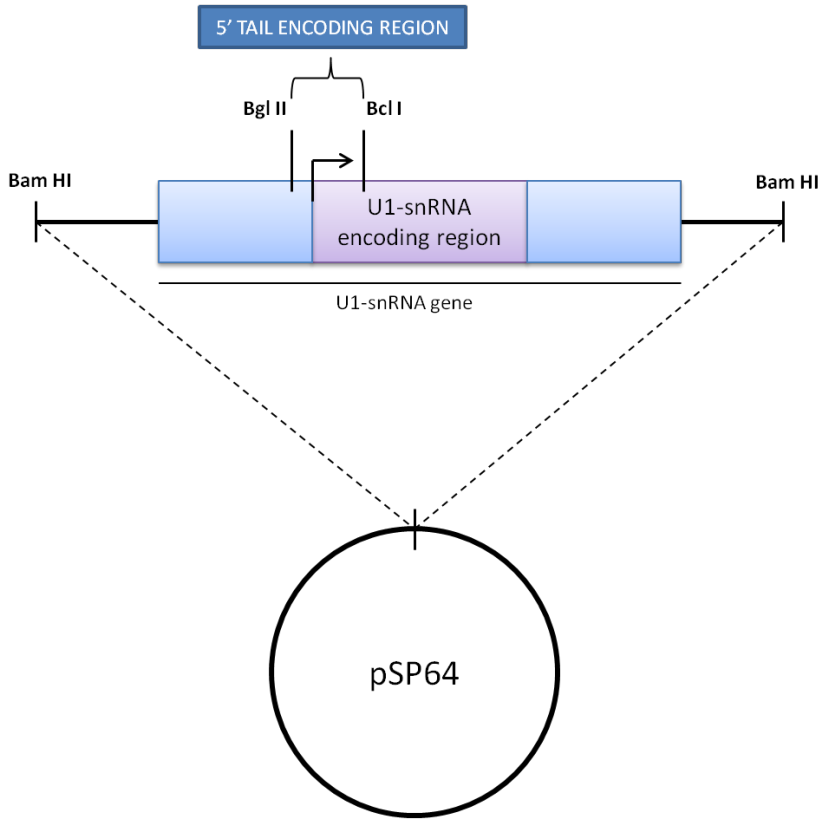

Figure 3.1 Schematic representation of cloning strategy for creation of modified-U1-snRNAs.
The wild-type U1-snRNA gene was cloned in *BamHI* restriction site located in the multiple cloning site of pSP64 vector. The region between *BglII* and *BclI* sites encoding for the 5'-tail of the U1 was replaced by specific annealed DNA oligonucleotides for create engineered U1-snRNAs able to recognize specific target sequences with their modified 5'-tails.

3.16 Expression vector for generation of U7smOPT

The original U7 SmOPT vector contains the murine U7 gene as a 570 bp *HaeIII* fragment inserted into the unique *SmaI* site of the pSP64 polylinker. The wild-type U7 Sm binding site has been converted to the Sm OPT sequence and a single *StuI* and *HpaI* sites have been inserted upstream and downstream of the U7 snRNA sequence. The U7 constructs (F8ex19 and IKBKAP) were generated by PCR amplification using a mutagenic primer in the appropriate region of U7 gene and a common primer in the Sp6 promoter region of the plasmid. The list of primers used to create these molecules is reported below.

oligo name	sequence 5' -> 3'
SP6 rev	ATTTAGGTGACACTATAGAA
U7 F8ex19 dir	ACAGAGGCCTTTCCGCAgcattccacccaccaaattccagcAATTTTTGGAG
U7 IKAP 15 dir	ACAGAGGCCTTTCCGCAGCAAACAGTAATTTTTGGAG
U7 IKAP 10 dir	ACAGAGGCCTTTCCGCAGCAAACAGTACAATAATTTTTGGAG

The PCR product was purified by electrophoresis on agarose gel, excision of the band of interest and elution as described previously. It was then digested with *HindIII* and *StuI*, re-purified and ligated into the *HindIII/StuI* opened pSP64-U7 Sm OPT vector. Plasmids from ampicillin-resistant colonies were then screened by restriction and sequence analysis (Fig. 3.2).

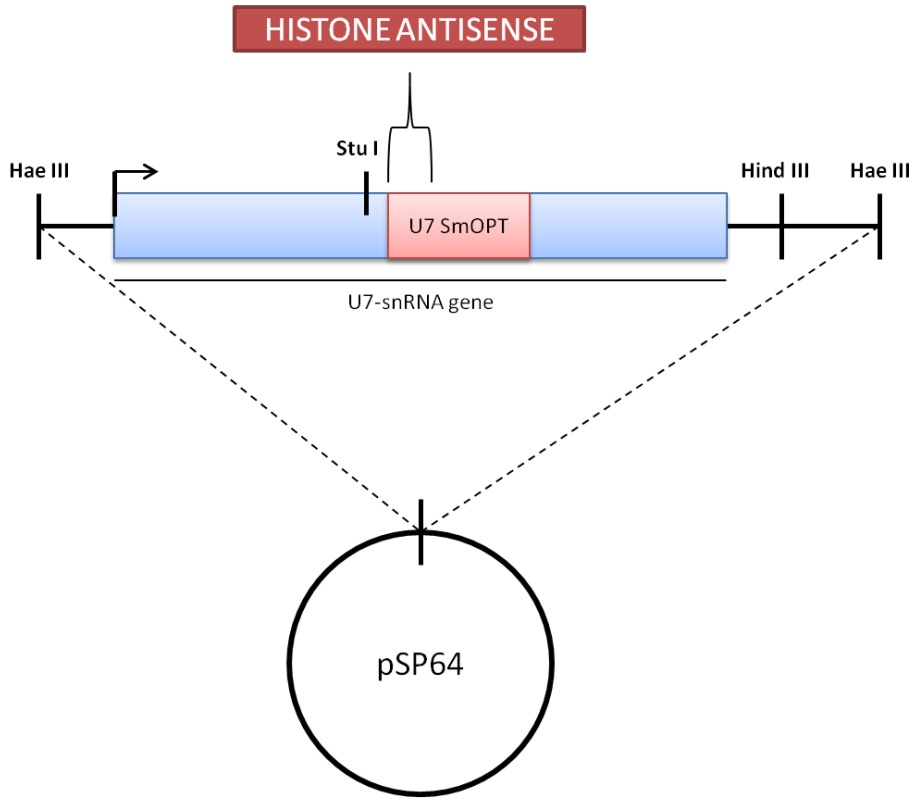

Figure 3.2 Schematic representation of cloning strategy for creation of modified-U7-snRNAs.
The murine U7 snRNA gene was cloned in *SmaI* restriction site of the pSP64 polylinker. The modified-U7-snRNAs were generated by PCR amplification using mutagenic primers. The PCR products were digested and then cloned into the *HindIII/StuI* opened pSP64-U7 Sm OPT vector.

3.17 Cell culture

3.17.1 Hek293, HepG2 and SH-SY5Y culture

The eukaryotic cell line used for transfection and co-transfection experiments of hybrid minigenes were Human hepatocyte carcinoma cell line (HepG2), for the F8 minigenes, and the Human embryonic kidney (Hek293) and the neuronal SH-SY5Y, for the IKBKAP minigenes.

Cells were grown in Dulbecco's modified eagle medium (with glutamine, sodium pyruvate, pyriodoxine and 4.5g/l glucose) supplemented with 10% fetal calf serum (EuroClone) and antibiotic antimycotic (Sigma) according to the manufacturer's instruction. A standard 100mm dish containing a confluent monolayer of cells was washed twice with 1X PBD solution, in order to remove all the medium residues as well as the dead cells, treated with 1ml Trypsin (PBS containing 0.045mM EDTA and 0.1% trypsin) and incubated at 37°C for 1 minutes or until cells were completely detached. After adding 5ml of medium, to block trypsin activity, cells were precipitated by centrifugation (1000 rpm for 5 minutes) and resuspended in pre-warmed medium. A subcultivation ratio of 1:6 to 1:8 was used for these cells. 1ml of this cells dilution was added to 9ml of fresh medium and plated in a new 100mm dish.

3.17.2 CHO culture

CHO DG44 cells were maintained in suspension by orbital shaking in ProCHO5 (Lonza Verviers SPRL) supplemented with 4 mM glutamine, 13,6 mg/L hypoxanthine and 3,84 mg/L thymidine (Muller et al., 2005). The culture will be maintained at 37°C in the presence of 5% CO2.

3.17.3 FD fibroblasts culture

Human FD fibroblasts were purchased from Coriell Institute (GM04959, GM04899). Human FD fibroblasts were cultured in Dulbecco's Modified MEM added with L-glutamine to a final concentration of 2mM, 125 U/ml Penicillin, 125 µg/ml Streptomycin and 10% fetal bovine serum (FBS). Cells were maintained at 37°C with 5% CO2. At day 0, human FD fibroblasts were seeded at a density of 6x104 cells/well. At day 1, the cells were transduced with lentiviral ExSpeU1 10 and lentiviral U1 wild-type with MOI 0, MOI 1, MOI 10 and MOI 20. Polybrene (Sigma) was used at a concentration of 10 µg/ml. Total RNA was extracted at day 4 using TRIzol (Invitrogen) according to manufacturer's instructions. Reverse transcription was performed using 1 µg of total RNA and PCR was carried out with IKAP Exon 19 F and IKAP Exon 21 R primers (Suppl. Table 1). PCR conditions were 95° C for 2 minutes, 95° C for 30 seconds, 60° C for 30 seconds, 72° for 30 seconds and 72° C for 5 minutes. PCR products were separated on 2% agarose gel by electrophoresis, quantified with Image J Software (NIH) and analyzed by sequencing to confirm their nature.

3.18 Transfection of recombinant DNA

$3x10^5$ cells were plated as described above into 6-well cell culture dishes in order to reach a final confluence of 40-70%. The plasmid DNA used for transfection was prepared with JetStar purification kit as previously described.

Transfection of cells was performed by applying Effectene transfection reagent (Qiagen) according to manufacturer's instructions. For 6-well plates, 500ng of DNA plasmid were first mixed with 150µl of EC buffer and 4 µl of Enhancer. This mixture was incubated at RT for 5 minutes to allow the condensation of DNA. Then was added 5 µl of Effectene reagent to the mixture and incubated for 10 minutes to allow Effectene-DNA complexes to form. After the time, was added 500 µl of complete growth medium to the mixture to block the Effectene reaction. This mixture was then transferred into 6-well dishes containing the cells previously washed with 1ml of PBS solution and successively added with 1.5ml of complete growth medium. The cells treated in this way were then incubated at 37°C for 24

hours. After the incubation time, cells were harvested and subjected to further analysis. Each transfection experiment was repeated at least three times in double.

3.19 Co-transfection of recombinant DNA

The co-transfection experiment consist of the transfection of two different plasmid at the same time in the same cultured cells. This procedure was used to analyze the effect of U1 snRNAs and U7 snRNAs constructs to the processing of hybrid minigene constructs, previously described.

The protocol was the same as that described above. The differences consists to use 500ng of minigene added with 500ng of U1 plasmid in the same eppendorf tube (1µg of total amount of DNA). This mixture was then incubated with 8µl of Enhancer reagent and 10µl of Effectene reagent. All other points of the experiment were the same reported above.

3.20 RNA preparation from cultured cells

Cultured cells were washed twice with 1X PBS solution and then 750µl of RNA TRI Pure reagent (Roche Diagnostics) was added. Then, chloroform extraction was performed and supernatant was precipitated with isopropanol. The pellet was resuspended in 70% ethanol. The final pellet was resuspended in 33µl of H_2O and stored at -80°C. The RNA quantity was checked by electrophoresis on a 0.8% agarose gel.

To verify if the RNA was contaminated by DNA, the extracted RNA was treated with RNase-Free DNase (Promega) in 1X DNase buffer. The DNA digestion was performed at 37°C for 30 minutes and the reaction was stopped by adding DNase Stop Solution and incubating at 65°C for 10 minutes. RNA was then purified using RNeasy Mini Kit – RNA Cleanup Protocol (Qiagen) according to manufacturer's instructions.

3.21 Estimation of nucleic acid concentration

As both DNA and RNA molecules absorb UV light, this feature is used for measuring the concentration of nucleic acids with UV spectrophotometer. The nitrogenous bases in nucleotides have an absorption peak at 260nm, so an optical density of 1.0 at this wavelength is usually taken to be equivalent to a concentration of 50µg/ml for double-stranded DNA, 40µg/ml for single-stranded DNA and RNA, and 20µg/ml for single-stranded oligonucleotide sample. The ratio of the absorbance at 260nm and 280nm is a measure of the purity of a sample: this ratio should be around 1.8 for pure DNA sample and 2.0 for RNA sample; these ratios are reduced in the case of protein contamination.

3.22 The mRNA functional splicing analysis

3.22.1 cDNA synthesis

The first-strand cDNA synthesis was performed with the M-MLV reverse transcriptase kit (Invitrogen) following manufacturer's instructions. 100ng of total RNA extracted from the cells were mixed with 2µl of random primers (100ng/µl, Invitrogen) and diluted in water to the final volume of 12µl. To denature the RNA, the mixture was put at 94°C for 2 minutes and quick chilled on ice. After denaturation, 6µl of 5X First-Strand buffer (250mM tris-HCl (pH8.3 at RT), 375mM KCl, 15mM $MgCl_2$), 3µl of 0.1M DTT, 3µl of dNTPs (100mM each), 0.5µl of M-MLV RT were added to the previously mixture. The final mixture was then incubated at 37°C for 90 minutes, after which were used 3µl as template for the PCR analysis.

3.22.2 PCR analysis

PCR amplifications were performed using previously described protocol in a final volume of 25µl. To perform the *in vivo* sequence analysis I used the primers reported below. Alpha 2,3 and Bra2 are primers used to specifically amplify the pTB-based minigenes (*F8* and

IKBKAP). The IKAP primers were used to amplify the endogenous *IKBKAP* from FD fibroblasts. The ExSpeU1 Ik10 primers were used to specifically amplify the ExSpeU1 Ik10 after transduction of FD fibroblasts. The SMN2 primers were used to amplify the *hSMN2* from mouse samples.

oligo name	sequence 5' -> 3'
alpha 2,3	caacttcaagctcctaagccactg
Bra2	tgatttaaccaacttcctggtgaccggatccta
oligo IKAP dir	ggccggcctgagcagcaatcatgtgtcc
oligo IKAP rev	gattctcagctttctcatgcattc
ExSpeU1 Ik10 dir	ATAGCAAACAGTACAATGC
ExSpeU1 Ik10 rev	CACTACCACAAATTATGCA
oligo SMN2 dir	CTCCCATATGTCCAGATTCTCTT
oligo SMN2 rev	CTACAACACCCTTCTCACAG

The results of all the transfections are the representative of at least three independent experiments. PCR products were resolved by 2% agarose electrophoresis gel. Whereas quantification of exon inclusion was performed using ImageJ2X program.

3.23 Bioinformatic analysis

Putative exonic splicing enhancer (ESE) motifs were identified using *ESEfinder* (http://rulai.cshl.edu/cgi-bin/tools/ESE3/esefinder.cgi?process=home), that is a web-based resource that facilitates rapid analysis of exon sequences to identify putative ESEs responsive to the human SR proteins SF2/ASF, SC35, SRp40 and SRp55, and to predict whether exonic mutations disrupt such elements [164].
The strength of both 3' and 5' splice sites of considered genes has been valuated using the bioinformatics tool (http://www.fruitfly.org/seq_tools/splice.html). This resource permits to evaluate the score of splicing only inserting the sequence that would want to analyze.

3.24 Lentiviral production and titration

Lentiviruses (LVs) were produced by transient transfection of Hek293FT cells (Invitrogen). A total of $2x10^7$ cells were seeded in one 175 cm^2 tissue culture flask and incubated overnight at 37°C, 5% CO_2 in a Dulbecco modified Eagle medium (Gibco) containing 10% fetal bovine serum (FBS), 0.1 mM Non-Essential Amino Acids (NEAA), 6 mM L-glutamine, 500 μg/mL Geneticin. A total of 100 μg plasmid was used for transfecting one flask: 50 μg FVIII and ExSpeU1 LV plasmid, 17.5 μg pMD.G2 (vesicular stomatitis virus glycoprotein envelope plasmid) and 32.5 μg pCMVΔ8.74 (gag-pol packaging plasmid). These plasmids were incubated for 20 minutes at room temperature in OptiMEM with 1 μl of a 10 mM polyethylenimine solution (Sigma-Aldrich). After the incubation, the solution was added to the cells for 3 hours and then replaced with 15 mL of complete DMEM medium. After 24 hours, the medium was replaced with a 15 mL of fresh complete medium. The supernatant was harvested at 48 and 72 hours post-transfection, filtrated and ultracentrifuged at 23000 rpm for 2 hours at 4°C. The pellet was resuspended with 50 μl of OptiMEM, aliquoted and stored at -80°C.

The physical titer of lentiviral particles was measured according to the manufacturer's instructions with the Lenti-X p24 Rapid Titer Assay (Clontech), an ELISA assay that quantitatively binds the HIV-1 p24 core/capsid protein. The obtained values were used to calculate the MOI according to the manufacturer's instructions.

3.25 Expression analysis of rFVIII variants

3.25.1 CHO transduction with LV-rFVIII variants

Chinese Hamster Ovarian wild-type cell line (CHO) was transduced with rFVIII lentiviral variants at MOI 2. These cells were grown in suspension at 37°C, 5% CO_2 at 120 rpm using the CD DG44 medium (Gibco) supplemented with 10% Pluronic F-68 (Gibco) and 4% GlutaMAX (Gibco). At day 0, CHO cell lines were seeded at $4x10^6$ cells in 10 mL of complete medium and transduced with MOI 2 of FVIII lentiviral variants. After 6 hours, the volume was increased up to 30 mL with fresh medium. 24 hours after transduction,

cells were centrifuged, washed with PBS 1X (Invitrogen) and resuspended with 30 mL of fresh complete medium. Cells were harvested at 48, 72 and 96 hours after infection and stored in RNAlater according to the manufacturer's instructions (Ambion). Medium samples were harvested at 48, 72 and 96 hours after infection and stored at -80°C. Cells viability was measured every day in duplicate using the TC20 Automated Cell Counter (Biorad).

3.25.2 Quantitative Real-Time PCR (qPCR) for the Determination of Proviral Copy Number

Real-time PCR was performed in triplicate on the genomic DNA of the cells harvested at 96 hours after infection. Genomic DNA was extracted with the DNeasy Blood&Tissue kit (Qiagen) according to the manufacturer's protocol and then quantified with the Qubit 3.0 Fluorometer (Invitrogen). 50 ng of genomic DNA was used as template for the SYBRgreen (Invitrogen) real-time PCR in order to quantify the lentiviral copy number for each FVIII variant. The sequences of the viral woodchuck hepatitis regulatory element (WPRE) are: WPRE F 5'-GTCCTTTCCATGGCTGCTC-3' and WPRE R 5'-CCGAAGGGACGTAGCAGA-3'. The internal reference gene used to normalize the data is the hamster actin, which primers are: ham_actin_F 5'-ACGATATCGCTGCGCTCGT-3' and ham_actin_R 5'-GCCCACGATGGATGGGAAG-3'. The real-time PCR conditions were 95°C for 5', 95°C for 15" and 60°C for 15" for 40 cycles. Values obtained by cells viability and real-time PCR were used to correct the rFVIII antigen and activity levels.

3.25.3 Factor VIII Antigen ELISA

The levels of factor VIII antigen in cell media were determined using the FVIII ELISA (F8C:EIA, Affinity Biologicals) as per manufacturers instructions. MaxisorpTM 96-well NUNC-Immuno ELISA plates (NUNC) were coated with 100µL/well with FVIII capture antibody diluted 1:100 in coating buffer, sealed, and incubated for two hours at 22°C. The plates were washed three times and 100µL of sample diluted 1:20 to 1:40 in dilution buffer added in duplicate. A standard curve in % FVIII protein was constructed by diluting

biophen normal control plasma (Quadratech Diagnostics) 1:40, carrying out ten 1:2 serial dilutions, and running in duplicate on the plate. Biophen abnormal control plasma was also used as a further quality control for the assay. Plates were incubated at room temperature for two hours at 22°C and subsequently washed three times times with wash buffer. 100µL/well of pre-diluted FVIII detection antibody was added to each well and plates incubated at 22°C for one hour. Plates were then washed three times and 200µL/well of OPD substrate solution was added. The plates were incubated for exactly approximately 15 minutes at 22°C in the dark, at which time the reaction was stopped by adding 50µL stop solution (2.5M H2SO4). The absorbance of each well was then read at 490nm on a spectrophotometer.

3.25.4 Factor VIII Chromogenic Activity Assay

The cofactor activity of blood plasma samples and in vitro cell culture media samples was assessed using the Biophen Factor VIII:C Chromogenic Assay (Quadratech Diagnostics) as per manufacturer's instructions. When activated by thrombin, activated Factor VIII forms an enzymatic complex with Factor IXa, phospholipids, and calcium, which activates Factor X to Factor Xa. In this assay factor IXa, phospholipids, calcium, and factor X are all supplied at a constant concentration and in excess to FXa, meaning the generation of FIXa is rate limited by, and directly proportional to, FVIIIa. Factor Xa generation is measured by its activity on a specific Factor Xa chromogenic substrate (SXa-11), cleaving the substrate and releasing pNA. The amount of pNA generated is directly proportional to the Factor Xa activity and can be read by colour development at 405nm. Samples were diluted 1:20 and 1:40 in sample diluent provided and run in duplicate on plates. A standard curve in % FVIII cofactor activity was constructed by diluting biophen normal control plasma (Quadratech Diagnostics) 1:20, carrying out four 1:2 serial dilutions, and running in duplicate on the plate. Biophen abnormal control plasma was also used as a further quality control for the assay.

3.26 Expression analysis of endogenous IKBKAP

3.26.1 Real-time IKBKAP analysis

IKBKAP real-time PCR was done on a BioRad thermal ICycler with the following PCR program: 1 cycle at 50°C for 15 min; 1 cycle at 95°C for 5 min; and 45 cycles at 95°C for 15 sec, and at 59 °C for 1 min. All reactions were carried out in triplicate in a 96-well plate format, with a final volume of 50 uL. The list of the IKBKAP-Taqman assay is reported below.

oligo name	sequence 5' -> 3'
WT-IKAP F	GCAGCAATCATGTGTCCCA
WT-IKAP R	ACCAGGGCTCGATGATGAA
WT-IKAP TAQMAN PROBE	GTTCACGGATTGTCACTGTTGTGCC
MUT-IKAP F	CACAAAGCTTGTATTACAGACT
MUT-IKAP R	GAAGGTTTCCACATTTCCAAG
MUT-IKAP TAQMAN PROBE	CTCAATCTGATTTATGATCATAACCCTAAGGTG
18S F	GGCCCTGTAATTGGAATGAG
18S R	GCTATTGGAGCTGGAATTAC
18S TAQMAN PROBE	TGCTGGCACCAGACTTGCCCTC

3.26.2 Western Blotting analysis of IKAP protein

For western blotting analysis 50ug of total protein from treated-fibroblasts' lysates incubated 5 min at 95°C and run on 4–12% SDS–PAGE (NuPAGE Bis–Tris gel, Invitrogen, Carlsbad, CA, USA). Proteins were transferred onto a 0.2 mm nitrocellulose membrane (Whatman, Dassel, Germany), which was blocked for 1 hour with PBS buffer supplemented with 0.1% Tween-20 (PBS-T) and 5% low fat dry milk (Bio-Rad, Hercules, CA, USA). Membrane was incubated overnight at 4°C with rabbit polyclonal antibody against the C-terminus region of the human IKAP protein (Anaspec, 1:2000) and with the rabbit polyclonal antibody against tubulin (Sigma, 1:2000). Membranes were washed and incubated with secondary antibodies for 1 hour at room temperature. Protein bands were visualized by chemiluminescence (Pierce® ECL Western Blotting Substrate, Thermo Scientific) followed by exposure to autoradiographic film.

3.27 *In-vivo* experiments

3.27.1 SMA animal models

All animals were kept in a controlled environment at 25°C with a 12 h light/dark photoperiod. Animal care and treatment were conducted in conformity with ICGEB institutional guidelines in compliance with national and international laws and policies (EU Directive 2010/63/EU) upon approval by the Italian Ministry of Health.

Two different SMA mouse models were used in this project. (i) The mild SMA model, that is characterized by the absence of the murine *smn* gene and carries four copies of the *SMN2* transgene, which was purchased from Jackson's Laboratory (Stock Number: 005058). (ii) The severe Taiwanese-SMA model, that was obtained by crossing back the original strain purchased from Jackson's Laboratories (No. 005058) to wild-type FVB/N mice for two generations. The mice being heterozygous for the SMN2 transgene on Smn null background developed a severe SMA phenotype with a mean age of survival of 10 days. They turned out to be an excellent SMA mouse model. In each litter, 50% of offspring was SMA mice (Smn -/-; SMN2tg/-) and 50% was control carriers (Smn +/-; SMN2tg/-). As a wild-type strain, the inbred strain FVB/NJ (Jackson´s Laboratory, Stock Number: 001800) was used.

3.27.2 Genotyping

Tails biopsies were incubated at 55 ºC overnight in lysis buffer (0.1 M Tris pH 8.0 0.2M NaCl, 5 mM EDTA, 0.4% SDS, proteinase K 0.2 mg/ml) and DNA was precipitated with isopropanol. The PCR reaction was performed with 35 cycles of amplification as follow: 94 ºC 30s, 58 ºC 30s, 72 ºC 30s. The three PCR primer pairs used to identify transgenic mice were:

oligo name	sequence 5' -> 3'
1F	ACTGCAACCTCCTGGGTTCAAGTG
1B	CAGTTCGAGACCAGCCTGACCAAT
2F	CGAATCACTTGAGGGCAGGAGTTTG
2B	AACTGGTGGACATGGCTGTTCATTG
3F	AAACCAGTCGGGCACAATACCTAGC
3B	TATGCTGATTGAAGGGAGGGGTGC

Table of primers used for the genotyping.

3.27.3 AAV9-treatments

The adeno-associated molecules used in the treatment of SMA animals were purchased from SignaGen Laboratories. I intraperitoneally injected (IP) newborns mice at post natal days 0 and 2 with approximately 25ul/animal. The titer of the AAV9 used in these experiments were:

1) AAV9-ExSpeU1 sm25 titer [7.58E13 GC/ml]
2) AAV9-ExSpeU1 sm37 titer [1.18E14 GC/ml]
3) AAV9-U1 wt titer [3.01E13 GC/ml]
4) Saline

3.27.4 Neurofunctional tests

The four limb hanging test was performed between the fifth and the ninth week after birth. The time recorded is the ability of mice to hold themselves on to the bars after the metal grid was inverted, with 60 sec being the maximum time.

The Rotarod test was performed between the fifth and the ninth week after birth. Using an accelerating profile, each trial ended when the mouse fell off the rod, and latency was recorded, with a maximum time of 300 sec. In all tests mice were tested 3 times per session and the results were averaged.

Chapter 4

RESULTS

4.1 Effect of the p.Arg2016Trp (c.6046C>T) mutation on FVIII protein and mRNA biology

Due to the amino acids properties, the missense change p.Arg2016Trp is supposed to have a significant structural impact on the FVIII protein, which might reduce either its secretion or its activity. Here, I evaluated the effect of the p.Arg2016Trp change on its secretion and its activity levels, by taking advantage of the codon-optimized FVIII (coFVIII) cDNA (Fig. 4.1A) [163]. The secretion levels of the original FVIII are usually very low due to several factors, like the wide protein size and the labile structure. For this reason, I used the recombinant coFVIII that is characterized by higher secretion levels due to its codon optimization that includes the removal of 14 cryptic splice sites, an increase in the GC-content, the addition of a Kozak sequence (to increase translation initiation) and two stop codons (to ensure efficient termination). Furthermore, this sequence is characterized by the absence of the FVIII B domain, which was replaced by a 14-amino acids SQ^m sequence. This region consists of a SFSQNPPVLTRHQR motif, where the RHQR represents the furin recognition site used to increase the FVIII intracellular cleavage. Thus, the resulting optimized sequence maintained a nucleotide homology with the original not optimized FVIII sequence of approximately 76%.

As shown in figure 4.1A, the coFVIII sequence was introduced into a SIN lentiviral backbone, that I successively used to create lentiviral particles (LPs). Before to generate LPs, I introduced the missense p.Arg2016Trp by site-specific mutagenesis on the cDNA sequence, which was confirmed by DNA sequencing. Therefore, I transduced the Chinese

hamster ovary (CHO) cell line, which is typically used to produce high-grade recombinant protein due to their efficiency, with a lentivirus expressing the wild-type coFVIII (rFVIIIwt) and one expressing the tryptophan in position 2016 (rFVIII-2016Trp). Seventy-two hours post-transduction, I harvested cells media and analyzed the secretion and activity levels of these two rFVIII proteins by ELISA and chromogenic assays, respectively. As shown in figure 4.1B, the mutant rFVIII-2016Trp displayed a secretion of 11.0±0.4% and activity of 6.0±2.9%, where the rFVIIIwt was set up to 100%. The corresponding FVIII specific activity, which is calculated by diving the FVIII activity per Ag values, resulted to be reduced of 50% (Fig. 4.1B).

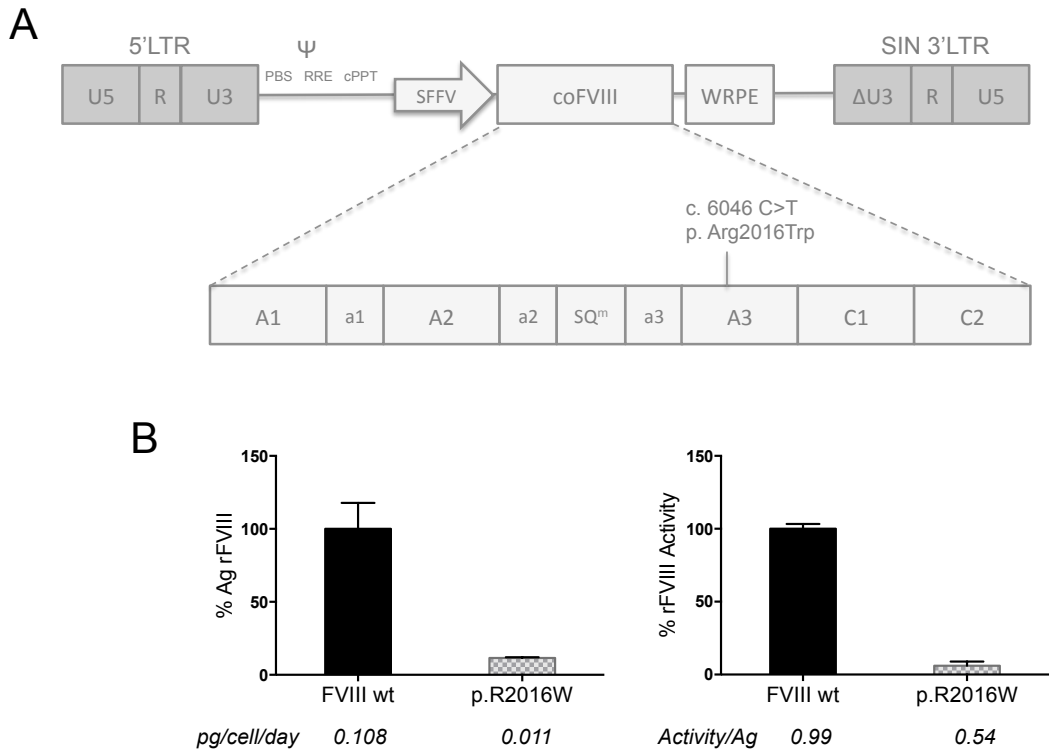

Figure 4.1 Effect of the p.Arg2016Trp (c.6046C>T FVIII) mutation on FVIII protein biology *in vitro*

A) Schematic representation of the lentiviral vector expressing the human codon optimized FVIII deleted of the B domain. The p.Arg2016Trp (c.6046C>T) substitution was inserted by site-specific mutagenesis and confirmed with DNA sequencing.

B) Secreted (left) and cofactor activity (chromogenic assay; right) levels of rFVIII variants measured upon lentiviral infection of CHO cells. The amount of secreted protein, expressed as picograms/cell/day, and the specific activity are also shown at the bottom of each graph.

The secretion and activity levels observed in this experiment with the rFVIII-2016Trp displayed a significant difference with the corresponding *in-vivo* values described in HA

patients who carry this missense mutation (<1-2%). For this reason, I decided to analyze the effect of the mutation at RNA level on the RNA from white-blood cells of three patients with this change. Since the nucleotide change (c.6046C>T) that causes the amino acid substitution p.Arg2016Trp occurs within the F8 exon 19, I amplified by RT-PCR the region spanning from exon 18 to exon 20, in order to observe whether the mutation has an effect on splicing or not. As shown in figure 4.2B, the amplification displayed an aberrant processing from the patients' samples, resulting into a percentage of exon 19 inclusion of approximately 70%. This phenomenon, however, did not appear in the amplification from RNA samples of unaffected candidates, demonstrating the involvement of the mutation on splicing.

To confirm this observation, I further analyzed the mutation using a hybrid minigene system. This artificial tool is a plasmid that contains a promoter, a series of exonic and intronic sequences that derive from a reporter gene (α-globin in this case), and a polyadenilation signal. The genomic region of interest is cloned in a precise site within the reporter gene, that allows the analysis of its effect on splicing afterwards. This construct, indeed, is transfected in cell lines, followed by RNA extraction and specifically RT-PCR amplified. The effect on splicing is then studied through a gel electrophoresis run of the amplified products.

Therefore, I created a F8 wild type minigene carrying the genomic region of FVIII spanning from intron 18 to intron 19, isolating in this manner the exon of interest (Fig. 4.2A).

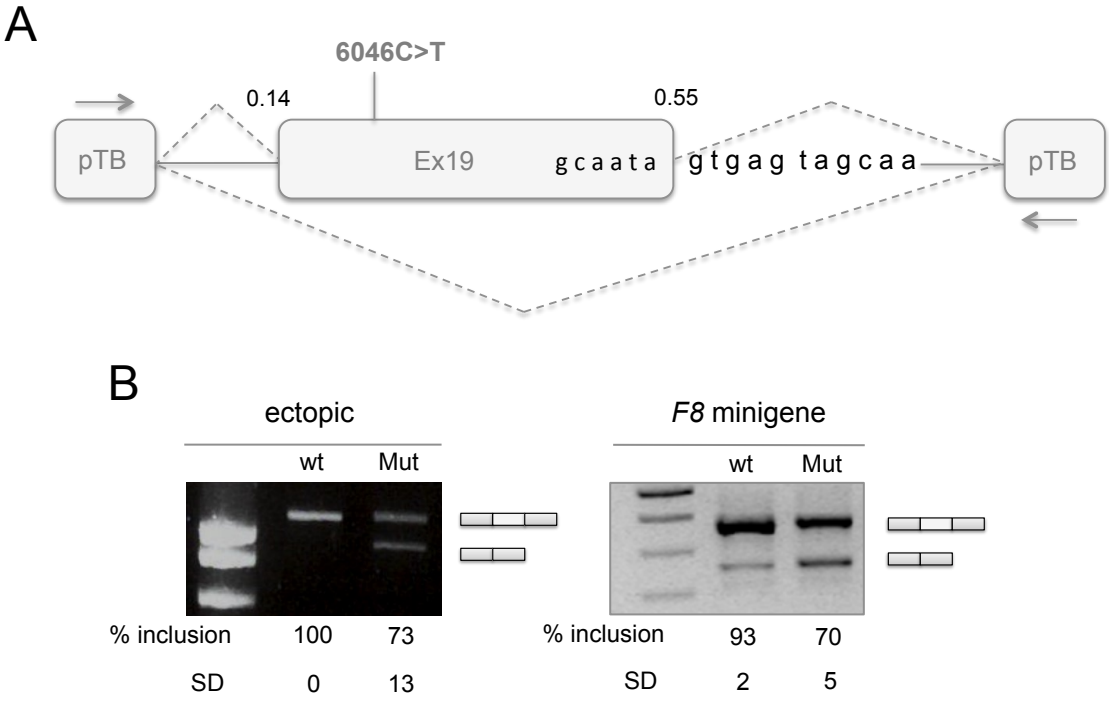

Figure 4.2 Effect of the p.Arg2016Trp (c.6046C>T FVIII) mutation on FVIII mRNA biology *in vitro*

A) Schematic representation of the F8 hybrid minigene highlighting the F8 exon 19 and its splicing scores. Arrows schematically indicate the binding regions of the PCR primers used for the specific amplification.

B) Splicing patterns of F8 measured from ectopic mRNA (left) and from F8 minigenes (right; wt, wild type; Mut, variant carrying the c.6046C>T transition). RT-PCR amplicons, including (375bp) or not (258bp) exon 19 were separated on 2% agarose gel. The relative percentages of exon inclusion, calculated with ImageJ software, and the standard deviations are reported below as a mean of three independent experiments.

Successively, as previously done for the recombinant molecule, I inserted the nucleotide change c.6046C>T by site-specific mutagenesis, generating the F8 mutant minigene. I transfected these two plasmids in the hepatic cell line HepG2, being the FVIII of liver origin. Twenty-four hours post-transfection, I extracted the total RNA and RT-PCR amplified to study the effect on splicing. As shown in figure 4.2C, both amplifications resulted in two different bands demonstrating a partially impaired RNA processing. In particular, the F8 wt minigene resulted in a percentage of exon inclusion of 93±2%, probably due to the artificial system itself since the wt ectopic product did not show any defect (Fig. 4.2B, lane 1). On the other hand, the F8 mutant minigene displayed a splicing pattern similar to the ectopic one, reaching a percentage of exon inclusion of 70±5% (Fig. 4.2C, lane 2).

This result confirms the aberrant splicing observed in HA patients' samples carrying the c.6046C>T substitution, providing an additional element for the explanation of the low levels of FVIII *in vivo*, where the exonic c.6046C>T mutation impairs both the protein and the RNA processing of the FVIII.

4.2 Characterization of *FVIII* pre-mRNA regulatory elements within exon 19

Sometimes exon skipping defects occur in exonic contexts with weak splice sites. A useful tool to predict it is given by a web platform (fruitfly.org), which calculates the splicing sites scores according to the nucleotide sequence. This analysis displayed that F8 exon 19

is characterized by weak splicing scores that could explain the observed alternative splicing in mutational context (Fig. 4.2A). Looking at F8 exon 19 sequence, it is evident that the complementarity between the donor site and the endogenous U1 snRNA is reduced by four mismatches (Fig. 4.3A). The U1 snRNA binding tail, indeed, consists of nine nucleotides that physically interacts with the donor site, recruiting the spliceosome and initiating the splicing process. The F8 exon 19 donor site, however, maintains only five Watson-Crick interactions, which explain the predicted weak splice site score. Therefore, to verify this hypothesis, I improved the authentic donor site of the F8 exon 19 in the mutant minigene, by replacing the four un-matching nucleotides with four nucleotides that are complementary to the wild type U1 snRNA (Fig. 4.3B). In particular, I replaced the ATA at the 3' end of exon 19 with the nucleotides CAG, and the intronic guanine in position +3 with an adenine. This replacement increased the affinity between the donor site and the endogenous U1 snRNA to 100%, for which reason I named this construct F8 exon 19 5'ss HC (High Complementary).

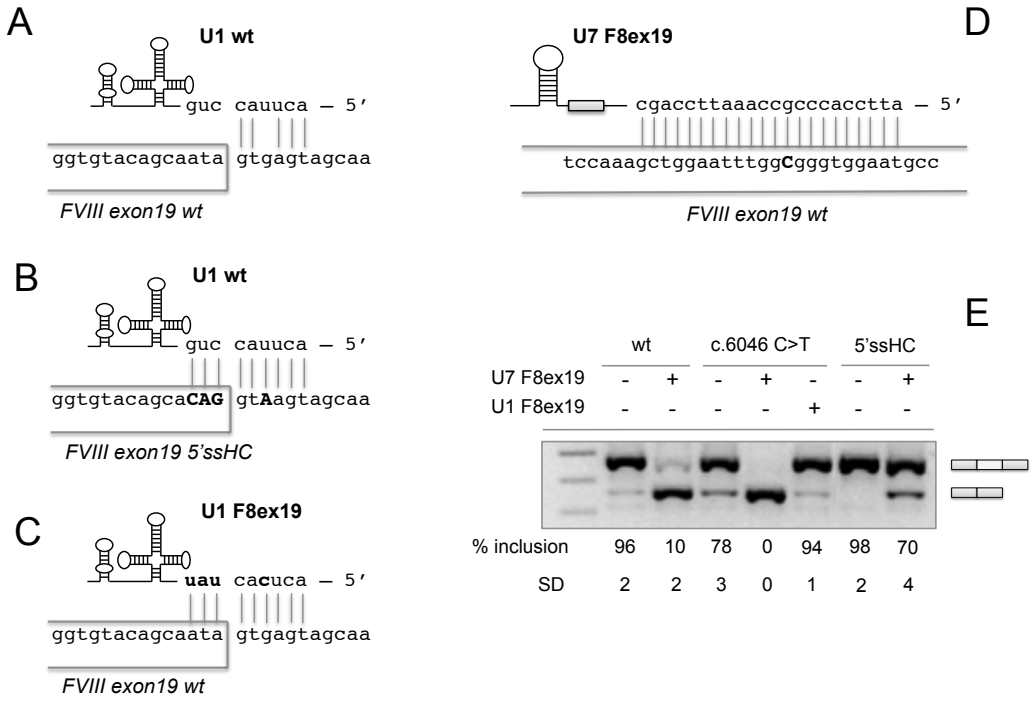

Figure 4.3 Characterization of the splicing regulatory elements within *F8* exon 19

A) Schematic representation of the wild type donor splice site of the *F8* exon 19 and its complementarity with the endogenous wild type U1 snRNA. Vertical lines highlight the Watson-Crick interactions between the two molecules.

B) Schematic representation of the implemented *F8* exon 19 donor site (F8 exon 19 5'ssHC) and its complementarity with the endogenous wt U1snRNA. The changed nucleotides are shown in bold,

displaying the complete interaction between the F8 exon 19 donor site and the 5' tail of the U1 snRNA.

C) Schematic representation of the wild type donor site of the *F8* exon 19 and its complementarity with the modified U1 snRNA (U1 F8ex19), which was designed to fully interact with the F8 exon19 5'ss.

D) Schematic representation of the binding region of the U7 F8ex19 that covers the exonic region affected by the c.6046C>T substitution.

E) Alternative pre-mRNA processing of F8 minigene transcripts, wild-type (wt), with the frequent c.6046C>T mutation alone or in the presence of the ameliorated 5'ss (5'ssHC) and upon co-expression (+) with the antisense U7 F8ex19 or the compensatory U1 F8ex19. RT-PCR amplicons, including (375bp) or not (258bp) exon 19 were separated on 2% agarose gel. The relative percentages of exon inclusion, calculated with ImageJ software, and standard deviations are reported below as a mean of three independent experiments.

Accordingly, I transfected the HepG2 cells with this new construct and, twenty-four hours later, I extract the total RNA to analyze it by RT-PCR. As shown in figure 4.3E (lane 6), the high complementary F8 variant recovered the aberrant splicing observed in the c.6046C>T mutant, displaying a percentage of exon 19 inclusion of approximately 98%.
These results demonstrate that, due to the presence of weak splice sites, the exon 19 is poorly defined and suggest that the c.6046C>T substitution might negatively influence the exon 19 recognition by affecting an exonic splicing regulatory element (ESRE). The *cis*-acting regulatory elements can improve (enhancers) or inhibit (silencers) the exon recognition via the recruitment of specific *trans*-acting factors. Therefore, to characterize the nature of the regulatory element affected by the c.6046C>T mutation, I used the U7 snRNA as antisense molecule to cover the exonic region affected by the mutation. The U7 snRNP is a ribonucleoprotein that belongs to the U snRNP family but, physiologically, does not play any role in splicing. For this reason, this molecule is usually modified in order to mask *cis*-acting elements and affect alternative splicing. In this case, I modified the 5' binding tail of the U7 snRNA (U7 F8ex19) in order to mask the exonic region 12 nucleotides upstream and 11 nucleotides downstream of the c.6046C>T change (Fig. 4.3D). Therefore, I co-transfected both the wild type and mutant F8 minigenes together with the U7 F8ex19 in HepG2 cells. Twenty-four hours later, I extracted the total RNA and analyzed it by RT-PCR. This experiments highlighted the presence of an exonic splicing regulatory element (ESRE) with enhancing properties, as observed by the significant exon skipping induced in both wild type and mutant minigenes (Fig. 4.3E, lanes 2 and 4). In particular, in the F8 exon 19 wild type context, the percentage of exon inclusion was approximately of 10%, whereas in the c.6046C>T mutant the percentage of exon inclusion

was 0%. To further evaluate the strength of this exonic regulatory element, I co-transfected the U7 F8ex19 with the high complementary F8 minigene. This experiment showed a significant effect on the amount of full length transcripts, reducing the exon inclusion with a percentage from 100% to 70% (Fig. 4.3E, lane 7). However, the ameliorated F8 exon 19 donor site provided enough strength to counteract the antisense effect of the U7 F8ex19.
All together, these results supports the hypothesis of a strong exonic splicing regulatory element located within the F8 exon 19, which is partially affected by the c.6046C>T mutation.

4.3 Characterization of FVIII missense variants at the FVIII protein and mRNA levels

To better understand the nature of the newly identified ESRE within the *F8* exon 19, I studied the FVIII database looking for other natural HA mutations within this region. According to this database, I identified several missense mutations, associated to moderate/severe HA, that were satisfying this condition: p.Gly2013Arg (c.6037G>A), p.Trp2015Cys (c.6045G>C), p.Arg2016Leu (c.6047G>T), p.Val2017Met (c.6049G>A), p.Glu2018Gly (c.6053A>G) (Fig. 4.4A). In addition, I focused also on other two missense variants that, being in the proximity of the exon 19 donor site, could have an impact on the F8 splicing, the p.Val2035Ala (c.6104T>C) and the p.Asn2038Ser (c.6113A>G). Therefore, I evaluated the molecular effect of these FVIII variants on splicing through the F8 minigene system (Fig. 4.4A).

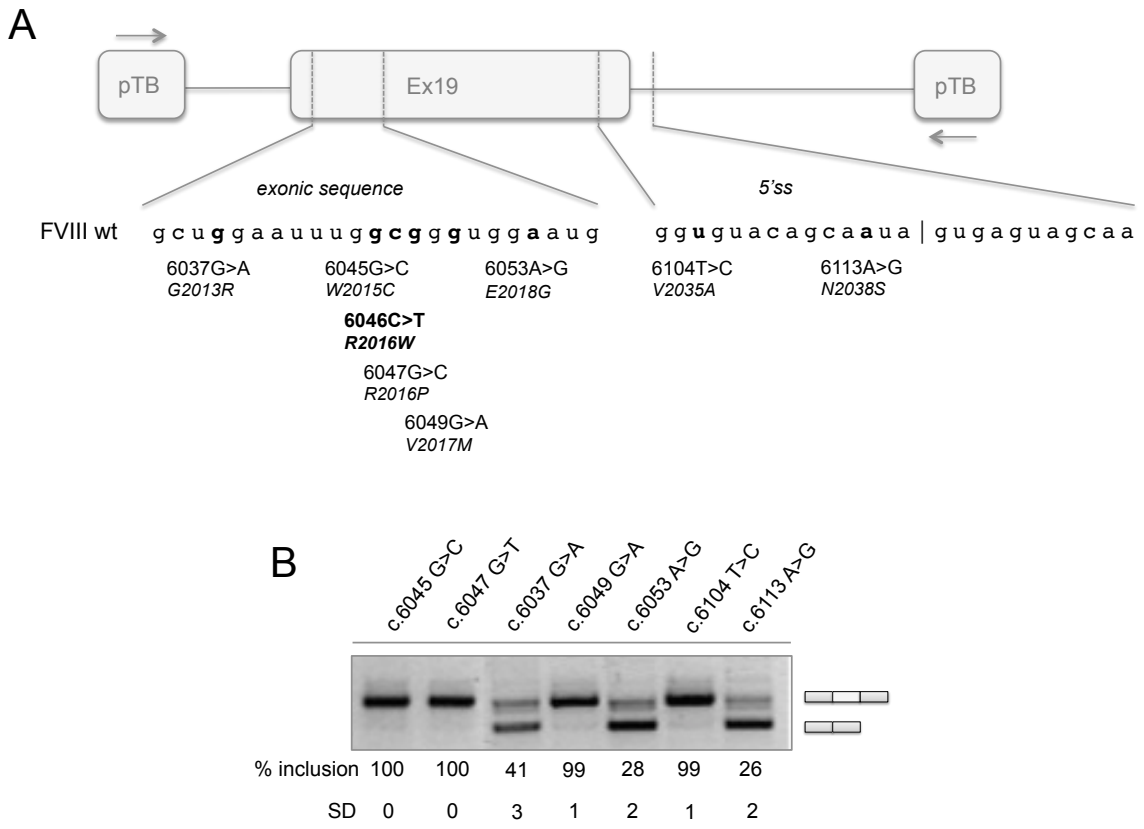

Figure 4.4 Characterization of FVIII missense variants at the FVIII mRNA level

A) Schematic representation of the FVIII missense variants identified within the exonic splicing regulatory element (c.6037G>A, c.6045G>C, c.6046C>T, c.6047G>C, c.6049G>A, c.6053A>G) and the two missense variants in the proximity of the *F8* exon 19 donor site (c.6104T>C, c.6113A>G). The nucleotides affected are shown in bold and the relative substitutions are shown below as both nucleotide and amino acid changes.

B) Alternative pre-mRNA processing of F8 minigene variants carrying the missense mutations. The upper band of 375bp corresponds to transcripts that include F8 exon 19, whereas the lower one of 258bp corresponds to F8 exon 19 skipping. RT-PCR products were run on 2% agarose gels. The percentage of exon 19 inclusion was calculated with ImageJ software and reported below along with the standard deviation as a mean of three independent experiments.

As before, I created each variant by site-specific mutagenesis and successively transfected in the hepatic cell line. Twenty-four hours post-transfection, I extracted the total RNA and RT-PCR amplified with the specific primers. As shown in figure 4.4B, three out of seven variants had a strong negative effect on F8 splicing, inducing a significant skipping of exon 19. In particular, the missense changes c.6037G>A (p.Gly2013Arg) and c.6053A>G (p.Glu2018Gly) remarkably reduced exon 19 inclusion from >90% to ~40% and 30%, respectively (Fig. 4.4B, lanes 3 and 5). I observed the strongest inhibitory effect with the

p.Asn2038Ser, that highly affected the recognition of exon 19, reducing the inclusion to 26% (Fig. 4.4B, lane 7). The other four missense mutations (c.6045G>C, c.6047G>T, c.6049G>A, c.6104T>C) did not negatively affect the F8 splicing, as observed by the total inclusion of the exon (Fig. 4.4B, lanes 1, 2, 4, 6), and therefore their pathological outcome could be explained only by an impaired protein biology.

On the other hand, the significant impairment of the *F8* pre-mRNA processing exerted by the three missense mutations (p.Gly2013Arg, p.Glu2018Gly and p.Asn2038Ser) could consistently reduce the amount of full length transcripts which, in turn, reduces the amount of secreted FVIII protein. To address this question, I created these three FVIII variants (rFVIII-2013Arg, rFVIII-2018Gly and rFVIII-2038Ser) using the previously described recombinant coFVIII (Fig. 4.5A). Furthermore, I produced an additional FVIII variant (rFVIIIΔ19) that might be translated by transcripts lacking of the exon 19. The deletion of this exon, indeed, does not compromise the reading frame, leading to the production of a protein with a deletion of 39 amino acids in the A3 domain of FVIII and, in the codon optimized sequence, the introduction of a Gly>Glu change at the exon 18-exon 20 junction (Fig. 4.5A).

A

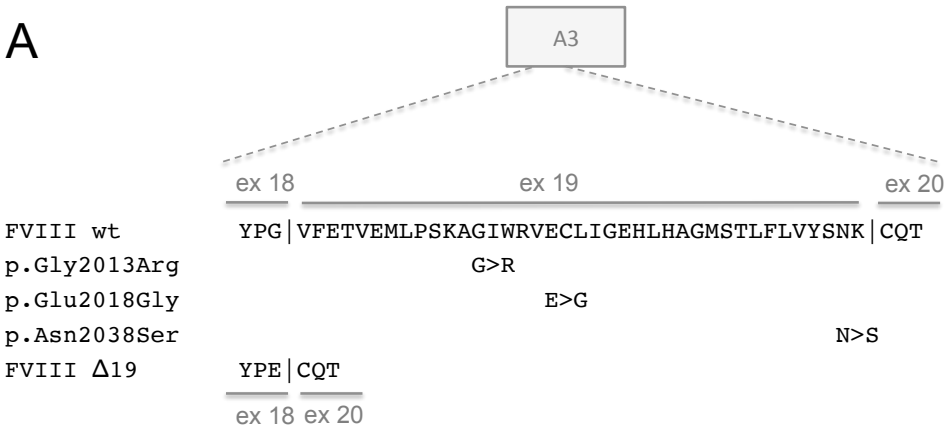

B

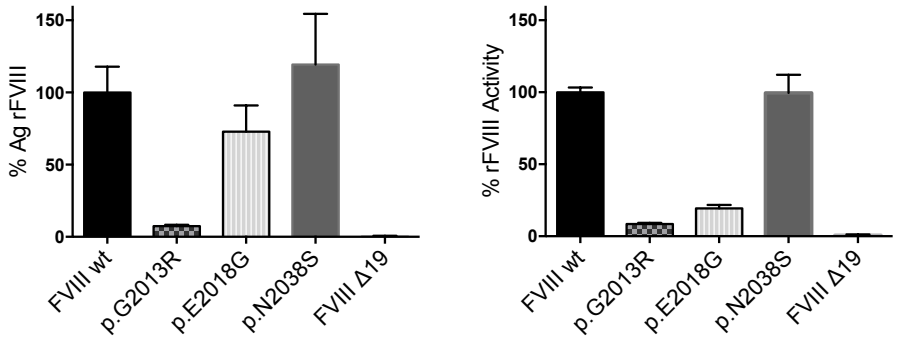

C

	FVIII wt	p.G2013R	**p.R2016W**	p.E2018G	p.N2038S	FVIII Δ19
pg/cell/day	0.10	0.00	**0.01**	0.08	0.10	n.d.
Specific activity	0.99	1.19	**0.54**	0.28	0.87	n.a.

Figure 4.5 Characterization of FVIII missense variants at the FVIII protein level

A) Schematic representation of the amino acid region affected by the FVIII missense variants. Amino acid substitutions and exon 19 deletion are shown in comparison to the wild type FVIII aa sequence.

B) Secreted and activity levels of the rFVIII missense variants (p.G2013R, p.E2018G, p.N2038S) whose nucleotide changes affected exon 19 splicing as well as of the rFVIIIΔ19 deleted variant.

C) The amount of rFVIII secreted levels, expressed as picograms/cell/day, and the specific activity, calculated as ratio Activity/Ag, are shown as table.

Accordingly, I produced lentiviral particles for each variant, which I successively used to transduce the CHO cell line. As before, seventy-two hours post-infection, I harvested cells media and analyzed by ELISA and chromogenic assays. As shown in figure 4.5B, the rFVIIIΔ19 variant was undetectable in both assays, whereas the rFVIII-2013Arg resulted in the lowest secretion of 7.0±0.9% of rFVIIIwt. The other two missense variants displayed significant antigen's levels. In particular, the rFVIII-2018Gly was secreted at 69.0±18.1% of rFVIIIwt, whereas the rFVIII-2038Ser was secreted at 112.9±35.2% of

rFVIIIwt (Fig. 4.5B, left panel). On the other hand, given 100% to the rFVIIIwt, the chromogenic assay showed an activity of 8.4±0.8% for the rFVIII-2013Arg, of 19.4±2.3% for the rFVIII-2018Gly and of 99.6±12.5% for the rFVIII-2038Ser (Fig. 4.5B, right panel). The corresponding specific activity, calculated by dividing FVIII activity per Ag, showed that: i) the rFVIII-2013Arg is poorly secreted but, however, maintains its functional activity; ii) the rFVIII-2018Gly is well secreted but has a severely reduced activity; iii) the secretion and activity of the rFVIII-2038Ser is not affected by this missense change (Fig. 4.5C).

All together, these results demonstrate that missense mutations can exert a negative effect also at the RNA level, and not only on the protein structure, providing a new concept for the evaluation of tailored therapeutic strategies, such as splicing-switching molecules.

4.4 Modified U1 snRNAs to correct the aberrant splicing caused by the FVIII exon 19 missense variants

The weak splice site scores of the F8 exon 19 have been counteracted by mutagenesis of the donor site, which increased the complementarity between the 5'ss and the binding tail of the wild type U1 snRNA. To confirm this result, I created a modified U1snRNA (U1 F8ex19) that has a binding tail fully complementary to the defective F8 exon 19 donor site (Fig. 4.3C). I replaced the GUC sequence within the U1 binding tail (the seventh to ninth nucleotides from the 5' end of the U1 tail) with a UAU sequence, that physically interacts with the ATA of the F8 exon 19 donor site. Furthermore, I replaced the second uracil of the U1 binding tail with a cytosine that binds to the intronic guanine of the F8 exon 19. Successively, I co-transfected the mutant (c.6046C>T) F8 exon 19 minigene along with the U1 F8ex19 in the hepatic cells and extracted the total RNA 24 hours after the experiment. The RT-PCR analysis displayed a correction of the aberrant splicing promoted by the co-presence of the U1 F8ex19, increasing the percentage of exon inclusion from 78% to 94% (Fig. 4.3E, lane 5).

This result confirmed the weakness of the F8 exon 19 donor site, providing also the basis for a splicing-corrective approach based on modified U1 snRNAs for those variants whose RNA processing was strongly affected by the missense change. For this reason, as proof of principle, I co-transfected the U1 F8ex19 with the F8 6113A>G variant, which displayed

the strongest inhibition of exon inclusion with a percentage of approximately 26%. As shown in figure 4.6, the RT-PCR showed a strong splicing correction induced by the presence of the U1 F8ex19 (lane 3). In particular, the exon 19 was included with a percentage of approximately 98%.

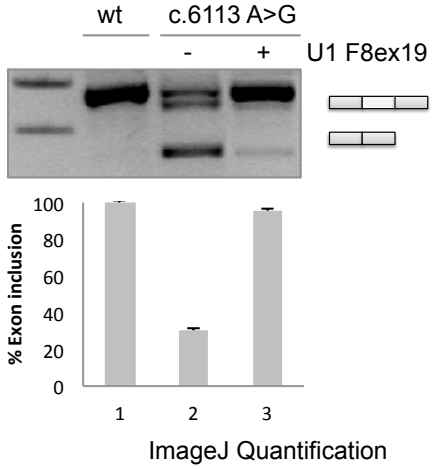

Figure 4.6 Effect of the modified U1 F8ex19 on the aberrant splicing caused by the FVIII missense variant p.Asn2038Ser

Alternative pre-mRNA processing of F8 minigene transcripts. The upper band of 375bp represents transcripts including the exon 19, whereas the lower band corresponds to exon 19 skipping. RT-PCR amplicons, including (375bp) or not (258bp) exon 19 were separated on 2% agarose gel. The relative percentages of exon inclusion, calculated with ImageJ software, and standard deviations are reported below as a mean of three independent experiments.

This result supports the therapeutic potential of splicing-switching molecules, such as modified U1 snRNAs, to correct splicing defects also in the context of missense mutations.

4.5 Effect of ExSpeU1s on the aberrant splicing caused by the *IKBKAP* IVS20+6T>C substitution

To further evaluate the therapeutic potential of modified U1 snRNAs, I took advantage of Familial dysautonomia (FD), a severe disease due to an intronic point mutation that causes a splicing defect. The *IKBKAP* IVS20+6T>C substitution, present in >99% of the patients, promotes skipping of the *IKBKAP* exon 20 leading to the FD disorder. To evaluate the

efficacy of a new class of modified U1 snRNAs (ExSpeU1s) that bind to the intronic sequences downstream the *IKBKAP* exon 20, I adopted the previously described methodology based on the pTB hybrid minigene (Fig. 4.7A). Firstly, a wild-type IKBKAP minigene was created by cloning the *IKBKAP* genomic region spanning from intron 18 to intron 22 into the pTB plasmid, that contains the promoter, the α-globin reporter gene and the polyadenilation site. Successively, the mutant IKBKAP minigene was produced by inserting the T>C change in position +6 of intron 20 through site-specific mutagenesis.

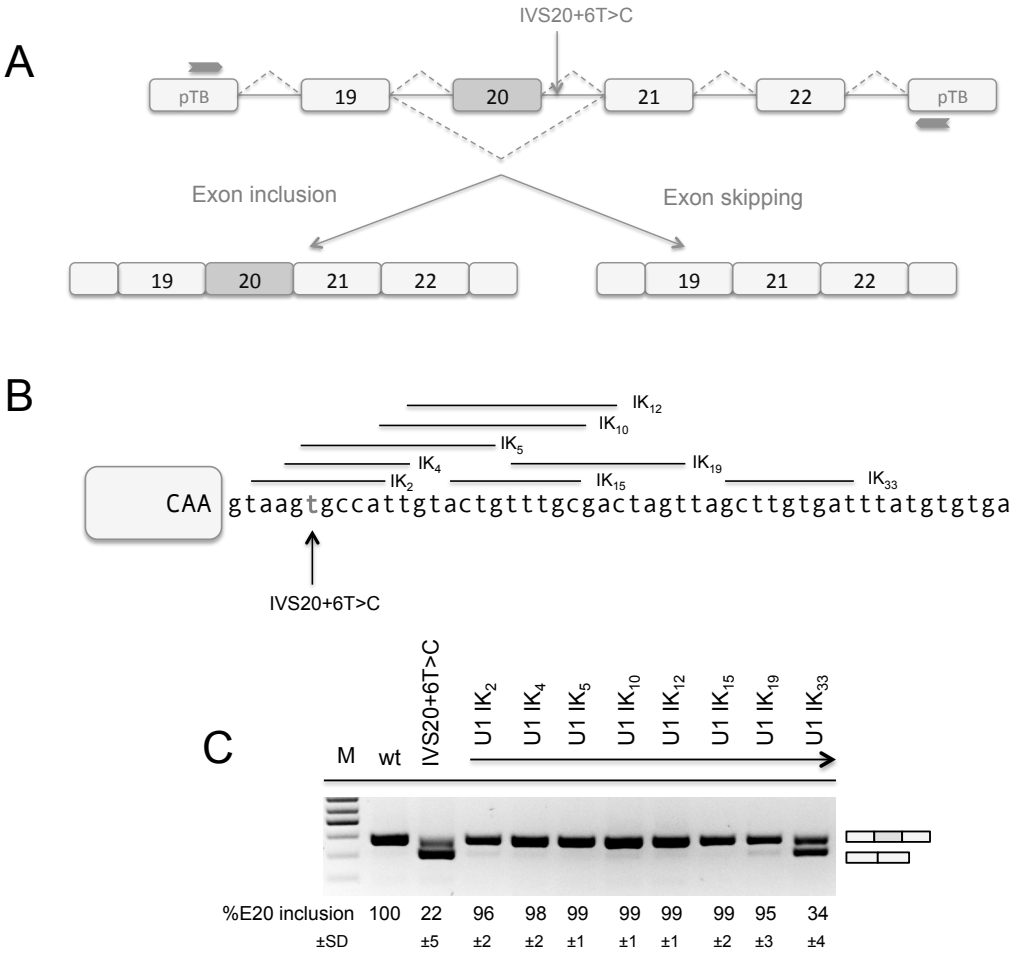

Figure 4.7 Effect of ExSpeU1s on *IKBKAP* mRNA biology *in-vitro*

A) Schematic representation of the pTB-IKBKAP minigenes. The genomic *IKBKAP* region from intron 18 to intron 22 was cloned in the hybrid pTB backbone, generating the wild type IKBKAP construct. The mutant IKBKAP minigene was created by site-specific mutagenesis, inserting the T>C substitution in position +6 of the intron 20. The affected exon is shown in darker grey and its processing is shown below as exon inclusion and exon skipping. The two dark grey arrows represents the binding region of the PCR primers used to specifically amplify the IKBKAP minigene.

B) Schematic representation of the binding regions of the IKBKAP-ExSpeU1s. The box on the left represents the 5'ss of exon 20, which is flanked by the IVS20 intronic sequence. The binding tail of the ExSpeU1s are schematically shown as lines above their targets.

C) IKBKAP splicing pattern analysis. Neuronal cells SH-SY5Y were co-transfected with fixed concentrations of pTB-IKBKAP minigenes and each IKBKAP-ExSpeU1. The RT-PCR products were separated on 2% agarose gels and the amount of exon 20 inclusion was quantified with ImageJ software. The upper band of 260bp corresponds to exon 20 inclusion, whereas the lower band of 187bp corresponds to transcripts lacking of the exon 20. The percentage of exon inclusion and standard deviations are shown below as a mean of three independent experiments.

Since the Relay-day syndrome is a neurological disorder caused by the *IKBKAP* aberrant splicing that occurs mostly in neurons, I expressed the IKBKAP minigenes in the neuronal cell line SH-SY5Y. Twenty-four hours post-transfection, I extracted the total RNA and analyzed it by RT-PCR.

As expected, the gel electrophoresis showed the presence of two pcr products of different molecular weight in the mutant context (Fig. 4.7C, lane 2). Direct sequencing of these fragments confirmed that the upper band corresponds to the transcript containing the IKBKAP exon 20, whereas the lower band is due to exon 20 skipping. In particular, the intronic mutation severely reduced the amount of exon inclusion with a percentage of approximately 22%. On the other hand, the wild type minigene did not show any aberrant splicing (Fig 4.7C, lane 1). This result confirms the clinical observations, supporting the negative role of the intronic mutation and providing the basis for the evaluation of ExSpeU1s' efficacy.

The donor site recognition is an important step of pre-mRNA processing that is mediated by the U1 snRNA, allowing the beginning of splicing. The *IKBKAP* IVS20+6T>C substitution reduces the interaction between the donor site and the binding tail of the endogenous U1 snRNA, leading to the observed aberrant splicing. Here, to evaluate the efficacy of modified U1 snRNAs to correct splicing, I designed eight ExSpeU1s that specifically target the intronic downstream region of *IKBKAP* exon 20, from position +2 to position +40 (Fig. 4.7B). To test the effect of these IKBKAP-ExSpeU1s, I co-transfected the IKBKAP mutant minigene along with each of the eight ExSpeU1s in the neuronal cell line. Twenty-four hours post-transfection, I extracted the total RNA and analyzed it by RT-PCR. The co-expression of these molecules along with the IKBKAP minigene showed a complete splicing correction, promoting the inclusion of exon 20 with a percentage up to 100% (Fig. 4.7C, lanes 3-10). In particular, seven out of eight molecules consistently

recovered the aberrant processing, with the only exception of the ExSpeU1 Ik33 that promoted an exon 20 inclusion with a lower efficiency (34%, Fig. 4.7C, lane 10).

To better understand the relative potency of the molecules at not saturating conditions, I evaluated their efficiency at lower doses by reducing the molar ratio between the ExSpeU1 and the minigene.

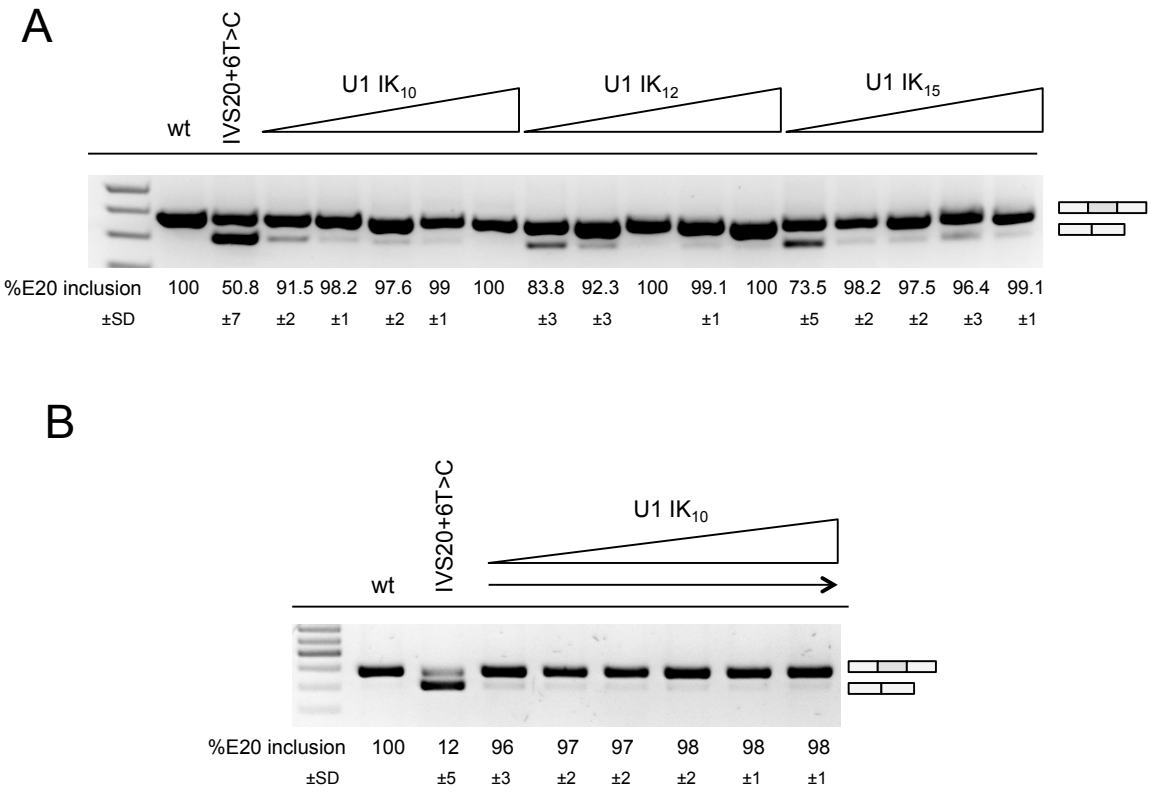

Figure 4.8 Dose-dependent effect of IKBKAP-ExSpeU1s

A) Splicing pattern of IKBKAP minigene co-transfected with an increased concentration of the ExSpeU1s Ik10, Ik12 and Ik15 in Hek293 cells. The amount of minigene was fixed to 500ng and co-transfected with increasing amount of ExSpeU1 (25ng, 50ng, 100ng, 200ng, 400ng).

B) Splicing pattern of IKBKAP minigene co-transfected with an increased concentration of the ExSpeU1 Ik10 in the neuronal SH-SY5Y cell line. The amount of minigene was fixed to 500ng and co-transfected with increasing amount of ExSpeU1 (25ng, 50ng, 100ng, 200ng, 400ng, 800ng).

The RT-PCR products were separated on 2% agarose gels. The upper bands correspond to transcripts including the exon 20, whereas the lower bands correspond to exon 20 skipping. The percentages of exon inclusion, calculated with ImageJ software, and standard deviations are reported below as a mean of three independent experiments.

Accordingly, I co-transfected the Hek293 cells with a fixed concentration of the *IKBKAP* mutant minigene and with increasing amounts of three ExSpeU1s (Ik10, Ik12, Ik15; Fig.

4.8A). These three ExSpeU1s showed a strong impact on the alternative splicing, promoting an exon inclusion with a percentage of 91%, 83% and 73% at the lowest molar ratio of 1:20 for the ExSpeU1s Ik10, Ik12 and Ik15, respectively (Fig. 4.8A, lanes 3, 8, 13). In this experiment, the ExSpeU1 Ik10 displayed the strongest correction already at the lowest molar ratio, which was also observed in the neuronal cell line, with a percentage of exon 20 inclusion of 96% at the lowest molar ratio of 1:20 (Fig. 4.8B, lane 3). Thus, even though the molecular mechanisms by which IKBKAP-ExSpeU1s exert their positive activity on the correction of the FD splicing defect, these experiments demonstrated the significant strength of these molecules, allowing the selection of the ExSkeU1 Ik10 as the most active modified U1 for the correction of the FD splicing defect.

4.6 Antisense U7smOPT snRNA targeting IKBKAP intron 20 does not improve exon recognition

To provide insights into the mechanism behind the splicing correction promoted by ExSpeU1s, I assessed the impact on *IKBKAP* splicing pattern using a U7snRNA targeting the identical intronic region of the IKBKAP-ExSpeU1s. The antisense properties of modified U7 snRNA make it a good tool to address the question whether our ExSpeU1s are acting as direct-involved splicing molecules or as antisense molecules masking an unknown intronic splicing silencer (ISS) within IKBKAP intron 20 (Fig. 4.9A). For this reason, I modified the previously used U7 snRNA by replacing the original binding tail with the binding region of two of the most active IKBKAP-ExSpeU1s, the Ik10 and Ik15. Accordingly, I co-transfected the IKBKAP mutant minigene with these two modified U7 snRNAs (U7 Ik10 and U7 Ik15) in the neuronal cell line. Twenty-four hours post transfection, I extracted the total RNA and analyzed it by specific RT-PCR amplification. The gel electrophoresis showed that both U7 Ik10 and U7 Ik15 induce skipping with a percentage of exon 20 inclusion that goes from 43% to 0% (Fig. 4.9B, lanes 4 and 5). The nature of the single band products was confirmed by direct-sequencing, corresponding to the transcript lacking of the exon 20.

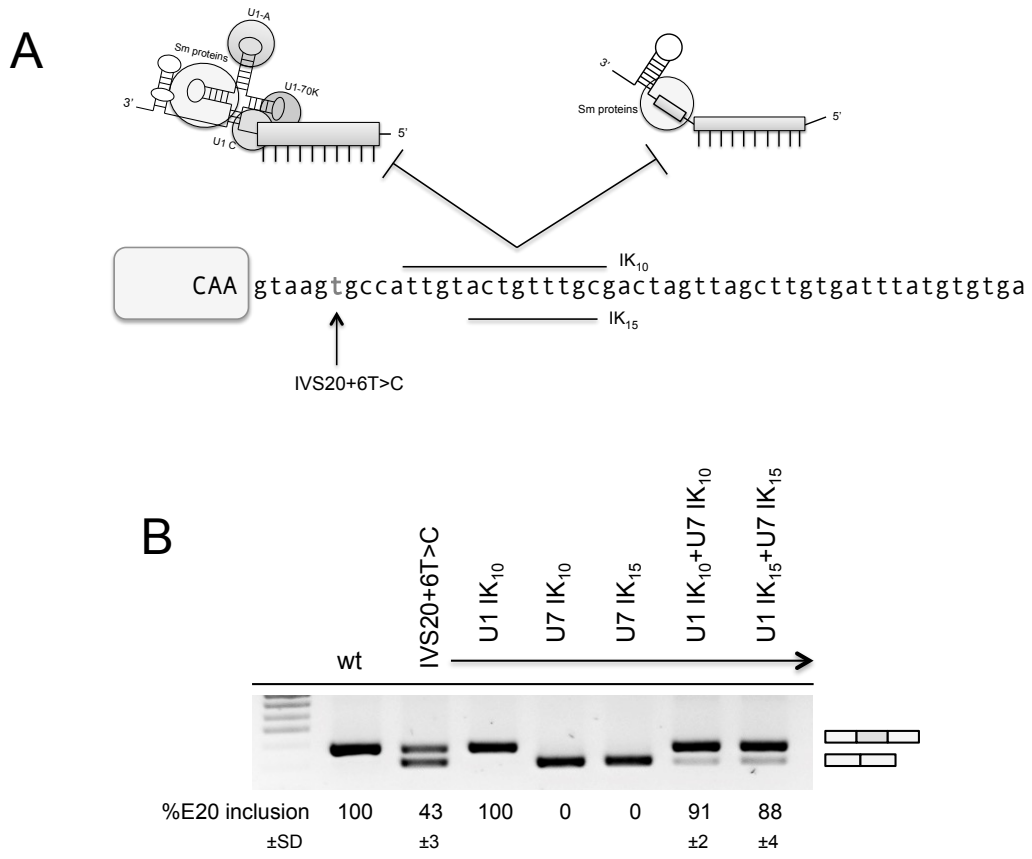

Figure 4.9 Characterization of the IKBKAP-ExSpeU1s molecular activity

A) Schematic representation of the binding regions of the U7 and U1 snRNAs Ik10 and Ik15 within the IVS20 sequence.

B) Splicing pattern of IKBKAP minigenes co-transfected with the U7 and U1 molecules in Hek293 cells. The modified U7 snRNAs contain the same binding sequences of the ExSpeU1s Ik10 and Ik15. The RT-PCR products were separated on 2% agarose gels. The upper band of 260bp corresponds to transcripts including the exon 20, whereas the lower band of 187bp represents exon 20 skipping. The amount of exon 20 inclusion was quantified with the software ImageJ. The percentages of exon inclusion and standard deviations are shown below as a mean of three independent experiments.

To ensure that the modified U7 snRNAs were produced and targeting the correct intronic sequences, I co-transfected the IKBKAP-U7 snRNAs together with their respective ExSpeU1s. In this experiment, the PCR amplification displayed a competition between the U7 and U1 snRNAs, as highlighted by the rescue of splicing with a percentage of exon inclusion of approximately 90% (Fig. 4.9B, lanes 6 and 7). As control, the co-transfection of the mutant IKBKAP minigene along with the ExSpeU1 Ik10 resulted in a complete correction of the aberrant splicing (Fig. 4.9B, lane 3). This result demonstrates that: i) the U7 snRNAs are produced and bind to the correct target; ii) the ExSpeU1s are not acting as

antisense molecules but their effect is probably due to U1 snRNP/spliceosome-mediated mechanism. Furthermore, the enhanced exon skipping observed after the addition of the IKBKAP-U7 snRNAs could be due to the presence of a positive *cis*-acting element (ISE) located within the *IKBKAP* IVS20, which is masked by the antisense molecule.

4.7 Effect of ExSpeU1 Ik10 at protein level

To further evaluate the ExSpeU1s activity, I took the advantage of a second minigene system that permits the splicing analysis at the protein level. In particular, I adopted the pFLARE-5GdP vector that is characterized by the co-presence of the coding sequences for the green fluorescent protein (GFP) and the red fluorescent protein (RFP). This useful tool is usually adopted for the screening of the effect of chemical compounds on splicing. The two fluorescent protein cDNAs are placed in tandem with the GFP coming first (Fig. 4.10A). At the beginning of the GFP's cDNA is placed an intronic sequence that can be used to insert a sequence of interest. In particular, the exogenous sequence must contain an adenine at its 3' end because the start codon of the GFP is missing it can be given only by the exogenous sequence of interest which has to be incorporated into the mature transcript. Accordingly, if the pre-mRNA processing promotes the inclusion of the exon of interest, it will result with the expression of the GFP; on the contrary, if splicing induces exon skipping, the start codon of GFP will be lost, resulting in the expression of the RFP.
Therefore, taking advantage of this GFP/RFP minigene system, I analyzed the IKBKAP-ExSpeU1s effect not only at the mRNA level but also at the protein one. Indeed, the adenine at 3' end of the *IKBKAP* exon 20 makes it a perfect candidate for the analysis through this pFLARE system. Accordingly, the wild type sequence of *IKBKAP* exon 20 has been cloned in the pFLARE backbone, generating the wt minigene, and the IVS20+6T>C was successively inserted by site-specific mutagenesis, creating the mutant minigene. I transfected these two plasmids in the neuronal SH-SY5Y cells and analyzed them forty-eight hours post-transfection by confocal microscopy.

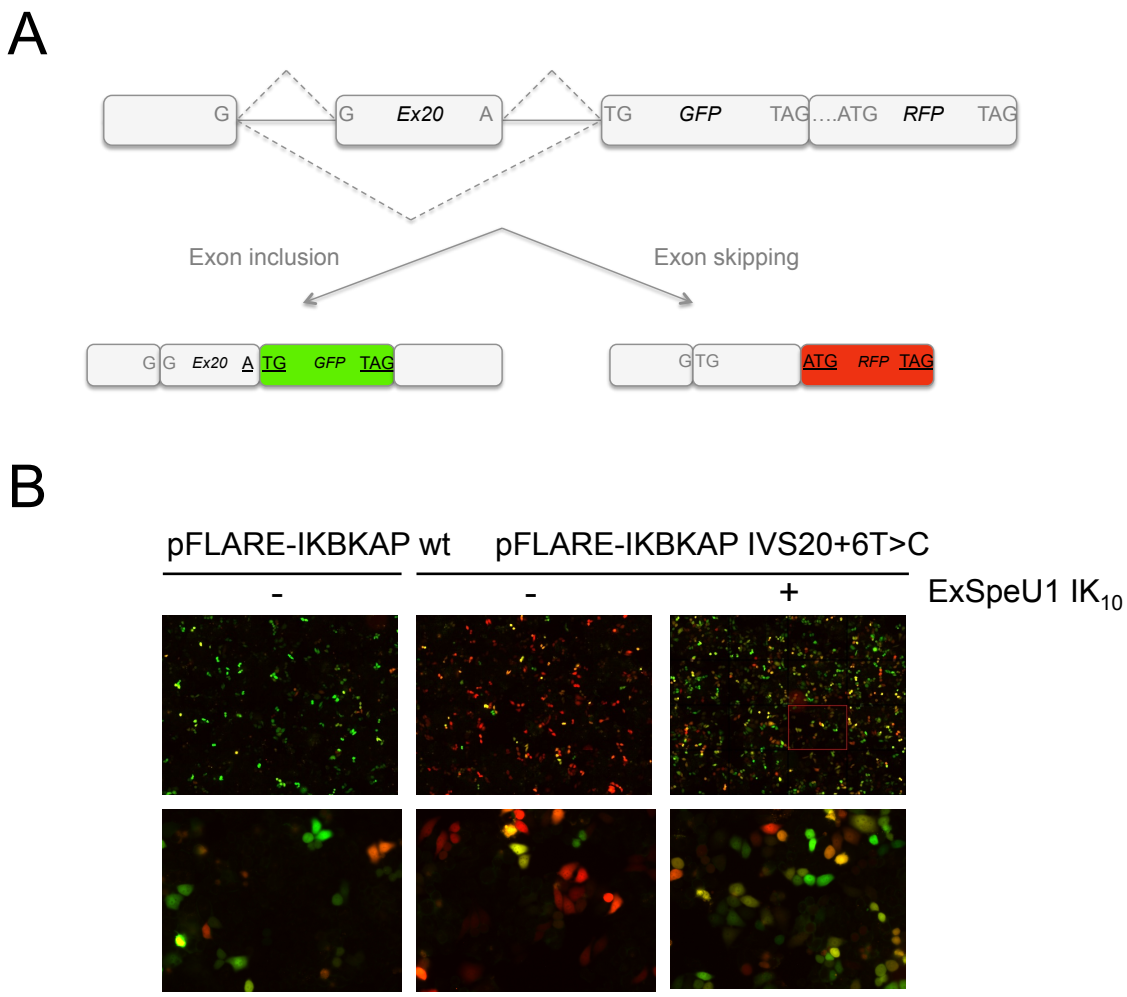

Figure 4.10 Effect of the ExSpeU1 Ik10 on the pFLARE-IKBKAP minigene

A) Schematic representation of the pFLARE-IKBKAP plasmid. The IKBKAP exon 20 and part of its flanking introns were cloned in the pFLARE backbone, before the coding sequences of the green fluorescent protein (GFP) and red fluorescent protein (RFP). Start and stop codons of fluorescent proteins are shown within boxes. Exon inclusion results in the expression of the GFP due to the last adenine of exon IKBKAP 20 that provides the start codon of the GFP. Exon skipping does not provide the start codon to the GFP, resulting in the expression of the RFP.

B) Confocal analysis of the splicing pattern of the IKBKAP exon 20 in wild type (left), mutant (center) and mutant plus ExSpeU1 Ik10 (right) conditions. The experiment was performed in SH-SY5Y cells and analyzed 48 hours after transfection. The relative expression of GFP and RFP was calculated with ImageJ sofware.

The aberrant splicing induced by the *IKBKAP* intronic mutation was confirmed also in this fluorescent minigene system, as showed by a relative percentage of GFP expression of 15% in the mutant minigene (Fig. 4.10B, center). On the other hand, the wild type minigene displayed a relative percentage of GFP expression of 97% (Fig. 4.10B, left). This

result confirmed the aberrant processing caused by FD mutation, providing a valuable model to further test the efficacy of the IKBKAP-ExSpeU1s.

Consequently, I repeated the experiment by co-transfecting the mutant pFLARE minigene together with the most active ExSpeU1 Ik10 in the neuronal cells. As previously done, forty-eight hours after transfection, I analyzed the expression of the two fluorescent proteins, observing a remarkable improvement in the aberrant splicing as displayed by a relative percentage of GFP expression of 92% (Fig. 4.10B, right). The relative expression of the GFP, indeed, was significantly improved from the 15%, in the mutant context, to the 92%, in the presence of the ExSpeU1 Ik10.

This result confirms the positive data obtained previously with our pTB-IKBKAP minigenes, providing a clear evidence that the activity exerted by the ExSpeU1s on splicing is reflected also at the protein level.

4.8 Effect of ExSpeU1 Ik10 at mRNA and IKAP protein levels in patients' fibroblasts

After two minigenes contexts, I challenged the corrective efficacy of the selected ExSpeU1 Ik10 in fibroblasts from FD patients, carrying the main IVS20+6T>C mutation. To overcome the known low transfection efficiency of this kind of cells I exploited the LV transduction. Therefore, two different lentiviral vectors were created by inserting the whole U1 cassette in the SIN lentiviral backbone, one carrying the gene encoding for the ExSpeU1 Ik10 and one encoding the wild type U1 snRNA (Fig. 4.11A).

To evaluate the ExSpeU1 Ik10 activity in *ex-vivo*, I firstly transduced the FD fibroblasts with different conditions: increasing values of multiplicity of infection (MOI), ranging from 0 (untreated) to the maximum of 20, and with the presence/absence of the compound polybrene (Fig. 4.11B). This molecule is usually adopted to reduce the electronegativity between the cells' surface and the viral particles, thus increasing the transduction's efficiency.

Seventy-two hours post-transduction, I harvested the cells and collected for the RNA analysis. After the extraction of total RNA, I used a set of primers to specifically amplify the *IKBKAP* region from exon 19 to exon 21. The RT-PCR amplification showed a significant effect of the ExSpeU1 Ik10 on the endogenous IKBKAP exon 20 inclusion

(Fig. 4.11B). The best splicing correction was obtained at MOI 10 and MOI 20 of the lentiviral particles expressing the ExSpeU1 Ik10 (Fig. 4.11B, lanes 3-6). The presence of polybrene improved the transduction efficiency, as shown by the complete exon 20 inclusion. On the other hand, the ExSpeU1 Ik10 MOI 1 displayed a significant improvement only in the presence of polybrene, with a percentage of exon inclusion of 82% (lane 2), while its absence did not ameliorate the aberrant splicing (lane 1). Untreated cells and cells transduced with different conditions of the LPs expressing the wild type U1 snRNA did not affect the aberrant processing, showing an approximate exon 20 inclusion of 65% (Fig. 4.11B, lanes 7-11).

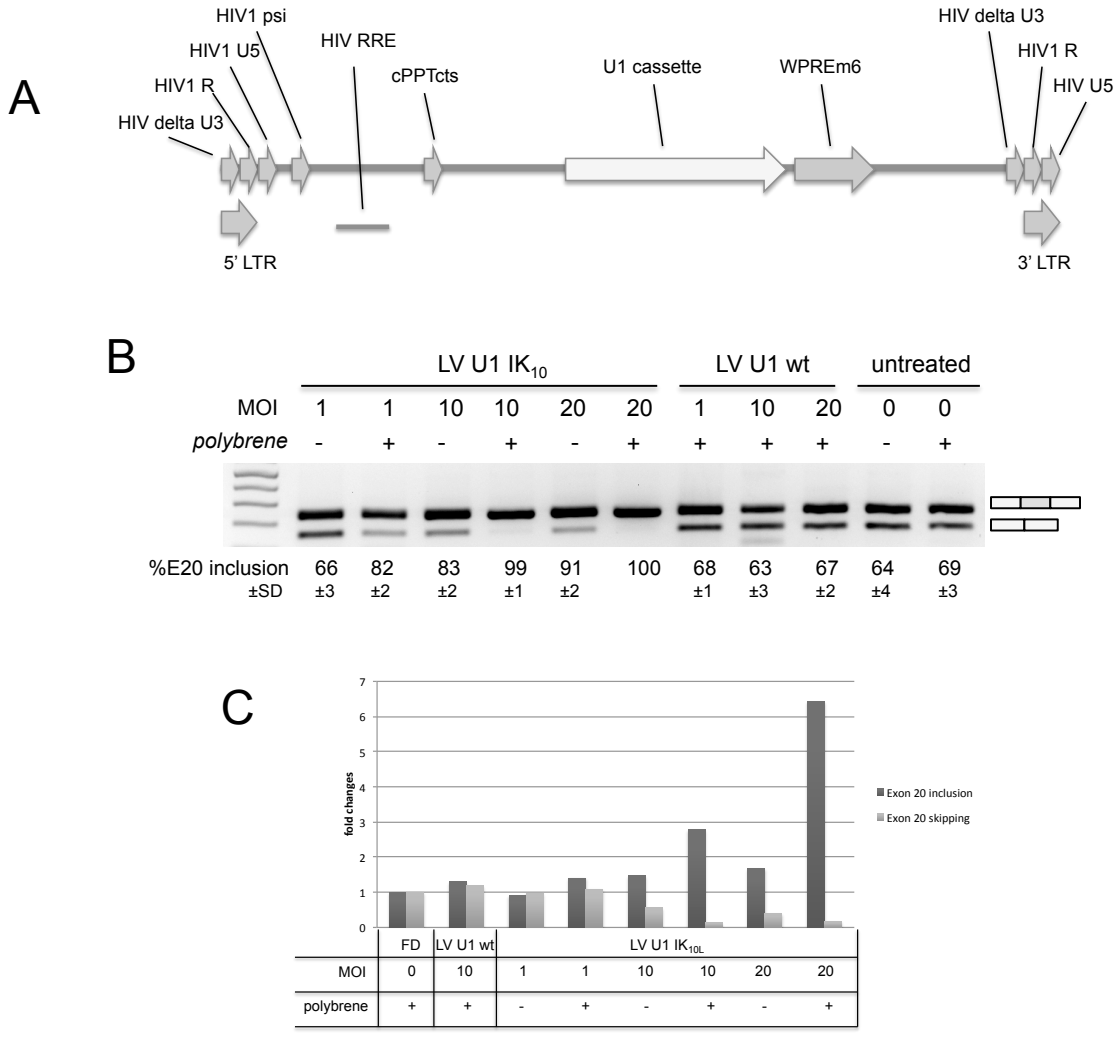

Figure 4.11 ***Ex-vivo*** **analysis of the ExSpeU1 Ik10 activity**

A) Schematic representation of the lentiviral backbone carrying the ExSpeU1 Ik10 cassette. The U1 cassette contains the entire gene with its own promoter elements and its 3' end box.

B) Splicing pattern of *IKBKAP* after lentiviral transduction with different values of MOI of FD fibroblasts. The RT-PCR products were separated on 2% agarose gels. The upper band of 260bp

corresponds to transcripts including the exon 20, whereas the lower band of 187bp represents exon 20 skipping. Exon 20 inclusion was quantified with the software ImageJ. The percentage of exon 20 inclusion and standard deviation is reported below as a mean of three different experiments.

C) Real time PCR analysis of the IKBKAP transcripts carrying the exon 20 and of IKBKAP transcripts lacking the exon 20 from the FD fibroblasts treated with LV-ExSpeU1 Ik10, LV-U1 wt and untreated. Samples were normalized for 18S.

The positive effect promoted by ExSpeU1 Ik10 was confirmed by real time PCR, where I observed a 3 to 6 fold change in the amount of IKBKAP full-length transcripts in the cells treated with MOI 10 and 20 of ExSpeU1 Ik10, respectively (Fig. 4.11C, lanes 6 and 8, dark grey). Concomitantly, the amount of aberrant transcripts was reduced almost to 0 (Fig. 4.11C, lanes 6 and 8, light grey). Cells treated with other conditions did not show any significant change on the amount of aberrant and normal transcripts, confirming the observations obtained by the qualitative PCR (Fig. 4.11C, lanes 1-4).

To confirm the obtained results, I repeated the experiment on fibroblasts from another FD patient (Fig. 4.12). Accordingly, I transduced the FD cells with different MOIs in the presence of polybrene. As before, seventy-two hours post infection, I extracted the total RNA and analyzed it by RT-PCR. The PCR amplification confirmed the efficacy of the ExSpeU1 Ik10 to correct the aberrant splicing of FD. As expected, the strongest correction was observed with MOI 10 and MOI 20, showing a complete exon 20 inclusion (Fig. 4.12A, lanes 2 and 3). The infection with MOI 1, on the other hand, displayed a lower but significant efficacy, with a percentage of exon inclusion of 83% (lane 1). Furthermore, untreated cells and cells treated with the U1 WT did not correct the aberrant splicing, showing a percentage of exon 20 inclusion of approximately 52% (lanes 4-6). Together, these results confirm the previous data, supporting the corrective effect of the ExSpeU1 Ik10 at the mRNA level.

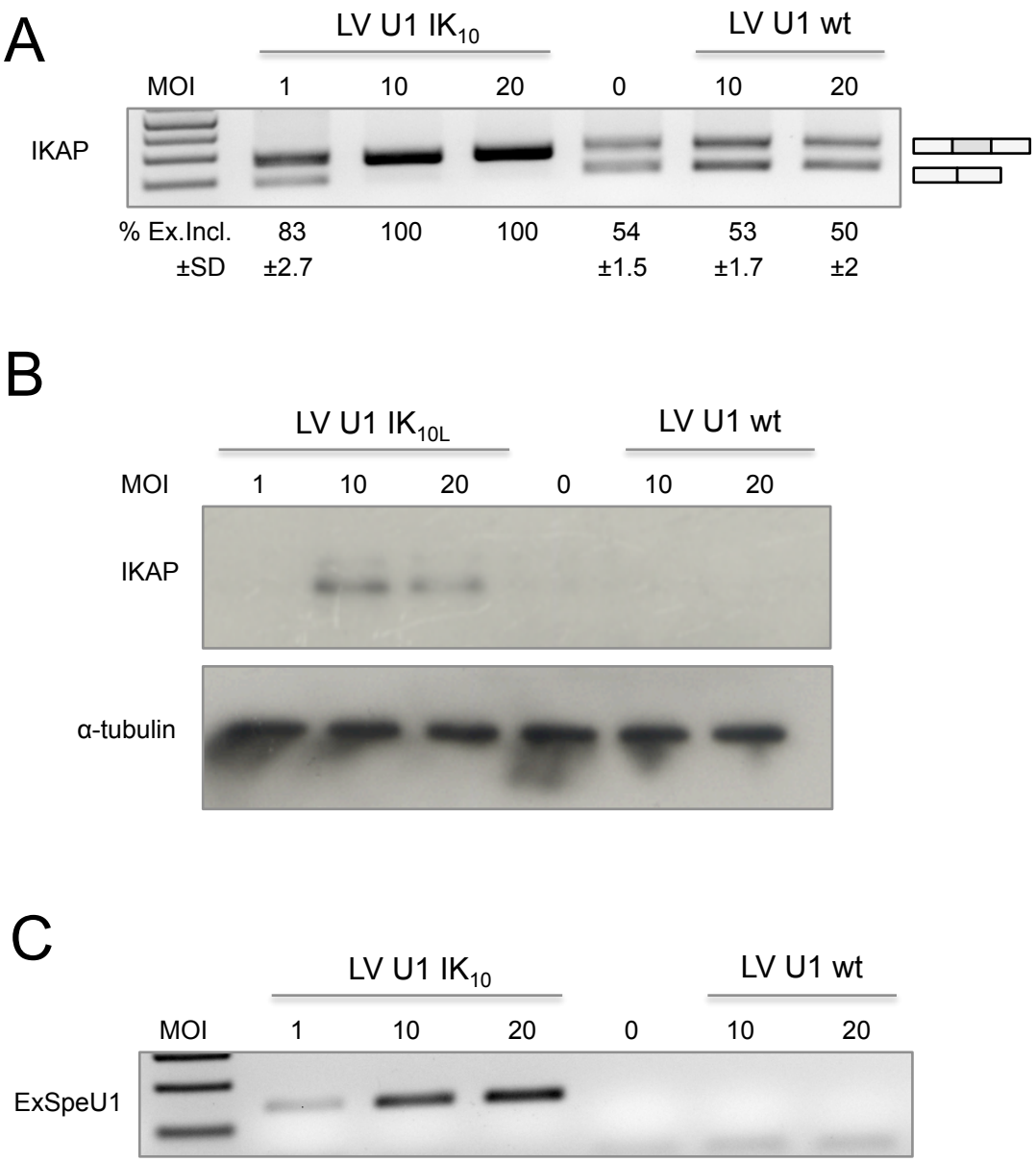

Figure 4.12 ***Ex-vivo*** **IKAP restoration mediated by the ExSpeU1 Ik10**

A) Splicing pattern of endogenous *IKBKAP* from FD fibroblasts after lentiviral delivery of ExSpeU1 Ik10, wild type U1 and from untreated fibroblasts. The RT-PCR products were separated on 2% agarose gel. The upper band of 260bp corresponds to transcripts including the exon 20, whereas the lower band of 187bp represents exon 20 skipping. The Exon 20 inclusion was quantified with the software ImageJ. The percentages of exon 20 inclusion and standard deviations were reported below as mean of three independent experiments.

B) Western blot analysis of the IKAP protein from FD fibroblasts transduced with ExSpeU1 Ik10, U1 wt and untreated. Samples were normalized with α-tubulin.

C) RT-PCR analysis of ExSpeU1 Ik10 expression from transduced FD fibroblasts. The PCR amplification was run on a 2% agarose gel.

To evaluate the ExSpeU1 Ik10 activity at the IKAP protein level, I addressed the treated fibroblasts by western blotting using a specific antibody. As shown in figure 4.12B, IKAP protein was detected in fibroblasts treated with MOI 10 and MOI 20 of the ExSpeU1 Ik10, whereas MOI 1 and control conditions did not display any signal.

To evaluate the expression levels of the ExSpeU1 Ik10, I performed a semi-quantitative PCR with a set of primers designed to specifically amplify the modified U1 snRNA. As shown in figure 4.12C, the RT-PCR displayed a dose-dependent amplification, confirming the increasing ExSpeU1s' expression according to its concentration. On the other hand, as expected, the RT-PCR on control samples did not show any amplification.

All together, these positive results in *ex-vivo* conditions demonstrate the therapeutic potential of ExSpeU1 Ik10 for the aberrant splicing of FD and provide the basis to move forward in the evaluation of their efficacy *in-vivo*.

4.9 In-vivo effects of ExSpeU1s sm25 and sm37 in the mild SMA animal model

The unavailability of an appropriate animal model that recapitulates the genotype and phenotype of Familial dysautonomia limited the *in-vivo* evaluation of the ExSpeU1s' approach. For this reason, I have investigated the *in-vivo* activity in the model of Spinal Muscular Atrophy (SMA), for which both animal models and specific SMN-ExSpeU1s are available.

To evaluate the ExSpeU1s' efficacy *in vivo*, I initially chose a mild mouse model of spinal muscular atrophy (SMA), the 5058 mouse. This model is a knock-out for the endogenous murine *smn* gene that, however, contains four copies of the human *SMN2* gene. Due to the relative high number of *SMN2* copies, this model exhibits a mild phenotype without any affection on the animal's survival. The main phenotypic feature that characterize this mouse model consists of a necrotic tail that is completely lost six weeks after birth. This mouse model is a good candidate for the evaluation of strategies aimed at splicing correction because of the only presence of the human *SMN2*.

In this thesis, I explored the *in-vivo* efficacy of two of the previously described ExSpeU1s for SMA, the ExSpeU1 sm25 and sm37 [2]. Since the α-motor neurons are the therapeutic targets for SMA, the two molecules were cloned into the adeno-associated virus serotype 9 (AAV9), which is known to pass the blood brain barrier (BBB) and reach the central

nervous system (CNS) [165]. Also the wild type U1 snRNA was inserted into the AAV9 backbone, in order to be used as control.

According to the number of treatments, I divided the newborn mice in four groups: AAV9-ExSpeU1 sm25, AAV9-ExSpeU1 sm37, AAV9-U1 wt and saline. Therefore, I treated each group by intraperitoneal (IP) injections with approximately 25ul/animal of the relative solution at post natal day 0 (PND0) and PND2. To firstly assess the response to the treatment, I weekly monitored both weight and tail lenght of the treated mice (Fig. 4.13A and B).

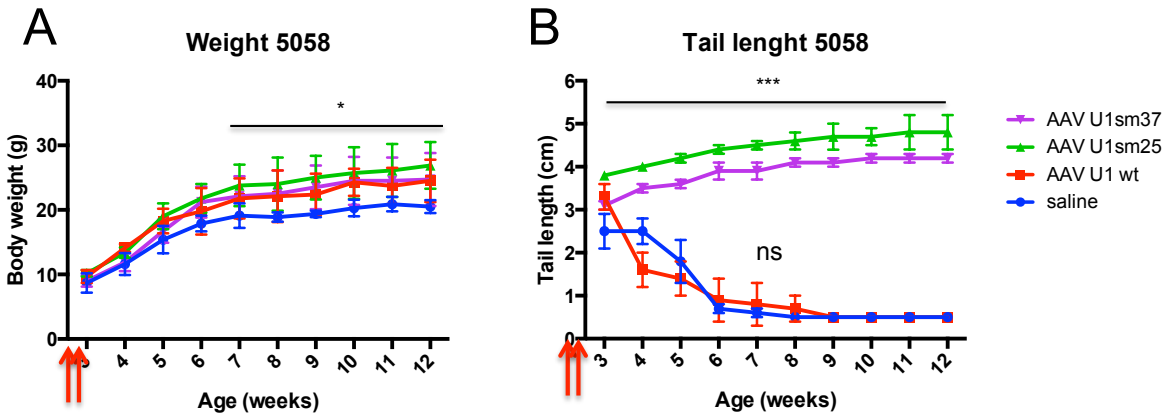

Figure 4.13 Systemic delivery of ExSpeU1 sm25 and sm37 prevents tail necrosis in SMA mild mouse.

A) Body weight and B) tail measurements of SMA mild mice treated with AAV9-U1sm25 (n=10), AAV9-U1sm37 (n=7), AAV9-U1 WT (n=6) and saline (n=14). Body weight and tail lenght were measured weekly for a period of three months. The red arrows at the bottom of graphs indicate the time of injections. Data are presented as mean + SD. *, P<0,05; **, P<0,01; ***, P<0,0001; all compared with saline controls.

As shown in figure 4.13B (and Fig. 4.14A, right mouse), treatment with AAV9-ExSpeU1 sm25 and sm37 significantly improved the phenotypic defect, without any sign of tails' necrosis. On the other hand, saline- and AAV9-U1 wt treated mice displayed the typical necrotic tails from the fourth week after birth, which were completely lost at nine weeks after birth (Fig. 4.14B, right mouse).

To date, nine months after birth, the tails of animals treated with AAV9-ExSpeU1 sm25 and sm37 are still present without showing the characteristic necrosis (Fig. 4.14B, left mouse). Body weights did not show any remarkable difference between the four groups,

only mice treated with AAV9-ExSpeU1 sm25 are slightly heavier, probably due to the longer tail. (Fig. 4.13A).

A

B

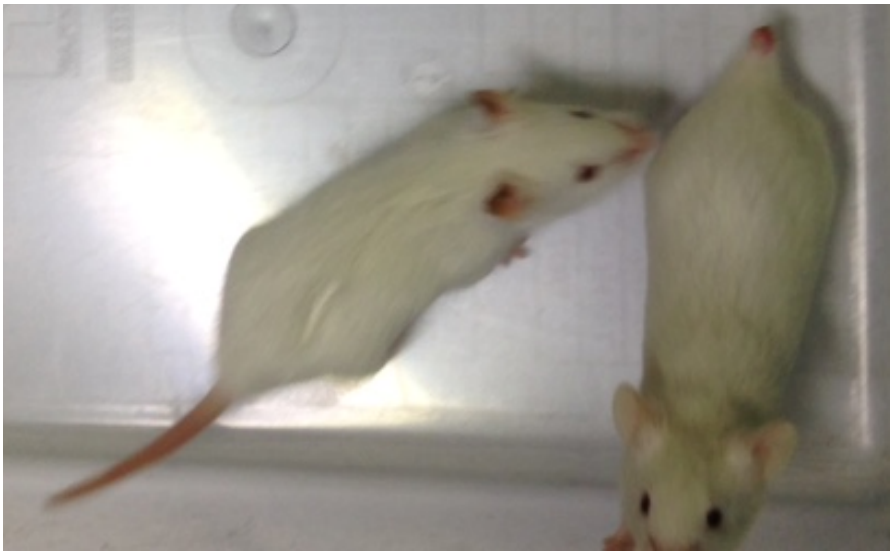

Figure 4.14 Phenotypic features of the mild 5058 SMA model

A) Four weeks old 5058 mice from the same litter. The mild SMA on the left was treated with saline, displaying the typical necrotic tail. The mild SMA mouse on the right was treated with the AAV9-ExSpeU1 sm25 and displays a healthy tail.

B) Nine weeks old 5058 mice from the same litter. The mild SMA on the left was treated at PND0 and PND2 with the AAV9-ExSpeU1 sm25, displaying a short but healthy tail; the mouse on the right was treated with saline and displays the typical phenotypic feature of this mouse model as shown by the complete absence of the tail.

Since the 5058 is a knockout for *smn* and carries only the human *SMN2* transgene, I also analyzed the ExSpeU1 effect on the *SMN2* splicing pattern. In order to evaluate the

efficacy of ExSpeU1s on splicing, another group of 5058 treated mice were sacrificed at PND 7 following the extraction of: brain (B), liver (L), heart (H), kidney (K), muscle (M) and spinal cord (SC). The splicing analysis was performed after RNA extraction and RT-PCR amplification. ExSpeU1 sm25 and ExSpeU1 sm37, but not the WT U1 and saline showed an increase in the *SMN2* splicing pattern in several tissues (Fig. 4.15).

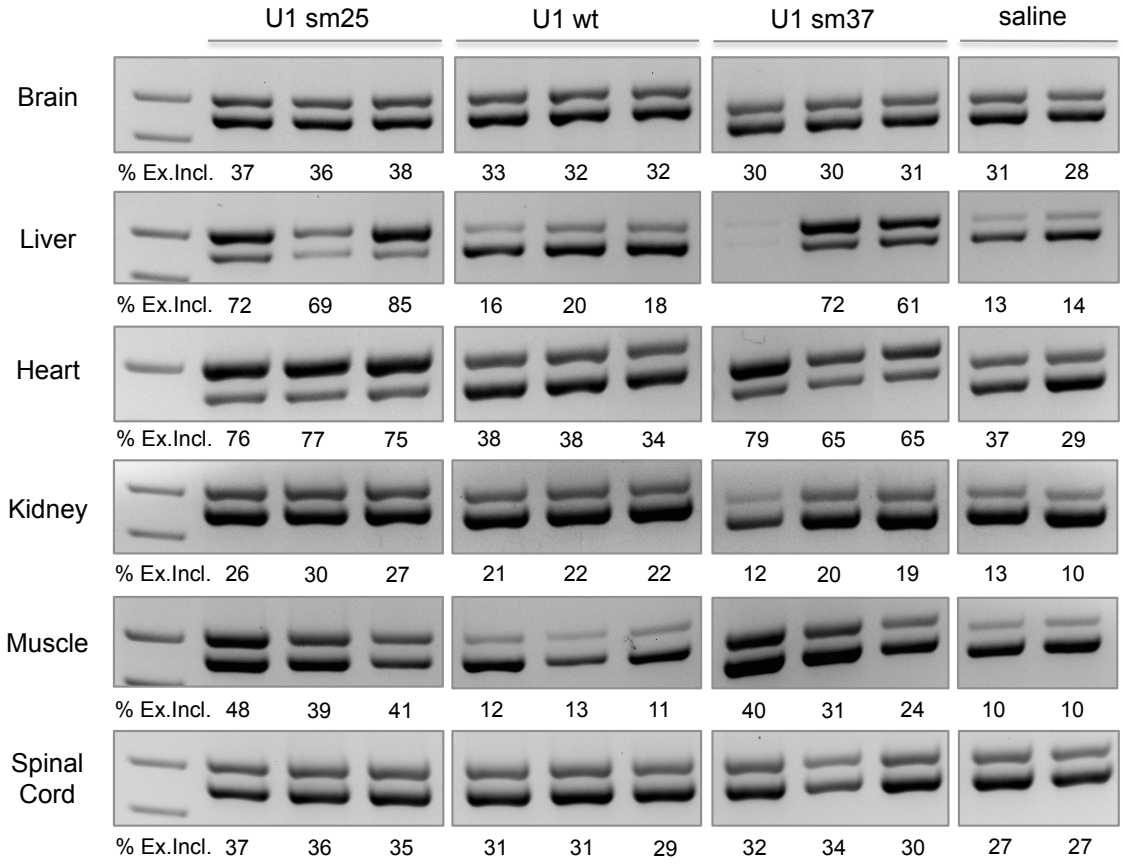

Figure 4.15 SMN splicing correction mediated by ExSpeU1 sm25 and sm37 in SMA mild mouse. Tissues from SMA mice were analyzed by RT-PCR at PND7 after injections at PND0 and PND2 with the different solutions (AAV9-U1sm25, AAV9-U1 WT, AAV9-U1 sm37 and saline). The upper band of 505 bp represents SMN2 exon 7 inclusion, whereas the lower band of 451 bp consists of SMN2 exon 7 skipping. Percentage of exon inclusion was quantified with ImageJ and reported below each amplification.

Their activity displayed an organ-dependent response, probably due to the AAV9 biodistribution after IP injection. With this analysis I distinguished high and low responsive tissues (Fig. 4.16A and B). Liver, heart and muscle are tissues with the highest percentage of splicing correction (Fig. 4.16A), in which the ExSpeU1 sm25 promoted the strongest effect with an increase in the percentage of exon inclusion from 13±0.3 to 75±8.6

in liver, from 33±6 to 76±1 in heart and from 10±0.1 to 42±4.7 in muscle. The ExSpeU1 sh37 showed a slightly lower effect in the same organs, promoting an exon inclusion from 13±0.3 to 66±7.8 in liver, from 33±6 to 69±8.3 in heart and from 10±0,1 to 32±7.8 in muscle. The treatment with the control U1 WT did not display any improvement compared to the saline. On the other hand, a lower splicing-correcting response was observed in brain, kidney and spinal cord, where the ExSpeU1 sm25 promoted exon inclusion with a percentage from 29.5±2.1 to 37±1 in brain, from 11±2.3 to 28±1.9 in kidney and from 27±0.3 to 36±1.1 in spinal cord (Fig. 4.16B). The ExSpeU1 sm37 was less efficient in these tissues, displaying a percentage of exon inclusion from 29.5±2.1 to 30.3±0.6 in brain, from 11±2.3 to 17±4.4 in kidney and from 27±0.3 to 32±2.2 in spinal cord. As observed for the high responsive tissues, also in these tissues the U1 WT did not promote any further improvement compared to saline.

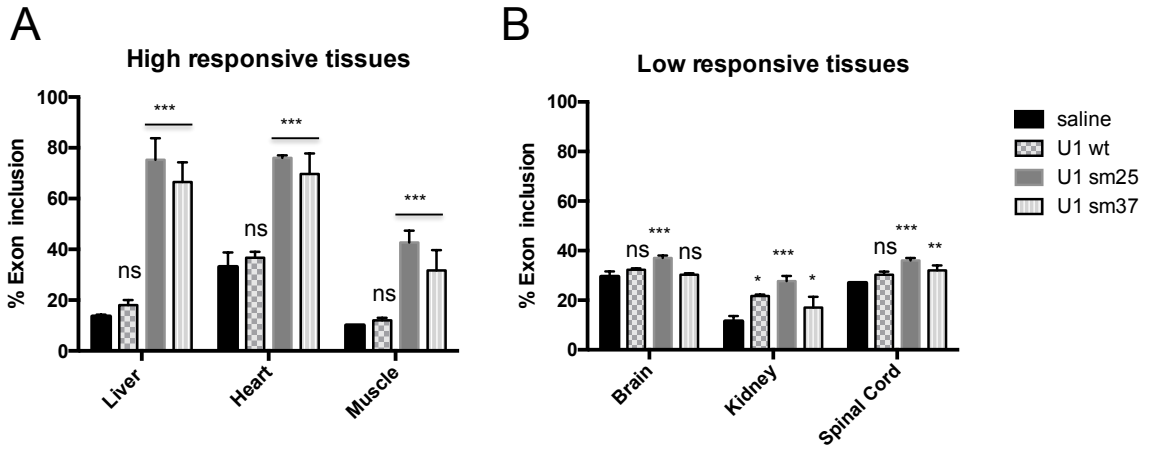

Figure 4.16 SMN splicing correction mediated by ExSpeU1 sm25 and sm37 in SMA mild mouse. RNA was extracted at PND7 from six different tissues of the SMA mild 5058 mouse model (n=3).

A) High responsive tissues: data obtained from RT-PCR analysis of liver, heart and muscle show a high percentage of exon inclusion promoted by ExSpeU1 sm25 and sm37.

B) Low responsive tissues: data obtained from RT-PCR analysis of brain, kidney and spinal cord show a lower splicing correction induced by ExSpeU1 sm25 and sm37. Data are presented as mean + SD. *, P<0,05; **, P<0,01; ***, P<0,0001; all compared with saline controls.

Even if both ExSpeU1 sm25 and ExSpeU1 sm37 promoted a significant exon inclusion, in general ExSpeU1 sm37 showed a slightly lower effect in comparison to ExSpeU1 sm25. This might be particularly important in brain and spinal cord tissues, where small increases

in the percentage of exon inclusion might result in a significant difference on the phenotype.

4.10 *In-vivo* effects of ExSpeU1s sm25 in the severe SMA TAIWANESE model

SMA is the primary genetic cause of infant mortality with a survival of approximately two years for the severe type I. Thus, the question was to evaluate the efficacy of our molecules at correcting the most important parameter, such as the survival. To evaluate the therapeutic activity of the AAV9-ExSpeU1, I used the severe Taiwanese SMA mouse model, that is characterized by a survival of 10-12 days due to the presence of two copies of *SMN2* and the absence of the murine *smn*.

In this model, I evaluated the effect of the most active ExSpeU1 sm25 on the following parameters: i) survival, ii) body weight and tail length, iii) neuromuscular behavior. Therefore, I divided the Taiwanese mice in three groups according to the treatments (AAV9-ExSpeU1 sm25, AAV9-U1 wt and saline), which I injected intraperitoneally with 25ul/animal of relative solutions at PND0 and PND2. Normally, the pathological phenotype is observable from the seventh day after birth, period at which is already possible to interpret the success of the treatment. At this age, the SMA-affected mice treated with the AAV9-ExSpeU1 sm25 did not show any typical SMA feature, providing a first evidence of the positive effect promoted by this molecule (Fig. 4.17A). Apart from a shorter tail and a smaller weight, these mice displayed a normal behavior without any compromised movement. On the other hand, SMA-affected mice treated with saline and AAV9-U1 wt displayed a reduced body weight, reduced movements and tremors (Fig. 4.17B and C).

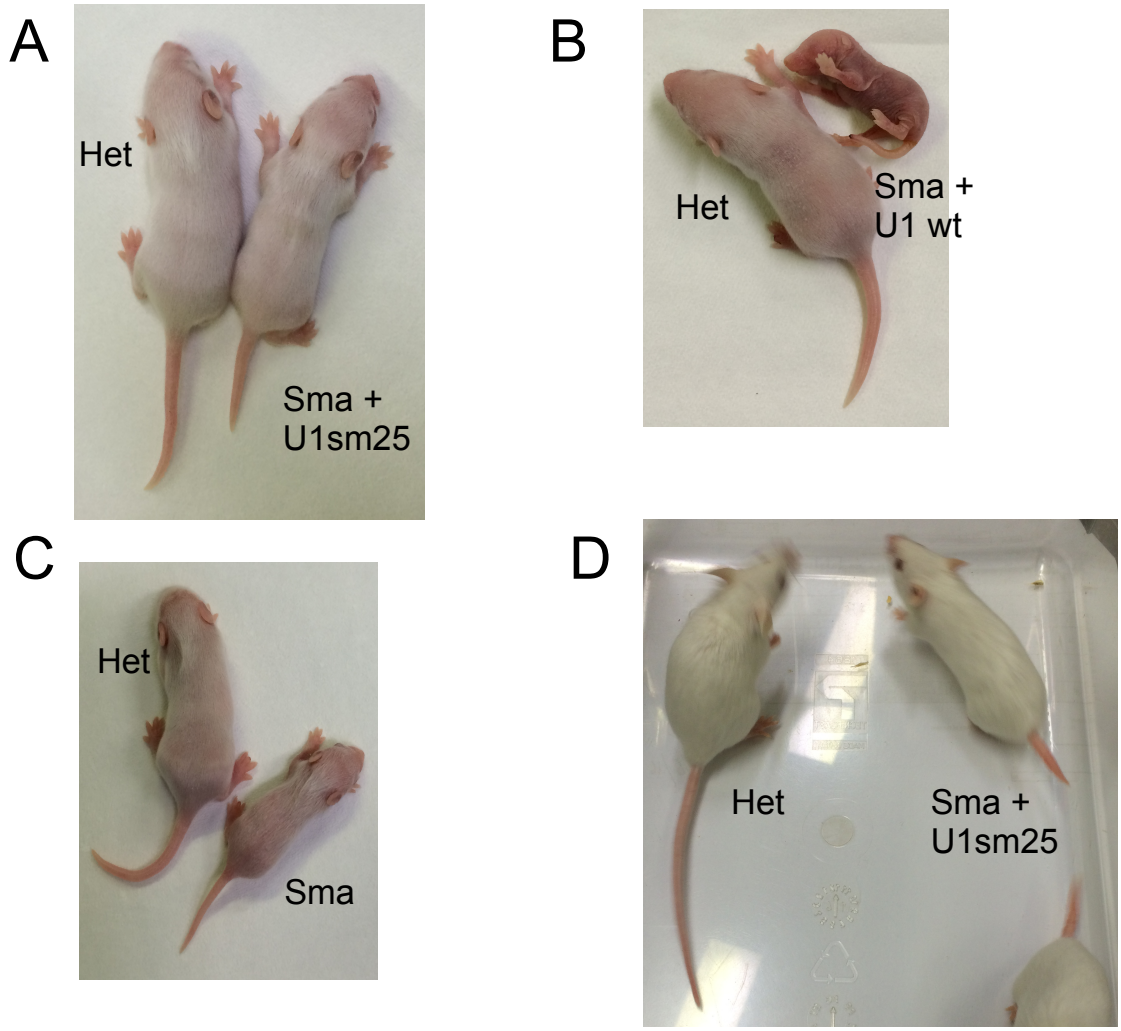

Figure 4.17 Phenotypic features of the severe Taiwanese model

A) Heterozygous (left) and SMA treated with ExSpeU1 sm25 (right) mice at PND7

B) Heterozygous (left) and SMA treated with U1 wt (right) mice at PND7

C) Heterozygous (left) and untreated-SMA affected (right) mice at PND7.

D) Heterozygous (left) and SMA treated with ExSpeU1 sm25 (right) mice at PND30.

As shown in figure 4.18, the treatment with the AAV9-ExSpeU1 sm25 significantly improved the survival of the Taiwanese model, rescuing the most important parameter from a survival of approximately 10 days to a survival that goes beyond a period of 250 days. To date, 40% of ExSpeU1 sm25-treated mice (four out of nine) are alive and healthy at 250 days after birth. On the other hand, the treatments with saline and AAV9-U1 wt did not revert the pathology, whereas all the heterozygous mice treated with saline, U1 WT or ExSpeU1 sm25 are alive and healthy at 250 days after birth. All the SMA Taiwanese mice treated with saline and AAV9-U1 wt died or were euthanized due to the serious pathological conditions by the twelfth day after birth.

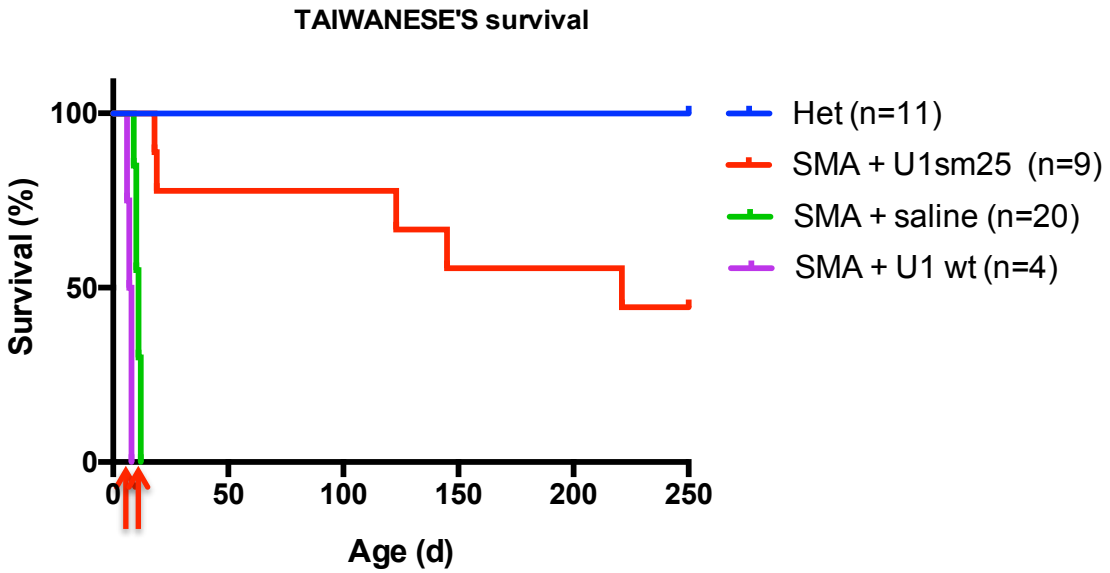

Figure 4.18 Survival analysis of the severe SMA Taiwanese mouse model.

Survival of severe SMA mouse was rescued by intraperitoneal injection with AAV9-ExSpeU1 sm25. Kaplan-Meier curves show the survival of SMA mice (smn -/-; SMN2 2Tg/-) treated with AAV9-U1sm25 (n=9), AAV9-U1 WT (n=4), saline (n=20) and a total of 11 heterozygous mice (Het, smn +/-; SMN2 2Tg/-), which consist of 3 animals treated with saline, 4 animals treated with AAV9-U1sm25, and 4 animals treated with AAV9-U1 WT. The red arrows indicate the time of injections.

Consequently, I monitored both body weight and tail length of the SMA-affected mice treated with the ExSpeU1 sm25 and of the heterozygous mice. As shown in figure 4.19A, both groups progressively improved the body weight, supporting the positive effect induced by the treatment with the ExSpeU1 sm25. SMA-affected mice treated with the ExSpeU1 sm25 displayed a lower body weight and a 2 centimeter shorter tail compared to the heterozygous mice (Fig. 4.19B). Heterozygous mice, instead, displayed a progressive increase in the tail length that reached the maximum length of 8 cm at one month after birth.

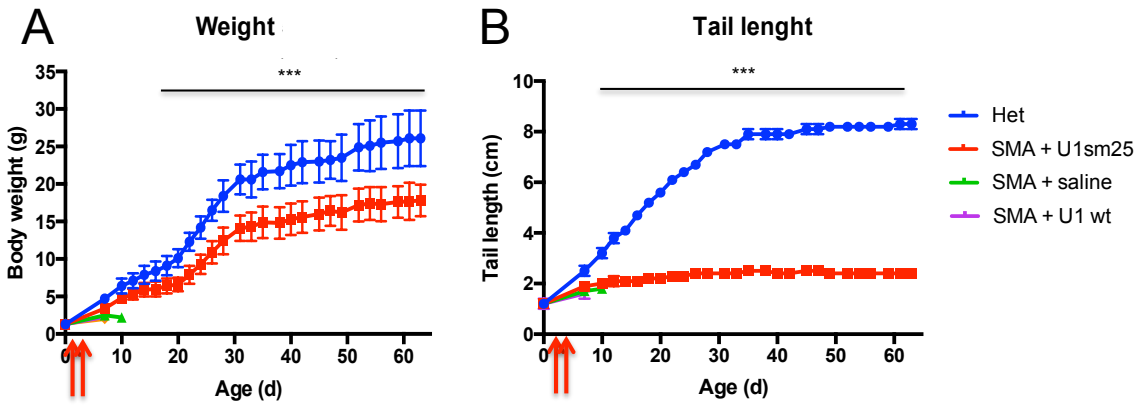

Figure 4.19 Body weight and tail lenght analysis in the severe SMA mice.

A) Body weight and B) tail's lenght were measured on a daily basis up to two months. A total of 11 heterozygous mice (smn +/-, SMN2 2Tg/-) were measured, consisting of 3 animals treated with saline, 4 animals treated with AAV9-U1sm25, and 4 animals treated with AAV9-U1 WT. A number of 9 SMA mice (smn -/-, SMN2 2Tg/-) have been treated with AAV9-U1sm25, 4 animals with AAV9-U1 WT and 20 animals with saline. The red arrows show time of injections. Data are presented as mean + SD. *, P<0,05; **, P<0,01; ***, P<0,0001 between Het mice and SMA mice treated with AAV9-U1sm25.

Finally, since the treatment with the ExSpeU1 sm25 displayed a significant improvement in both survival and pathological phenotype, I further investigated its effect on the neuromuscular behavior. Loss of motor neurons, indeed, results in a neuromuscular deficiency that compromises the physiological movements. To establish the positive effect developed by ExSpeU1 sm25 on the severe SMA mice, SMA-treated and heterozygous mice were submitted to two neurofunctional tests, such as rotarod and the four limbs hanging tests (Fig. 4.20).

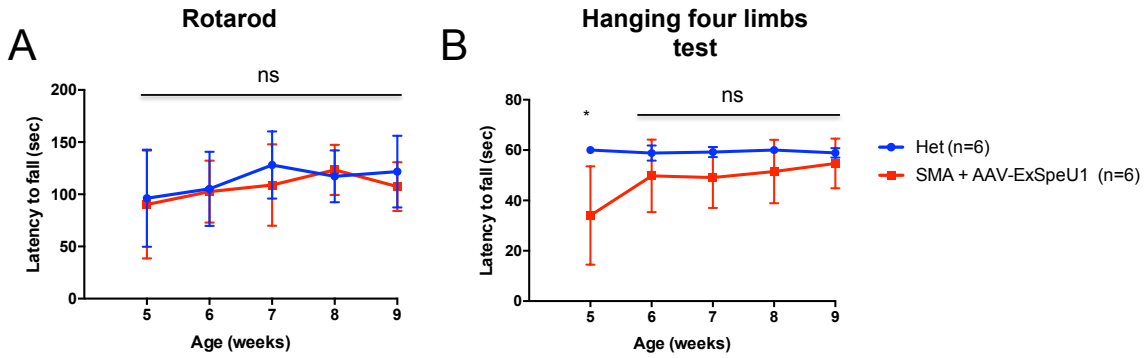

Figure 4.20 Systemic treatment with ExSpeU1 sm25 recover the neuromuscular functionality in the severe SMA mouse.

Five weeks old heterozygous (n=6) and SMA-affected treated with AAV9-U1 sm25 (n=6) mice were tested to establish a baseline performance and successively retested weekly for a total of 5 weeks.

A) Rotarod test: animals were subjected to an accelerating profile rotarod, receiving three trials per time. The means ± SD of the duration of balance or latency to fall (maximum 150 seconds) for the three trials were recorded.

B) Hanging four limbs test: grip strength of animals was measured by testing the ability of the mice to remain clinging to an inverted cage lid for a maximum of 60 seconds. The means ± SD of the latency to fall was recorded for three trials. Data are presented as mean + SD. *, P<0,05; all compared with heterozygous.

The four limbs grip test measures the capacity of a mouse to hold itself against gravity, while the rotarod is a functional test that measures the capacity to stay on a small-moving rotating surface. As represented in figure 4.20A, the rotarod test did not show any difference between the groups. Also in the hanging test (Fig. 4.20B) mice treated with the ExSpeU1 sm25 were not different from the controls (Het animals treated with saline): the only significant difference was observed at 5 weeks when mice first experienced these tests. Overall, in both rotarod and hanging tests the heterozygous and the SMA-treated with sm25 mice did not show any significant difference, demonstrating the efficacy of this molecule and, more in general, of the ExSpeU1s strategy to positively revert the pathological conditions caused by splicing defects.

Chapter 5

DISCUSSION

5.1 Coupled RNA and protein processing impaired by the frequent HA missense mutation p.Arg2016Trp

Missense mutations, through amino acids substitution, are known to impair either the biosynthesis or the activity of the corresponding protein. Recently, several evidences highlighted the impact of this type of mutations also at the RNA level, exerting a negative influence on the pre-mRNA processing that compromises the protein outcome [54]. In this thesis, I initially investigated the effect of the FVIII missense mutation p.Arg2016Trp (c.6046C>T) that represents the second most frequent cause (8%) of Haemophilia A in Italy and one of the most frequent missense changes in the HA database [71]. This mutation has been found associated with moderate/severe forms and variable FVIII antigen (<1% to 5%) and activity (<1 to 2%) levels in patients. The nucleotide change in position c.6046C>T is located within the exon 19 of the coagulation FVIII, which encodes for part of the FVIII A3 domain. The resulting arginine to tryptophan substitution might have an important biochemical impact on the polypeptide chain, which could involve in a significant structural change with negative effects on either the secretion or the function of the blood coagulation FVIII (Table 1).

Mutation	Context	Nucleotide	Amino acid	Type	Cyclic	Size	Hydrophobicity	Charge
p.Gly2013Arg	wild type	6037 G	Gly	aliphatic	acyclic	small	Hydrophobic	Neutral
	mutant	*6037 A*	*Arg*	*basic*	*acyclic*	*large*	*Hydrophilic*	*Positive*
p.Trp2015Cys	wild type	6045 G	Trp	aromatic	Cyclic	large	Hydrophobic	Neutral
	mutant	*6045 C*	*Cys*	-	*acyclic*	*medium*	*Hydrophilic*	*Neutral*
p.Arg2016Trp	wild type	6046 C	Arg	basic	acyclic	large	Hydrophilic	Positive
	mutant	*6046 T*	*Trp*	*aromatic*	*cyclic*	*large*	*Hydrophobic*	*Neutral*
p.Arg2016Leu	wild type	6047 G	Arg	basic	acyclic	large	Hydrophilic	Positive
	mutant	*6047 T*	*Leu*	*aliphatic*	*acyclic*	*large*	*Hydrophobic*	*Neutral*
p.Val2017Met	wild type	6049 G	Val	aliphatic	acyclic	medium	Hydrophobic	Neutral
	mutant	*6049 A*	*Met*	-	*acyclic*	*large*	*Hydrophobic*	*Neutral*
p.Glu2018Gly	wild type	6053 A	Glu	acidic	acyclic	large	Hydrophilic	Negative
	mutant	*6053 G*	*Gly*	*aliphatic*	*acyclic*	*small*	*Hydrophobic*	*Neutral*
p.Val2035Ala	wild type	6104 T	Val	aliphatic	acyclic	medium	Hydrophobic	Neutral
	mutant	*6104 C*	*Ala*	*aliphatic*	*acyclic*	*small*	*Hydrophobic*	*Neutral*
p.Asn2038Ser	wild type	6113 A	Asn	-	acyclic	medium	Hydrophilic	Neutral
	mutant	*6113 G*	*Ser*	-	*acyclic*	*small*	*Hydrophilic*	*Neutral*

Table 1 Biochemical differences between wild type and mutant amino acids in FVIII variants within exon 19.

Therefore, I started my study by analyzing the biochemical effect of the missense mutation on both the secretion and the activity of this FVIII variant. By taking advantage of a codon-optimized FVIII cDNA devoid of the FVIII B-domain [163] and of a lentiviral expression system in CHO cells, I found that the recombinant rFVIII-2016W variant is secreted at appreciable levels (11.0±0.4% of rFVIIIwt) and, in chromogenic assay, displayed an half-reduced specific activity (6.0±2.9% of rFVIIIwt) (Fig. 4.1B). These *in-vitro* results showed a discrepancy with the described FVIII activity levels in patients (<1-2%). A possible explanation of the difference between the *in-vitro* and the *in-vivo* results could be given by an impaired RNA processing that, reducing the amount of full-length transcripts, decreases also the final protein's quantity. Accordingly, I have examined the FVIII exon 19 splicing in three patients of the Italian cohort that carry this missense mutation. Albeit at the ectopic level, RT-PCR amplifications of the FVIII genomic region from exon 18 to exon 20 displayed an altered splicing pattern with a percentage of exon 19 inclusion of approximately 70% (Fig. 4.2B), which is consistent with the analysis of ectopic RNAs in two patients as showed by *Theopillus et al* [72]. In order to characterize the effect of the mutation on the pre-mRNA processing of the *F8* exon 19, I created an artificial system based on a hybrid F8 minigene that contains the FVIII genomic region affected by the missense mutation. The expression of this system in hepatic cells confirmed the aberrant splicing observed in patients' samples, reducing the exon 19

inclusion from 93±2% to 70±5% (Fig. 4.2B). This result supports the negative effect of the p.Arg2016Trp substitution on the pre-mRNA processing of the FVIII, providing a first evidence of pleiotropic effects at the RNA processing, protein secretion and protein activity.

5.2 FVIII exon 19 contains an Exonic Splicing Regulatory Element (ESRE) and is affected by several HA missense mutations that induce exon skipping

To understand the molecular mechanisms involved in the exon 19 skipping, I initially evaluated the strength of its splice sites through bioinformatics analysis that displayed weak donor and acceptor sites, explaining the alternative splicing caused by the c.6046C>T mutation (Fig. 4.2A). To verify the hypothesis that the effect of the mutation depends on the inherently "weak" exon 19, I improved by mutagenesis the authentic F8 exon 19 5'ss of the mutant minigene (F8 exon 19 5'ss HC). Indeed, the complementarity between the F8 exon 19 donor site and the wild type U1 snRNA is reduced by four mismatches (Fig. 4.3A). The U1 snRNA usually interacts with the 5' ss through its 5' binding tail that physically targets nine nucleotides on the exon-intron boundary of the donor site. Therefore, the improvement of the F8 exon 19 donor site increased the communication between the wild type U1 snRNA and the 5'ss (Fig. 4.3B). The *in-vitro* experiment with this implemented F8 minigene showed a strong splicing correction, demonstrating the weakness of the donor site and suggesting that the HA-causing nucleotide change could affect an exonic splicing regulatory element (ESRE) (Fig. 4.3E lane 6).

Therefore, in order to characterize the nature of this exonic splicing regulatory element, I exploited a U7 snRNA antisense molecule (U7 F8exon19) masking the exonic region affected by the missense mutation (Fig. 4.3D). If the exonic regulatory element has enhancing properties (ESE), by masking this region with the antisense molecule, the exon inclusion would be inhibited; on the contrary, if the splicing regulatory element acts as silencer (ESS), by masking it with the U7 F8ex19, the exon inclusion would be positively enhanced. Co-transfection of F8 wild type and c.6046C>T minigenes with the U7 F8ex19 molecule clearly showed a negative effect on the exon 19 inclusion, reducing it to approximately 10% and 0% in wild type and mutant contexts, respectively (Fig. 4.3E lanes

2 and 4). The inhibitory effect of the U7 F8ex19 has been observed also in the F8 minigene with the implemented donor site, decreasing its inclusion from 100% to 70% approximately (Fig. 4.3E lane 7). These results indicate that F8 exon 19 contains an exonic regulatory splicing element (ESRE) with enhancing properties that is partially affected by the p.Arg2016Arg mutation.

The identification of an ESRE within the *F8* exon 19 prompted me looking for other natural HA mutations that, affecting this regulatory element might induce exon skipping. Among the mutations described in the FVIII database, I identified in this region five natural F8 missense mutations that are associated to moderate/severe HA: the p.Gly2013Arg (c.6037G>A), p.Trp2015Cys (c.6045G>C), p.Arg2016Leu (c.6047G>T), p.Val2017Met (c.6049G>A), p.Glu2018Gly (c.6053A>G) (Fig. 4.4A). To study their effect on the F8 splicing, I introduced these mutations in the F8 hybrid minigene system. Transfection experiments demonstrated that two of these missense changes significantly displayed a negative effect on the exon 19 processing. In particular, c.6037G>A (p.Gly2013Arg) and c.6053A>G (p.Glu2018Gly) remarkably reduced exon 19 inclusion from >90% to ~40% and 30%, respectively (Fig. 4.4B, lanes 3 and 5).

Since mutations that are in proximity of splice sites are likely to impair splicing, I also addressed the missense mutations p.Val2035Ala (c.6104T>C) and p.Asn2038Ser (c.6113A>G). These two missense variants are in proximity of the F8 exon 19 donor site and, thus, could potentially affect the recognition of exon 19 inducing its skipping. The experiment in hepatic cells showed the p.Asn2038Ser significantly affects the recognition of exon 19, reducing its inclusion to 26% (Fig. 4.4B, lane 7), whereas the p.Val2035Ala did not induce any aberrant splicing.

The identification of three missense mutations (c.6037G>A, c.6053A>G and c.6113A>G) that significantly influence the F8 exon 19 inclusion, with >60% of exon skipping, prompted me to investigate their effect on the protein biology taking advantage of the previously described rFVIII. Indeed, due to the significant properties of the amino acid changes (Table 1), they are likely to have a repercussion also on the structure and function of the crucial FVIII A3 domain.

Therefore, I expressed the three variants (rFVIII-2013Arg, rFVIII-2018Gly and rFVIII-2038Ser) in the CHO cells through the lentiviral-mediated delivery, analyzing their secretion and activity levels by ELISA and chromogenic assays, respectively (Fig. 4.5). In addition, I also considered the FVIII variant that results from the skipping of exon 19 (rFVIIIΔ19), since the deletion of this exon does not change the reading frame and encodes for a FVIII protein deleted of 39 amino acids in the A3 domain.

The expression of these rFVIII molecules showed that:

i) the rFVIII-2013Arg is poorly secreted (7.0±0.9% of rFVIIIwt) and maintains a normal specific activity (8.4±0.8% of rFVIIIwt);

ii) the rFVIII-2018Gly is well secreted (69.0±18.1% of rFVIIIwt) and displays a significant reduced specific activity (19.4±2.3% of rFVIIIwt);

iii) the rFVIII-2038Ser is well secreted (112.9±35.2% of rFVIIIwt) and maintains a normal specific activity (99.6±12.5% of rFVIIIwt);

iv) the rFVIIIΔ19 was not detected in both assays, demonstrating that is not responsible of the low FVIII levels in HA patients.

These results clearly demonstrates that missense mutations do not exclusively impair the protein biology, but they might also influence the pre-mRNA processing. In this thesis, indeed, I characterized several FVIII missense mutations with a coupled impairment of the RNA and protein processing, providing additional information for the interpretation of the low FVIII levels *in-vivo* (Table 2).

FVIII exon 19 variants		rFVIII:C* (%)	ex19 inclusion (%)	FVIII:C inferred (%)	FVIII:C (%)	HA Patients n°	Concordance
HGVS	Legacy AA No.						
p.G2013R	1994	8.4±0.8	41±3	2.8-4.0	<1	1	+
p.R2016W	**1997**	**6.0±2.9**	**70±5**	**2.0-6.7**	**0-5**	**61**	**+++**
p.E2018G	1999	19.4±2.3	28±2	4.4-6.5	1-4	7	++
p.N2038S	2019	99.6±12.5	26±2	20.9-31.4	5-20	10	+++

Table 2 Comparison between *in-vitro* and *in-vivo* FVIII levels.

The expression of rFVIII variants does not undergo to RNA-processing. Therefore, I calculated an "expected FVIII level" considering the results obtained in the splicing assay in relation with the Ag and chromogenic results of rFVIII, in order to compare it with the plasma FVIII levels in patients.

Furthermore, these results provide a second important aspect, such as the opportunity to develop new tailored therapeutic strategies aimed at correcting the splicing defect.

5.3 FVIII exon 19 skipping: a model for innovative therapeutic strategies based on modified U1 snRNAs

To date, several splicing-switching strategies have been described to correct splicing defects, one of those is based on modified U1 snRNAs [166]. In my previous experiments I showed that a reduced interaction with the U1 snRNP at the donor site results in a poor definition of the exon 19 inducing some degree of exon skipping even in the absence of exonic mutations. Therefore, this experiment provided me the rationale for the evaluation of modified U1 snRNAs as therapeutic strategy to rescue the aberrant F8 exon 19 splicing. As shown in the mutant c.6046C>T context, the exogenous *trans*-acting factor efficiently restored the aberrant splicing, promoting exon 19 inclusion with a percentage of 94% (Fig. 4.3E, lane 5). Therefore, since I identified three additional natural HA missense mutations (c.6037G>A, c.6053A>G and c.6113A>G) whose splicing was severely affected, I investigated the potential of this molecule on the aberrant splicing caused by the F8 mutation c.6113A>G, which displayed the strongest negative effect on the inclusion of F8 exon 19. Co-transfection with the U1 F8ex19 efficiently rescued the aberrant splicing with a percentage of exon 19 inclusion of approximately 98% (Fig. 4.6). This significant result demonstrates the therapeutic potential of splicing-switching molecules, such as modified U1 snRNAs, to correct splicing defects caused by missense mutations. Indeed, even if the missense mutations exert a negative impact on the protein biology (reduced secretion or activity), the splicing correction increases the amount of full-length transcripts, leading to the production of more protein that, even if defective, might significantly improve the pathological phenotype. In this example, the c.6113A>G variant represents a perfect candidate for a splicing-correction approach, since both the secretion and the activity were not affected by the amino acid change. The rescue of its aberrant splicing would result in higher secretion levels of FVIII, reverting the HA phenotype of the patients carrying this variant.

5.4 Therapeutic potentials of ExSpeU1s for Familial dysautonomia

Recently, our laboratory demonstrated the therapeutic potential of a new class of modified U1 snRNAs that are designed to specifically bind to intronic sequences downstream of aberrantly spliced exons, the Exon Specific U1s (ExSpeU1s) [1]. This important feature significantly reduces the potential off-targets due to the recognition of less-conserved sequences. In the past years, we demonstrated the applicability of these molecules in

several diseases, including haemophilia B, cystic fibrosis, spinal muscular atrophy and Netherton syndrome[1][162][161][2]. These molecules efficiently corrected the splicing defects caused by different type of mutations, such as synonymous, missense and intronic substitutions [1].

Here, in order to further evaluate the efficacy of these molecules and to amplify the diseases models for which ExSpeU1s might represent a therapeutic opportunity, I focused on a neurological disorder caused by an intronic mutation (IVS20+6C>T) that impairs the pre-mRNA processing of the *IKBKAP* gene, leading to the exclusion of exon 20 [78]. This disease, known as Familial dysautonomia (FD), represented a good model to test the efficacy of the ExSpeU1s because, as demonstrated by the Ast's group, the IVS20+6 T>C substitution significantly reduces the affinity between the donor site and the endogenous U1 snRNA [167]. In addition, to date, there are no specific therapies available for this pathology and, unfortunately, gene therapy replacement is not a feasible approach due to the wide *IKBKAP* size. For these reasons, I addressed the question whether ExSpeU1s could be a potential answer to treat FD patients, by developing eight IKBKAP-ExSpeU1s that specifically bind to the intronic downstream region of exon 20 (from position +2 to position +40) (Fig. 4.7B).

To investigate the splicing-correcting activity of these molecules, I took advantage of two different minigene systems. The first one, based on our pTB-globin hybrid plasmid in which was cloned the *IKBKAP* genomic region from intron 18 to intron 22, allowed the analysis at the RNA level; whereas the second one, based on a pFLARE-GFP/RFP reporter expression according to the inclusion/exclusion of the *IKBKAP* exon 20, allowed the study at protein level using a reporter. In both systems, the intronic point mutation displayed the characteristic aberrant splicing observed in FD patients with a strong exon 20 skipping (Fig. 4.7 and 4.10). On the other hand, the wild type context did not affect the pre-mRNA splicing, leading to a complete exon 20 inclusion. Therefore, looking at the RNA and protein levels, these two systems recapitulated the in-vivo splicing defect of FD.

Since FD is a neurological disorder with the most pronounced exon 20 skipping in the dorsal root ganglia, I tested all the eight IKBKAP-ExSpeU1s in a neuronal cell line along with the pTB-IKBKAP minigene, observing a significant positive effect promoted by these molecules (Fig. 4.7C). In particular, seven out of eight ExSpeU1s completely restored the aberrant splicing with a 100% of exon inclusion. Dose-dependent experiments confirmed the efficiency of ExSpeU1s at low concentrations, identifying the ExSpeU1 Ik10 as the most performing molecule with a percentage of exon 20 inclusion of 96±3% in a 1:20 molar ratio (Fig. 4.8). Consequently, I evaluated the efficacy of this selected ExSpeU1

Ik10 in the second pFLARE-IKBKAP minigene. Co-transfection of the mutant minigene along with the ExSpeU1 Ik10 significantly improved the relative GFP expression from 15% to 92%, confirming the correction of the *IKBKAP* splicing defect (Fig. 4.10).
These results clearly demonstrate that ExSpeU1s represent an innovative therapeutic opportunity to correct the aberrant splicing caused by the intronic FD mutation and indicate the ExSpeU1 Ik10 as the most performing molecule.

5.5 IKBKAP-ExSpeU1 Ik10 does not act as antisense but actively promotes exon 20 recognition

ExSpeU1s efficiently rescued the aberrant *IKBKAP* splicing in two minigene systems, but the molecular mechanism by which they exert the corrective activity remains unclear. The large amount of *cis*- and *trans*-acting factors involved into the exon-intron recognition make splicing a complicate process that has to be looked under the hand lens in every different pathological context. These factors can play either a positive or negative role, enhancing or inhibiting the exon definition, and mutations within transcripts can alter their information leading to pathological conditions [40]. In the past decade, one of the most used molecular tool used to correct aberrant splicing is based on antisense oligonucleotide (ASO) sequences that, binding to specific regions of the transcript, physically block the recognition of certain regulatory elements and therefore improve splicing. It might be possible that IKBKAP-ExSpeU1s are masking an intronic splicing silencer (ISS) within the intron 20 and, therefore, correcting the aberrant *IKBKAP* splicing through an antisense mechanism. For this reason, in order to evaluate that the IKBKAP-ExSpeU1s are actively involved in the splicing reaction and that are not masking an intronic regulatory element, I took advantage of the U7 snRNA as antisense molecule.
Accordingly, I modified the U7 snRNA by replacing its original binding tail with the binding sequences of the IKBKAP-ExSpeU1s Ik10 and Ik15 (Fig. 4.9). Co-transfection experiments with the pTB-IKBKAP minigenes and the U7 snRNAs Ik10 and Ik15 resulted in a complete exon 20 skipping. This result supports the hypothesis of a splicing regulatory elements within the intron 20 that, instead of behaving like a silencer, possesses enhancing properties (ISE). Therefore, the IKBKAP-ExSpeU1s are not acting as antisense molecules but are more likely working as spliceosome-related active molecules. To further

demonstrate that the outcomes obtained with the U7 molecules were not artifacts, I co-transfected the mutant IKBKAP minigene with both the U7 snRNA and the corresponding ExSpeU1. This experiment resulted in a competition between the two molecules, where the ExSpeU1s gained the upper hand. Indeed, the aberrant *IKBKAP* splicing was rescued with a percentage of exon 20 inclusion of approximately 90%. This result confirms the active role of IKBKAP-ExSpeU1s that might be working as a spliceosome-directly involved molecule with no antisense masking effects. Furthermore, the negative effect exerted by the IKBKAP-U7 highlighted the presence of a positive *cis*-acting element (ISE) located within the intronic *IKBKAP* 20 sequence.

5.6 Ex-vivo efficacy of ExSpeU1 Ik10

Hybrid minigenes are useful artificial tools developed to isolate specific genomic contexts and to analyze the molecular elements involved in their RNA processing. However, due to their restricted properties, it might happen that the *in-vitro* outcomes differ from the physiological context. For this reason, I investigated the role of the ExSpeU1 Ik10 in a natural pathological condition, such as the one in fibroblasts from FD patients. Even though fibroblasts are not a perfect cellular model to test the *IKBKAP* aberrant splicing, due to the tissue-dependent splicing response, these cells naturally carry the intronic IVS20+6T>C mutation, providing a physiological context where to study the efficacy of the ExSpeU1 Ik10.

In this thesis, I assessed the ExSpeU1 Ik10 activity by the transduction with a lentivirus carrying the entire genetic sequence of this modified U1 snRNA and, as control, a lentivirus carrying the wild type U1 snRNA (Fig. 4.11A). Accordingly, I transduced FD fibroblasts with different experimental conditions, in order to assess the best parameters for a proper response. I observed the strongest effect at MOI 10 and MOI 20 of the lentivirus carrying the ExSpeU1 Ik10, showing a complete *IKBKAP* splicing correction (Fig. 4.11B and 4.12). This positive result was then confirmed by real time PCR, displaying a 3 to 6 times fold change of the full length IKBKAP transcript in the cells treated with MOI 10 and 20 of the ExSpeU1 Ik10, respectively (Fig. 4.11C). Further confirmation was given by western blot analysis for the IKAP protein, which was detected only in cells treated with these two MOI conditions (Fig. 4.12B). Polybrene showed up as a useful additive,

enhancing the viral infection and, thus, displaying beneficial results already at the lowest multiplicity of infection (MOI) 1. On the other hand, untreated and cells treated with the WT U1 snRNA did not improve the aberrant processing, showing an unaltered splicing pattern also at the highest concentrations of the U1 wt.

All together, these *in-vitro* and *ex-vivo* data demonstrate that IKBKAP-ExSpeU1s represent a valuable therapeutic opportunity to treat the splicing defect of FD. To date, indeed, there are no available therapies for this devastating disease, for which the only therapeutic approach consists of reducing the symptoms. In addition, unfortunately, gene therapy replacement does not represent an alternative because of the huge *IKBKAP* size that does not fit into the adeno-associated viruses. Therefore, to our knowledge, the only possible therapeutic strategy to effectively cure this disease is given by splicing-switching. In this direction, several compounds have been tested, displaying positive results [98][102][103]. However, although the positive impact on the *IKBKAP* aberrant splicing, the nature of these molecules is likely to have a negative and widespread repercussion on the processing of other genes. On the contrary, ExSpeU1s are specifically developed to bind the less-conserved intronic sequences, reducing the number of potential off-targets. Recently, indeed, it has been demonstrated that ExSpeU1s have a minimal genome-wide effect as observed with RNAseq analysis in a transgenic mouse model, that constitutively expressed a SMN-ExSpeU1 to correct the aberrant splicing of *SMN2* in SMA [2]. Therefore, the next step for the evaluation of ExSpeU1s as a therapeutic opportunity to treat Familial dysautonomia would be the investigation of their efficacy *in-vivo*. However, at that time, I could not perform this analysis due to the unavailability of a mouse model that recapitulated both phenotypic and genotypic features of FD. For this reason, I took on the ExSpeU1s' efficacy *in-vivo* in another pathological condition, such as spinal muscular atrophy.

5.7 ExSpeU1s activity *in-vivo*: gene therapy 2.0

Spinal muscular atrophy is a severe disease caused by the loss of the *survival of motor neuron* (*smn*) *1* gene, whose severity depends on the number of copies of its paralog *SMN2*. However, the *SMN2* gene carries a synonymous mutation in the exon 7 (c.840C>T) that causes exon skipping, highly affecting the amount of full-length transcripts[110]. Up

to date, several therapeutic approaches have been tested to treat this detrimental disease, where the two most successful strategies consist of i) gene therapy replacement through a scAAV9 carrying the coding sequence of the *smn1* gene [151][159][152][154] and ii) the usage of antisense oligonucleotides (ASO) targeting an intronic regulatory elements within the *SMN2* intron 7 that corrects the aberrant splicing [146][126][156][146][168]. Both strategies displayed a significant efficacy through the correction of the severe pathological phenotype in SMA animal models, for which reason both of them are currently under clinical trial investigation[159][126].

Recently, we proposed a third therapeutic alternative based on modified U1 snRNAs that bind to the intronic sequences downstream exon 7, the SMN-ExSpeU1s [1]. During the last years, it was demonstrated the activity and the efficiency of these molecules i) *in-vitro* with a minigene system [1], ii) *ex-vivo* with SMA fibroblasts [150]and iii) *in-vivo* with a transgenic mouse model that constitutively expressed the ExSpeU1 sm25 [2]. Thus, the next step to evaluate the efficacy of SMN-ExSpeU1s *in-vivo* was to deliver these molecules through an AAV system to treat an affected SMA mouse model.

Therefore, during my last year of PhD, I investigated the SMN-ExSpeU1s' *in-vivo* efficacy in two animal models of SMA through an AAV-based delivery. I initially chose a mild mouse model of SMA, known as the 5058 model. Because of its genotype, this mouse has been largely used to investigate the *in-vivo* therapeutic potential of SMA splicing-switching molecules, such as antisense oligonucleotides [146]. The 5058, indeed, is a transgenic mouse model that lacks of the murine *smn* gene, which is replaced by four copies of the human *SMN2* gene. Although the *hSMN2* gene undergoes alternative splicing, reducing the amount of final SMN protein, the number of transgene copies is sufficient to allow the conduction a normal life but, at the same time, impairing two morphological aspects: the loss of the tail six weeks after birth and the ears' necrosis. Therefore, this mouse model represented a good model to investigate the splicing correction of ExSpeU1s at RNA level, analyzing the effect on *SMN2* splicing, but also at the phenotype, observing both tails and ears development.

Since the main therapeutic targets of SMA are the α-motor neurons, I investigated the SMN-ExSpeU1s delivery through an adeno-associated virus serotype 9, which was previously described to pass the blood brain barrier, reaching the central nervous system [165]. *Machida et al.*, indeed, were able to reach the dorsal root ganglia and motor neurons by intraperitoneal injections with AAV9 in newborn mice. In addition, ASO treatment of SMA mice by intraperitoneal injections at PND0 and PND2 successfully corrected the *SMN2* aberrant splicing, improving both survival and phenotype [126].

Accordingly, I evaluated the *in-vivo* effects by treating newborn 5058 mice with intraperitoneal injections of four different conditions (AAV9-ExSpeU1 sm25, AAV9-ExSpeU1 sm37, AAV9-U1 wt, saline) at two time points (PND0 and PND2). The monitoring of body weight and tail length displayed a positive response to the ExSpeU1s' treatments (Fig. 4.13). Indeed, as shown in figure 4.13, both the groups treated with the AAV9-ExSpeU1 sm25 and sm37 did not exhibit the typical necrosis that usually appears at four weeks after birth. On the contrary, mice treated with the AAV9-U1 wt and saline presented dark tails as symptom of initiated necrosis. Nonetheless, all the four treatments did not influence the body weight, providing a first outcome on the ExSpeU1s' safety (Fig. 4.13A). As expected, the two control groups (saline and U1 wt-treated) completely lost the tails at nine weeks after birth, whereas the ExSpeU1s-treated siblings still (at nine months after birth) maintain healthy tails and ears. These first encouraging results pushed me to analyze the ExSpeU1s' effect at RNA level. Indeed, our goal was to demonstrate that ExSpeU1s delivered by AAV9 are able to reach specific target tissues, promoting *SMN2* exon 7 inclusion and improving the SMA phenotype. Therefore, I analyzed the splicing patter of *SMN2* in six different tissues (brain, liver, heart, kidney, muscle and spinal cord) from seven days old 5058 mice treated with the four different solutions (Fig. 4.15 and 4.16). ExSpeU1 sm25 and ExSpeU1 sm37, but not the U1 wt and saline showed an increase in the *SMN2* splicing pattern in a tissue-dependent manner. In particular, according to the percentage of exon 7 inclusion, I could distinguish high and low responsive tissues. Overall, both ExSpeU1 sm25 and sm37 responded similarly. The higher splicing correction was achieved in liver, heart and muscle with percentages ranging from 13% to 75% in liver, from 33% to 70% in heart and from 10% to 35% in muscle. On the other hand, the lower answer was observed in brain, kidney and spinal cord with percentages ranging from 30% to 35% in brain, from 11% to 20% in kidney and from 27% to 33% in spinal cord. Although there was a physiological variability between each animal, I did not observe significant variations in the control-treated (saline and U1 wt) animals. However, I noticed a stronger response mediated by the ExSpeU1 sm25 which, in general, promoted a higher exon 7 inclusion than the ExSpeU1 sm37. The slightly lower efficiency of the ExSpeU1 sm37 could have due to multiple reasons, such as a lower efficacy of the molecule itself or an apparent lower titer of the AAV9.

To further validate the efficacy of SMN-ExSpeU1s *in-vivo*, I adopted a severe SMA mouse with affected survival, known as Taiwanese model. This mouse model is characterized by a survival of 10-12 days, which offers a sufficient temporal window to study the effect of

our SMN-ExSpeU1s. As previously described with the 5058 model, I treated the Taiwanese mice with intraperitoneal injections of the three different conditions (AAV9-ExSpeU1 sm25, AAV9-U1 wt, saline) at two time points (PND0 and PND2). Since the effect on splicing was already investigated in the mild SMA model, here I focused on the survival, phenotype and neurofunctional behavior.

At PND7, SMA-affected mice treated with the AAV9-ExSpeU1 sm25 did not show any symptomatic SMA features (Fig. 4.17). The severe Taiwanese mouse, indeed, usually displays the first pathological symptoms at six-seven days after birth with a decreased motility and tremors. In fact, SMA-affected mice treated with U1 wt and saline showed evident symptoms of the disease with affected body weight and impaired movements. As supposed, the treatment with ExSpeU1 sm25 significantly improved the animal survival, with 40% of the treated mice (four out of nine) alive and healthy at 250 days after birth (Fig. 4.18). Differently, Taiwanese mice treated with saline and U1 WT died or were euthanized due to the serious pathological conditions by the twelfth day after birth.

Treated SMA mice varied in size compared to the heterozygous mice, their average weight was lower and their tails were much shorter than normal (Fig. 4.19). This result is in concordance with the results obtained with the ASO-treatment in animal models [126], which is currently in phase 3 of clinical trial.

Rescued SMA mice could run and climb normally, with no evident sign of motor dysfunction. SMA, indeed, is a severe disease that impairs the neurofunctional communication between the central nervous system and the muscle. Therefore, to further support this extraordinary result, I evaluated the neurobehavioral response of ExSpeU1 sm25-treated and heterozygous mice with two neurofunctional test, such as rotarod and the four limbs hanging test (Fig. 4.20). As shown in figure 4.20, the rotarod test did not show any difference between the two groups. Also in the hanging test, sm25-treated mice were not different from the controls (Het animals treated with saline): the only significant difference was observed at 5 weeks when mice first experienced these tests. Considering that SMA is a neuromuscular disease, these performances represent a remarkable phenotypic improvement.

In addition, these data offered other important information concerning the toxicity of ExSpeU1s. Both the SMA animal models treated with ExSpeU1s sm25 and sm37 did not show any evident sign of toxicity nor side effects. Indeed, all the 5058 mice treated with these molecules are still alive and healthy. As shown in Fig. 4.13, I did not detect any significant difference between weights of saline-, AAV-ExSpeU1 sm25- and ExSpeU1 sm37- treated *5058* mice. Furthermore, the Taiwanese mice treated with the ExSpeU1

sm25 did not show any neuromuscular dysfunction, supporting the safeness of the treatment and confirming that the minimal genome-wide effect observed by *Malgorzata et al.* does not compromise the efficacy of the treatment [2].

Further *in-vivo* experiments are required to address the questions related to delivery routes, dosages and timing for the treatment of SMA with the ExSpeU1 sm25.

Overall, these results support the potential of ExSpeU1 sm25 as a new therapeutic option for the treatment of SMA and, more in general, of ExSpeU1 as a strategy to cure splicing-caused diseases.

To date, there are two ongoing clinical studies for the treatment of SMA, which are based on antisense molecules and gene therapy replacement. Although both approaches successfully improved the SMA pathology *in-vivo*, these strategies might outcome some limitations. The ASO treatment, for example, requires repeated infusions because of its dilution over the time. Therefore, our ExSpeU1s strategy represents a valuable alternative because it maintains the physiological chromosomal context with no apparent side effects and it is delivered once in the life.

Concluding, all together, these results offer the opportunity to ExSpeU1s to be a potential therapy for SMA and, hopefully, to other splicing-caused diseases, such as Familial dysautonomia and Haemophilia.

Chapter 6

CONCLUSIONS & FUTURE PLANS

In the past decades, genetics and molecular biology along with advanced technology brought to light a new era. Worldwide, researchers have been working together to highlight the molecular mechanisms behind the central dogma of biology: DNA is transcribed into RNA to be translated into PROTEIN. The entire genome has also been sequenced. So, a lot of efforts have been made and what we now know is that probably we cannot even talk about a "central dogma", because in biology nothing seems that straight anymore. Indeed, a lot of different molecular and cellular processes occur in each step of life, a lot of processes that normally function with no visible consequences but that could be negatively influenced by just a single nucleotide change, like those described in this thesis, changing the good for the worse.

In this thesis, I focused on a specific cellular process that plays an essential role into the maturation of messenger RNAs, the splicing. This fundamental process eliminates the intronic sequences from pre-mRNA molecules, joining exons together and producing an uninterrupted coding sequence ready to be translated into protein. Unfortunately, this mechanism is so complicated that can be significantly influenced by just a single point mutation, leading to severe diseases. However, the recent advances in biotechnology allowed researchers to develop new therapeutic strategies aimed at correcting these cellular mistakes. One of these innovative approaches was recently developed by our laboratory, which is based on modified U1 snRNAs, called ExSpeU1s [1]. These molecules are designed to specifically target the intronic regions downstream of aberrant exons, increasing their recognition through the spliceosome and, therefore, correcting splicing defects. Their potential has been already demonstrated *in-vitro* and *in-vivo* for several disorders like cystic fibrosis, spinal muscular atrophy, Netherton syndrome and

haemophilia B [161][162][150][2]. Here, in this thesis, in order to provide new models of diseases for which ExSpeU1s might represent a valid therapeutic opportunity, I took on the problem of point mutations in other pathological conditions, such as Haemophilia A and Familial dysautonomia. In particular, I used Haemophilia A as a model which permits to quantitatively and functionally investigate the molecular effect of missense mutations, identifying an exonic splicing regulatory element (ESRE) within the *F8* exon 19 and identifying three missense variants that strongly affected the pre-mRNA processing of the coagulation FVIII. I demonstrated that the aberrant splicing could be counteracted by a modified U1 snRNA, providing the basis for the development of an alternative therapeutic strategy for HA. Then, I investigated the ExSpeU1s' potential on Familial dysautonomia, whose aberrant splicing is caused by an intronic point mutation that reduces the *IKBKAP* exon 20 definition. I developed several ExSpeU1s that actively corrected the aberrant *IKBKAP* splicing and demonstrated the *ex-vivo* efficacy of the most active ExSpeU1 in FD fibroblasts. Furthermore, since a proper FD mouse model was not available, I evaluated the *in-vivo* efficacy of ExSpeU1s in two mouse models of spinal muscular atrophy. Here, I demonstrated that the ExSpeU1s sm25 and sm37 strongly correct the *SMN2* aberrant splicing in the mild SMA mouse model, and I showed that the ExSpeU1 sm25 efficiently rescues the survival of the severe SMA mouse.

Therefore, in this thesis, I had the opportunity to study the aberrant splicing in a 360° fashion, starting from the *in-vitro* and concluding with the *in-vivo* analysis. All together, the results described in this thesis demonstrate the potential of ExSpeU1s as an innovative therapeutic tool aimed at curing rare diseases through the correction of aberrant splicing.

Looking ahead, the next main steps of the present work will be i) the evaluation of the *in-vivo* efficacy of the IKBKAP-ExSpeU1s in the newly created FD mouse model that displays both phenotypic and genotypic defects and ii) the evaluation of delivery routes, dosages and timing for the treatment of SMA with the ExSpeU1 sm25 aimed at moving to the clinical phase.

BIBLIOGRAPHY

[1] E. F. Alanis, M. Pinotti, A. D. Mas, D. Balestra, N. Cavallari, M. E. Rogalska, F. Bernardi, and F. Pagani, "An exon-specific U1 small nuclear RNA (snRNA) strategy to correct splicing defects," *Hum. Mol. Genet.*, vol. 21, no. 11, pp. 2389–2398, 2012.

[2] M. E. Rogalska, M. Tajnik, D. Licastro, E. Bussani, L. Camparini, C. Mattioli, and F. Pagani, "Therapeutic activity of modified U1 core spliceosomal particles.," *Nat. Commun.*, vol. 7, p. 11168, 2016.

[3] S. McCracken, N. Fong, K. Yankulov, S. Ballantyne, G. Pan, J. Greenblatt, S. D. Patterson, M. Wickens, and D. L. Bentley, "The C-terminal domain of RNA polymerase II couples mRNA processing to transcription.," *Nature*, vol. 385, no. 6614. pp. 357–361, 1997.

[4] T. Maniatis and R. Reed, "An extensive network of coupling among gene expression machines.," *Nature*, vol. 416, no. 6880, pp. 499–506, 2002.

[5] C. L. Will and R. Lührmann, "Spliceosome structure and function," *Cold Spring Harb. Perspect. Biol.*, vol. 3, no. 7, pp. 1–2, 2011.

[6] M. C. Wahl, C. L. Will, and R. Lührmann, "The Spliceosome: Design Principles of a Dynamic RNP Machine," *Cell*, vol. 136, no. 4. pp. 701–718, 2009.

[7] R. Sperling, "The nuts and bolts of the endogenous spliceosome," *Wiley Interdiscip. Rev. RNA*, 2016.

[8] S. M. Berget, "Exon recognition in vertebrate splicing," *Journal of Biological Chemistry*, vol. 270, no. 6. pp. 2411–2414, 1995.

[9] C. J. Langford, F. J. Klinz, C. Donath, and D. Gallwitz, "Point mutations identify the conserved, intron-contained TACTAAC box as an essential splicing signal sequence in yeast," *Cell*, vol. 36, no. 3, pp. 645–653, 1984.

[10] R. Reed and T. Maniatis, "The role of the mammalian branchpoint sequence in pre-mRNA splicing.," *Genes Dev.*, vol. 2, no. 10, pp. 1268–1276, 1988.

[11] R. F. Roecigno, M. Weiner, and M. A. Garcia-Blanco, "A mutational analysis of the polypyrimidine tract of introns: Effects of sequence differences in pyrimidine tracts on splicing," *J. Biol. Chem.*, vol. 268, no. 15, pp. 11222–11229, 1993.

[12] L. Cartegni, S. L. Chew, and A. R. Krainer, "Listening To Silence and Understanding Nonsense : Exonic Mutations That," vol. 3, no. April, 2002.

[13] F. Pagani, C. Stuani, M. Tzetis, E. Kanavakis, A. Efthymiadou, S. Doudounakis, T. Casals, and F. E. Baralle, “New type of disease causing mutations: The example of the composite exonic regulatory elements of splicing in CFTR exon 12,” *Hum. Mol. Genet.*, vol. 12, no. 10, pp. 1111–1120, 2003.

[14] S. Sharma, C. Maris, F. H. T. Allain, and D. L. Black, “U1 snRNA Directly Interacts with Polypyrimidine Tract-Binding Protein during Splicing Repression,” *Mol. Cell*, vol. 41, no. 5, pp. 579–588, 2011.

[15] J. F. Cáceres, T. Misteli, G. R. Screaton, D. L. Spector, and A. R. Krainer, “Role of the modular domains of SR proteins in subnuclear localization and alternative splicing specificity,” *J. Cell Biol.*, vol. 138, no. 2, pp. 225–238, 1997.

[16] T. Misteli and D. L. Spector, “Protein phosphorylation and the nuclear organization of pre-mRNA splicing.,” *Trends Cell Biol.*, vol. 7, no. 4, pp. 135–138, 1997.

[17] G. Dreyfuss, V. N. Kim, and N. Kataoka, “Messenger-RNA-binding proteins and the messages they carry.,” *Nat. Rev. Mol. Cell Biol.*, vol. 3, no. 3, pp. 195–205, 2002.

[18] S. Piñol-Roma and G. Dreyfuss, “hnRNP proteins: localization and transport between the nucleus and the cytoplasm.,” *Trends Cell Biol.*, vol. 3, no. 5, pp. 151–155, 1993.

[19] S. Piñol-Roma and G. Dreyfuss, “Shuttling of pre-mRNA binding proteins between nucleus and cytoplasm.,” *Nature*, vol. 355, pp. 730–732, 1992.

[20] O. Gozani, R. Feld, and R. Reed, “Evidence that sequence-independent binding of highly conserved U2 snRNP proteins upstream of the branch site is required for assembly of spliceosomal complex A,” *Genes Dev.*, vol. 10, no. 2, pp. 233–243, 1996.

[21] K. K. Nelson and M. R. Green, “Mammalian U2 snRNP has a sequence-specific RNA-binding activity.,” *Genes Dev.*, vol. 3, no. 10, pp. 1562–1571, 1989.

[22] P. D. Zamore and M. R. Green, “Identification, purification, and biochemical characterization of U2 small nuclear ribonucleoprotein auxiliary factor.,” *Proc. Natl. Acad. Sci. U. S. A.*, vol. 86, no. 23, pp. 9243–7, 1989.

[23] M. C. Wahl and R. Lührmann, “SnapShot: Spliceosome Dynamics III,” *Cell*, vol. 162, no. 3, pp. 690–690, 2015.

[24] F. Rossi, T. Forń, E. Antoine, J. Tazi, C. Brunel, and G. Cathala, “Involvement of U1 small nuclear ribonucleoproteins (snRNP) in 5’ splice site-U1 snRNP interaction,” *J. Biol. Chem.*, vol. 271, no. 39, pp. 23985–23991, 1996.

[25] H. Stark, P. Dube, R. Lührmann, and B. Kastner, “Arrangement of RNA and

proteins in the spliceosomal U1 small nuclear ribonucleoprotein particle.," *Nature*, vol. 409, no. 6819, pp. 539–42, 2001.

[26] H. Du and M. Rosbash, "The U1 snRNP protein U1C recognizes the 5' splice site in the absence of base pairing.," *Nature*, vol. 419, no. 6902, pp. 86–90, 2002.

[27] V. A. Raker, K. Hartmuth, B. Kastner, and R. Lührmann, "Spliceosomal U snRNP Core Assembly: Sm Proteins Assemble onto an Sm Site RNA Nonanucleotide in a Specific and Thermodynamically Stable Manner," *Mol. Cell. Biol.*, vol. 19, no. 10, pp. 6554–6565, 1999.

[28] S. Paushkin, A. K. Gubitz, S. Massenet, and G. Dreyfuss, "The SMN complex, an assemblyosome of ribonucleoproteins," *Current Opinion in Cell Biology*, vol. 14, no. 3. pp. 305–312, 2002.

[29] S. L. Naylor, B. U. Zabel, T. Manser, R. Gesteland, and A. Y. Sakaguchi, "Localization of human U1 small nuclear RNA genes to band p36.3 of chromosome 1 by in situ hybridization," *Somat. Cell Mol. Genet.*, vol. 10, no. 3, pp. 307–313, 1984.

[30] S. Pereira-Simon, J. M. Sierra-Montes, K. Ayesh, L. Martinez, A. Socorro, and R. J. Herrera, "Variants of U1 small nuclear RNA assemble into spliceosomal complexes," *Insect Mol. Biol.*, vol. 13, no. 2, pp. 189–194, 2004.

[31] N. Hernandez, "Formation of the 3' end of U1 snRNA is directed by a conserved sequence located downstream of the coding region.," *EMBO J.*, vol. 4, no. 7, pp. 1827–37, 1985.

[32] Q. Huang, M. R. Jacobson, and T. Pederson, "3' processing of human pre-U2 small nuclear RNA: a base-pairing interaction between the 3' extension of the precursor and an internal region.," *Mol. Cell. Biol.*, vol. 17, no. 12, pp. 7178–85, 1997.

[33] M. P. Terns, J. E. Dahlberg, and E. Lund, "Multiple cis-acting signals for export of pre-U1 snRNA from the nucleus," *Genes Dev.*, vol. 7, no. 10, pp. 1898–1908, 1993.

[34] N. Hernandez and A. M. Weiner, "Formation of the 3??? end of U1 snRNA requires compatible snRNA promoter elements," *Cell*, vol. 47, no. 2, pp. 249–258, 1986.

[35] M. Ohno, A. Segref, A. Bachi, M. Wilm, and I. W. Mattaj, "PHAX, a mediator of U snRNA nuclear export whose activity is regulated by phosphorylation," *Cell*, vol. 101, no. 2, pp. 187–198, 2000.

[36] I. Palacios, M. Hetzer, S. A. Adam, and I. W. Mattaj, "Nuclear import of U snRNPs requires importin beta.," *EMBO J.*, vol. 16, no. 22, pp. 6783–92, 1997.

[37] T. W. Nilsen and B. R. Graveley, "Expansion of the eukaryotic proteome by alternative splicing.," *Nature*, vol. 463, no. 7280, pp. 457–63, 2010.

[38] D. Schmucker, J. C. Clemens, H. Shu, C. A. Worby, J. Xiao, M. Muda, J. E. Dixon, and S. L. Zipursky, "Drosophila Dscam is an axon guidance receptor exhibiting extraordinary molecular diversity," *Cell*, vol. 101, no. 6, pp. 671–684, 2000.

[39] K. S. Manning and T. A. Cooper, "The roles of RNA processing in," *Nat. Publ. Gr.*, 2016.

[40] A. J. Ward and T. A. Cooper, "The pathobiology of splicing," *Journal of Pathology*, vol. 220, no. 2. pp. 152–163, 2010.

[41] D. L. Black, "Mechanisms of Alternative Pre-Messenger RNA Splicing," *Annu. Rev. Biochem.*, vol. 72, no. 1, pp. 291–336, 2003.

[42] B. K. Dredge, G. Stefani, C. C. Engelhard, and R. B. Darnell, "Nova autoregulation reveals dual functions in neuronal splicing.," *EMBO J.*, vol. 24, no. 8, pp. 1608–20, 2005.

[43] D. M. Mauger, C. Lin, and M. a Garcia-Blanco, "hnRNP H and hnRNP F Complex with Fox2 To Silence Fibroblast Growth Factor Receptor 2 Exon IIIc," *Mol. Cell. Biol.*, vol. 28, no. 17, pp. 5403–5419, 2008.

[44] J. Ule, G. Stefani, A. Mele, M. Ruggiu, X. Wang, B. Taneri, T. Gaasterland, B. J. Blencowe, and R. B. Darnell, "An RNA map predicting Nova-dependent splicing regulation.," *Nature*, vol. 444, no. 7119, pp. 580–586, 2006.

[45] G. W. Yeo, N. G. Coufal, T. Y. Liang, G. E. Peng, X.-D. Fu, and F. H. Gage, "An RNA code for the FOX2 splicing regulator revealed by mapping RNA-protein interactions in stem cells," *Nat. Struct. Mol. Biol.*, vol. 16, no. 2, pp. 130–137, 2009.

[46] B. K. Dredge and R. B. Darnell, "Nova regulates GABA(A) receptor gamma2 alternative splicing via a distal downstream UCAU-rich intronic splicing enhancer.," *Mol. Cell. Biol.*, vol. 23, no. 13, pp. 4687–700, 2003.

[47] M. Chen and J. L. Manley, "Mechanisms of alternative splicing regulation: insights from molecular and genomics approaches.," *Nat. Rev. Mol. Cell Biol.*, vol. 10, no. 11, pp. 741–54, 2009.

[48] T. A. Cooper, L. Wan, and G. Dreyfuss, "RNA and Disease," *Cell*, vol. 136, no. 4. pp. 777–793, 2009.

[49] M. Krawczak, J. Reiss, and D. N. Cooper, "The mutational spectrum of single base-pair substitutions in mRNA splice junctions of human genes: Causes and consequences," *Hum. Genet.*, vol. 90, no. 1–2, pp. 41–54, 1992.

[50] E. Daguenet, G. Dujardin, and J. Valcárcel, "The pathogenicity of splicing defects : mechanistic insights into pre-mRNA processing inform novel therapeutic approaches," vol. 16, no. 12, 2015.

[51] M. Krawczak, N. S. T. Thomas, B. Hundrieser, M. Mort, M. Wittig, J. Hampe, and D. N. Cooper, “Single base-pair substitutions in exon-intron junctions of human genes: Nature, distribution, and consequences for mRNA splicing,” *Hum. Mutat.*, vol. 28, no. 2, pp. 150–158, 2007.

[52] L. Cartegni and A. R. Krainer, “Disruption of an SF2/ASF-dependent exonic splicing enhancer in SMN2 causes spinal muscular atrophy in the absence of SMN1.,” *Nat. Genet.*, vol. 30, no. 4, pp. 377–84, 2002.

[53] L. Cartegni, M. L. Hastings, J. A. Calarco, E. de Stanchina, and A. R. Krainer, “Determinants of exon 7 splicing in the spinal muscular atrophy genes, SMN1 and SMN2.,” *Am. J. Hum. Genet.*, vol. 78, no. 1, pp. 63–77, 2006.

[54] M. Tajnik, M. E. Rogalska, E. Bussani, and E. Barbon, “Molecular Basis and Therapeutic Strategies to Rescue Factor IX Variants That Affect Splicing and Protein Function,” pp. 1–16, 2016.

[55] N. A. Orlova, S. V. Kovnir, I. I. Vorobiev, A. G. Gabibov, and A. I. Vorobiev, “Blood clotting factor VIII: From evolution to therapy,” *Acta Naturae*, vol. 5, no. 17. pp. 19–39, 2013.

[56] N. O. Viiala, S. R. Larsen, and J. E. J. Rasko, “Gene therapy for hemophilia: Clinical trials and technical tribulations,” *Seminars in Thrombosis and Hemostasis*, vol. 35, no. 1. pp. 81–92, 2009.

[57] P. J. Fay, “Activation of factor VIII and mechanisms of cofactor action,” *Blood Reviews*, vol. 18, no. 1. pp. 1–15, 2004.

[58] K. Sichler, E. Kopetzki, R. Huber, W. Bode, K. P. Hopfner, and H. Brandstetter, “Physiological fIXa activation involves a cooperative conformational rearrangement of the 99-loop,” *J. Biol. Chem.*, vol. 278, no. 6, pp. 4121–4126, 2003.

[59] A. D. Shapiro, “Anti-hemophilic factor (recombinant), plasma/albumin-free method (octocog-alpha; ADVATE??) in the management of hemophilia A,” *Vascular Health and Risk Management*, vol. 3, no. 5. pp. 555–565, 2007.

[60] M. Franchini and P. M. Mannucci, “Hemophilia A in the third millennium,” *Blood Rev.*, vol. 27, no. 4, pp. 179–184, 2013.

[61] E. Santagostino, “A new recombinant factor VIII: from genetics to clinical use,” *Drug Des Devel Ther*, vol. 8, pp. 2507–2515, 2014.

[62] W. H. Kane and E. W. Davie, “Cloning of a cDNA coding for human factor V, a blood coagulation factor homologous to factor VIII and ceruloplasmin,” *Proc Natl Acad Sci U S A*, vol. 83, no. 18, pp. 6800–6804, 1986.

[63] J. L. Pellequer, a J. Gale, J. H. Griffin, and E. D. Getzoff, “Homology models of the

C domains of blood coagulation factors V and VIII: a proposed membrane binding mode for FV and FVIII C2 domains.," *Blood Cells. Mol. Dis.*, vol. 24, no. 4, pp. 448–61, 1998.

[64] S. W. Pipe, "Functional roles of the factor VIII B domain," *Haemophilia*, vol. 15, no. 6, pp. 1187–1196, 2009.

[65] M. J. Hollestelle, T. Thinnes, K. Crain, A. Stiko, J. K. Kruijt, T. J. C. Van Berkel, D. J. Loskutoff, and J. A. Van Mourik, "Tissue distribution of factor VIII gene expression in vivo - A closer look," *Thromb. Haemost.*, vol. 86, no. 3, pp. 855–861, 2001.

[66] T. Shahani, K. Covens, R. Lavend'homme, N. Jazouli, E. Sokal, K. Peerlinck, and M. Jacquemin, "Human liver sinusoidal endothelial cells but not hepatocytes contain factor VIII.," *J Thromb Haemost*, vol. 12, pp. 36–42, 2014.

[67] P. J. Lenting, J. a van Mourik, and K. Mertens, "The life cycle of coagulation factor VIII in view of its structure and function.," *Blood*, vol. 92, no. 4, pp. 3983–3996, 1998.

[68] E. Y. Chi, S. Krishnan, B. S. Kendrick, B. S. Chang, J. F. Carpenter, and T. W. Randolph, "Roles of conformational stability and colloidal stability in the aggregation of recombinant human granulocyte colony-stimulating factor.," *Protein Sci.*, vol. 12, no. 5, pp. 903–13, 2003.

[69] R. D. Bagnall, N. Waseem, P. M. Green, and F. Giannelli, "Recurrent inversion breaking intron 1 of the factor VIII gene is a frequent cause of severe hemophilia A," *Blood*, vol. 99, no. 1, pp. 168–174, 2002.

[70] D. Lakich, H. H. Kazazian, S. E. Antonarakis, and J. Gitschier, "Inversions disrupting the factor VIII gene are a common cause of severe haemophilia A," *Nat. Genet.*, vol. 5, no. 3, pp. 236–41, 1993.

[71] I. Garagiola, S. Seregni, M. Mortarino, M. E. Mancuso, M. R. Fasulo, L. D. Notarangelo, and F. Peyvandi, "A recurrent F8 mutation (c . 6046C > T) causing hemophilia A in 8 % of northern Italian patients : evidence for a founder effect," 2015.

[72] B. D. M. Theophilus, M. S. Enayat, M. D. Williams, and F. G. H. Hill, "Site and type of mutations in the factor VIII gene in patients and carriers of haemophilia A," *Haemophilia*, vol. 7, no. 4, pp. 381–391, 2001.

[73] F. B. Axelrod, "Familial dysautonomia," *Muscle Nerve*, vol. 29, no. 3, pp. 352–363, 2004.

[74] F. B. Axelrod and J. Pearson, "Congenital Sensory Neuropathies: Diagnostic

Distinction From Familial Dysautonomia," *Am. J. Dis. Child.*, vol. 138, no. 10, pp. 947–954, 1984.

[75] C. M. RILEY, R. L. DAY, D. M. C. L. GREELEY, and W. S. LANGFORD, "CENTRAL AUTONOMIC DYSFUNCTION WITH DEFECTIVE LACRIMATION," *Pediatrics*, vol. 3, no. 4, pp. 468–478, 1949.

[76] F. B. Axelrod, "Hereditary sensory and autonomic neuropathies. Familial dysautonomia and other HSANs.," *Clin. Auton. Res.*, vol. 12 Suppl 1, pp. I2-14, 2002.

[77] F. B. Axelrod, "A world without pain or tears.," *Clin. Auton. Res.*, vol. 16, no. 2, pp. 90–97, 2006.

[78] S. L. Anderson, R. Coli, I. W. Daly, E. a. Kichula, M. J. Rork, S. a. Volpi, J. Ekstein, and B. Y. Rubin, "Familial Dysautonomia Is Caused by Mutations of the IKAP Gene," *Am. J. Hum. Genet.*, vol. 68, no. 3, pp. 753–758, 2001.

[79] M. P. Cuajungco, M. Leyne, J. Mull, S. P. Gill, W. Lu, D. Zagzag, F. B. Axelrod, C. Maayan, J. F. Gusella, and S. a Slaugenhaupt, "Tissue-specific reduction in splicing efficiency of IKBKAP due to the major mutation associated with familial dysautonomia.," *Am. J. Hum. Genet.*, vol. 72, no. 3, pp. 749–758, 2003.

[80] L. Cohen, W. J. Henzel, and P. a Baeuerle, "IKAP is a scaffold protein of the IkappaB kinase complex," *Nature*, vol. 395, no. 6699, pp. 292–6, 1998.

[81] D. Krappmann, E. N. Hatada, S. Tegethoff, J. Li, A. Klippel, K. Giese, P. A. Baeuerle, and C. Scheidereit, "The I??B kinase (IKK) complex is tripartite and contains IKK?? but not IKAP as a regular component," *J. Biol. Chem.*, vol. 275, no. 38, pp. 29779–29787, 2000.

[82] N. A. Hawkes, G. Otero, G. Sebastiaan Winkler, N. Marshall, M. E. Dahmus, D. Krappmann, C. Scheidereit, C. L. Thomas, G. Schiavo, H. Erdjument-Bromage, and J. Q. Svejstrup, "Purification and characterization of the human elongator complex," *J. Biol. Chem.*, vol. 277, no. 4, pp. 3047–3052, 2002.

[83] C. Holmberg, S. Katz, M. Lerdrup, T. Herdegen, M. Jäättelä, A. Aronheim, and T. Kallunki, "A novel specific role for I??B kinase complex-associated protein in cytosolic stress signaling," *J. Biol. Chem.*, vol. 277, no. 35, pp. 31918–31928, 2002.

[84] P. Close, N. Hawkes, I. Cornez, C. Creppe, C. A. Lambert, B. Rogister, U. Siebenlist, M. P. Merville, S. A. Slaugenhaupt, V. Bours, J. Q. Svejstrup, and A. Chariot, "Transcription Impairment and Cell Migration Defects in Elongator-Depleted Cells: Implication for Familial Dysautonomia," *Mol. Cell*, vol. 22, no. 4, pp. 521–531, 2006.

[85] D. Cheishvili, C. Maayan, R. Cohen-Kupiec, S. Lefler, M. Weil, G. Ast, and A. Razin, “IKAP/Elp1 involvement in cytoskeleton regulation and implication for familial dysautonomia,” *Hum. Mol. Genet.*, vol. 20, no. 8, pp. 1585–1594, 2011.

[86] L. D. Johansen, T. Naumanen, a. Knudsen, N. Westerlund, I. Gromova, M. Junttila, C. Nielsen, T. Bottzauw, a. Tolkovsky, J. Westermarck, E. T. Coffey, M. Jaattela, and T. Kallunki, “IKAP localizes to membrane ruffles with filamin A and regulates actin cytoskeleton organization and cell migration,” *J. Cell Sci.*, vol. 121, no. 6, pp. 854–864, 2008.

[87] M. Z. Jackson, K. a. Gruner, C. Qin, and W. G. Tourtellotte, “A neuron autonomous role for the familial dysautonomia gene ELP1 in sympathetic and sensory target tissue innervation,” *Development*, vol. 141, no. 12, pp. 2452–2461, 2014.

[88] L. George, M. Chaverra, L. Wolfe, J. Thorne, M. Close-Davis, A. Eibs, V. Riojas, A. Grindeland, M. Orr, G. A. Carlson, and F. Lefcort, “Familial dysautonomia model reveals Ikbkap deletion causes apoptosis of Pax3+ progenitors and peripheral neurons,” *Proc Natl Acad Sci U S A*, vol. 110, no. 46, pp. 18698–18703, 2013.

[89] O. Lehavi, O. Aizenstein, D. Bercovich, D. Pavzner, R. Shomrat, A. Orr-Urtreger, and Y. Yaron, “Screening for familial dysautonomia in Israel: evidence for higher carrier rate among Polish Ashkenazi Jews.,” *Genet. Test.*, vol. 7, no. 2, pp. 139–42, 2003.

[90] M. Leyne, J. Mull, S. P. Gill, M. P. Cuajungco, C. Oddoux, A. Blumenfeld, C. Maayan, J. F. Gusella, F. B. Axelrod, and S. A. Slaugenhaupt, “Identification of the first non-Jewish mutation in familial Dysautonomia.,” *Am. J. Med. Genet. A*, vol. 118A, no. 4, pp. 305–308, 2003.

[91] H. Xu, Z. Lin, F. Li, W. Diao, C. Dong, H. Zhou, X. Xie, Z. Wang, Y. Shen, and J. Long, “Dimerization of elongator protein 1 is essential for Elongator complex assembly.,” *Proc. Natl. Acad. Sci. U. S. A.*, vol. 112, no. 34, pp. 10697–702, 2015.

[92] L. Norcliffe-Kaufmann and H. Kaufmann, “Familial dysautonomia (Riley-Day syndrome): When baroreceptor feedback fails,” *Auton. Neurosci. Basic Clin.*, vol. 172, no. 1–2, pp. 26–30, 2012.

[93] P. Dietrich, S. Alli, R. Shanmugasundaram, and I. Dragatsis, “IKAP expression levels modulate disease severity in a mouse model of familial dysautonomia,” *Hum. Mol. Genet.*, vol. 21, no. 23, pp. 5078–5090, 2012.

[94] E. Morini, P. Dietrich, M. Salani, H. M. Downs, G. R. Wojtkiewicz, S. Alli, A. Brenner, M. Nilbratt, J. W. LeClair, A. L. Oaklander, S. A. Slaugenhaupt, and I. Dragatsis, “Sensory and autonomic deficits in a new humanized mouse model of

familial dysautonomia," *Hum. Mol. Genet.*, vol. 25, no. 6, pp. 1116–1128, 2015.

[95] D. S. Goldstein, B. Eldadah, Y. Sharabi, and F. B. Axelrod, "Cardiac sympathetic hypo-innervation in familial dysautonomia," *Clin. Auton. Res.*, vol. 18, no. 3, pp. 115–119, 2008.

[96] S. a. Slaugenhaupt, J. Mull, M. Leyne, M. P. Cuajungco, S. P. Gill, M. M. Hims, F. Quintero, F. B. Axelrod, and J. F. Gusella, "Rescue of a human mRNA splicing defect by the plant cytokinin kinetin," *Hum. Mol. Genet.*, vol. 13, no. 4, pp. 429–436, 2004.

[97] G. Lee, C. N. Ramirez, H. Kim, N. Zeltner, B. Liu, C. Radu, B. Bhinder, Y. J. Kim, I. Y. Choi, B. Mukherjee-Clavin, H. Djaballah, and L. Studer, "Large-scale screening using familial dysautonomia induced pluripotent stem cells identifies compounds that rescue IKBKAP expression.," *Nat. Biotechnol.*, vol. 30, no. 12, pp. 1244–8, 2012.

[98] M. M. Hims, E. C. Ibrahim, M. Leyne, J. Mull, L. Liu, C. Lazaro, R. S. Shetty, S. Gill, J. F. Gusella, R. Reed, and S. a. Slaugenhaupt, "Therapeutic potential and mechanism of kinetin as a treatment for the human splicing disease familial dysautonomia," *J. Mol. Med.*, vol. 85, no. 2, pp. 149–161, 2007.

[99] F. B. Axelrod, L. Liebes, G. G. Von Simson, S. Mendoza, J. Mull, M. Leyne, L. Norcliffe-Kaufmann, H. Kaufmann, and S. A. Slaugenhaupt, "Kinetin improves IKBKAP mRNA splicing in patients with familial dysautonomia," *Pediatr. Res.*, vol. 70, no. 5, pp. 480–483, 2011.

[100] B. Liu, S. L. Anderson, J. Qiu, and B. Y. Rubin, "Cardiac glycosides correct aberrant splicing of IKBKAP -encoded mRNA in familial dysautonomia derived cells by suppressing expression of SRSF3," *FEBS J.*, vol. 280, no. 15, pp. 3632–3646, 2013.

[101] R. Bochner, Y. Ziv, D. Zeevi, M. Donyo, L. Abraham, R. Ashery-Padan, and G. Ast, "Phosphatidylserine increases IKBKAP levels in a humanized knock-in IKBKAP mouse model," *Hum. Mol. Genet.*, vol. 22, no. 14, pp. 2785–2794, 2013.

[102] H. Keren, M. Donyo, D. Zeevi, C. Maayan, T. Pupko, and G. Ast, "Phosphatidylserine increases IKBKAP levels in familial dysautonomia cells," *PLoS One*, vol. 5, no. 12, 2010.

[103] M. Yoshida, N. Kataoka, K. Miyauchi, K. Ohe, K. Iida, S. Yoshida, T. Nojima, Y. Okuno, H. Onogi, T. Usui, A. Takeuchi, T. Hosoya, T. Suzuki, and M. Hagiwara, "Rectifier of aberrant mRNA splicing recovers tRNA modification in familial dysautonomia.," *Proc. Natl. Acad. Sci. U. S. A.*, vol. 112, no. 9, pp. 2764–9, 2015.

[104] S. Ogino, D. G. B. Leonard, H. Rennert, W. J. Ewens, and R. B. Wilson, "Genetic risk assessment in carrier testing for spinal muscular atrophy," *Am. J. Med. Genet.*, vol. 110, no. 4, pp. 301–307, 2002.

[105] T. W. Prior, P. J. Snyder, B. D. Rink, D. K. Pearl, R. E. Pyatt, D. C. Mihal, T. Conlan, B. Schmalz, L. Montgomery, K. Ziegler, C. Noonan, S. Hashimoto, and S. Garner, "Newborn and carrier screening for spinal muscular atrophy," *Am. J. Med. Genet. Part A*, vol. 152, no. 7, pp. 1608–1616, 2010.

[106] E. Mercuri, E. Bertini, and S. T. Iannaccone, "Childhood spinal muscular atrophy: Controversies and challenges," *The Lancet Neurology*, vol. 11, no. 5. pp. 443–452, 2012.

[107] M. R. Lunn and C. H. Wang, "Spinal muscular atrophy.," *Lancet*, vol. 371, no. 9630, pp. 2120–33, 2008.

[108] S. Lefebvre, L. Burglen, S. Reboullet, O. Clermont, P. Burlet, L. Viollet, B. Benichou, C. Cruaud, P. Millasseau, M. Zeviani, and Et Al., "Identification and characterization of a spinal muscular atrophy- determining gene [see comments]," *Cell*, vol. 80, no. 1, pp. 155–165, 1995.

[109] U. R. Monani, C. L. Lorson, D. W. Parsons, T. W. Prior, E. J. Androphy, A. H. M. Burghes, and J. D. McPherson, "A single nucleotide difference that alters splicing patterns distinguishes the SMA gene SMN1 from the copy gene SMN2," *Hum. Mol. Genet.*, vol. 8, no. 7, pp. 1177–1183, 1999.

[110] C. L. Lorson, E. Hahnen, E. J. Androphy, and B. Wirth, "A single nucleotide in the SMN gene regulates splicing and is responsible for spinal muscular atrophy.," *Proc. Natl. Acad. Sci. U. S. A.*, vol. 96, no. 11, pp. 6307–11, 1999.

[111] C. L. Lorson and E. J. Androphy, "An exonic enhancer is required for inclusion of an essential exon in the SMA-determining gene SMN.," *Hum. Mol. Genet.*, vol. 9, no. 2, pp. 259–265, 2000.

[112] B. G. Burnett, E. Muñoz, A. Tandon, D. Y. Kwon, C. J. Sumner, and K. H. Fischbeck, "Regulation of SMN protein stability.," *Mol. Cell. Biol.*, vol. 29, no. 5, pp. 1107–15, 2009.

[113] S. Lefebvre, P. Burlet, Q. Liu, S. Bertrandy, O. Clermont, a Munnich, G. Dreyfuss, and J. Melki, "Correlation between severity and SMN protein level in spinal muscular atrophy.," *Nat. Genet.*, vol. 16, no. 3, pp. 265–269, 1997.

[114] N. N. Singh, M. N. Lawler, E. W. Ottesen, D. Upreti, J. R. Kaczynski, and R. N. Singh, "An intronic structure enabled by a long-distance interaction serves as a novel target for splicing correction in spinal muscular atrophy," *Nucleic Acids Res.*,

vol. 41, no. 17, pp. 8144–8165, 2013.

[115] N. N. Singh, R. N. Singh, and E. J. Androphy, "Modulating role of RNA structure in alternative splicing of a critical exon in the spinal muscular atrophy genes," *Nucleic Acids Res.*, vol. 35, no. 2, pp. 371–389, 2007.

[116] Y. Hofmann, C. L. Lorson, S. Stamm, E. J. Androphy, and B. Wirth, "Htra2-beta 1 stimulates an exonic splicing enhancer and can restore full-length SMN expression to survival motor neuron 2 (SMN2).," *Proc. Natl. Acad. Sci. U. S. A.*, vol. 97, no. 17, pp. 9618–23, 2000.

[117] Y. Hofmann and B. Wirth, "hnRNP-G promotes exon 7 inclusion of survival motor neuron (SMN) via direct interaction with Htra2-beta1.," *Hum. Mol. Genet.*, vol. 11, no. 17, pp. 2037–2049, 2002.

[118] M. T. Nasim, T. K. Chernova, H. M. Chowdhury, B. G. Yue, and I. C. Eperon, "HnRNP G and Tra2??: Opposite effects on splicing matched by antagonism in RNA binding," *Hum. Mol. Genet.*, vol. 12, no. 11, pp. 1337–1348, 2003.

[119] J. P. Venables, D. J. Elliott, O. V Makarova, E. M. Makarov, H. J. Cooke, and I. C. Eperon, "RBMY, a probable human spermatogenesis factor, and other hnRNP G proteins interact with Tra2beta and affect splicing.," *Hum. Mol. Genet.*, vol. 9, no. 5, pp. 685–694, 2000.

[120] Y. Hua, T. a. Vickers, H. L. Okunola, C. F. Bennett, and A. R. Krainer, "Antisense Masking of an hnRNP A1/A2 Intronic Splicing Silencer Corrects SMN2 Splicing in Transgenic Mice," *Am. J. Hum. Genet.*, vol. 82, no. 4, pp. 834–848, 2008.

[121] T. Kashima, N. Rao, C. J. David, and J. I. Manley, "hnRNP A1 functions with specificity in repression of SMN2 exon 7 splicing," *Hum. Mol. Genet.*, vol. 16, no. 24, pp. 3149–3159, 2007.

[122] H. Miyajima, H. Miyaso, M. Okumura, J. Kurisu, and K. Imaizumi, "Identification of a cis-acting element for the regulation of SMN exon 7 splicing," *J. Biol. Chem.*, vol. 277, no. 26, pp. 23271–23277, 2002.

[123] N. K. Singh, N. N. Singh, E. J. Androphy, and R. N. Singh, "Splicing of a critical exon of human Survival Motor Neuron is regulated by a unique silencer element located in the last intron.," *Mol. Cell. Biol.*, vol. 26, no. 4, pp. 1333–46, 2006.

[124] T. Kashima, N. Rao, and J. L. Manley, "An intronic element contributes to splicing repression in spinal muscular atrophy.," *Proc. Natl. Acad. Sci. U. S. A.*, vol. 104, no. 9, pp. 3426–3431, 2007.

[125] J. N. Sleigh, T. H. Gillingwater, and K. Talbot, "The contribution of mouse models to understanding the pathogenesis of spinal muscular atrophy," *Dis Model Mech*,

vol. 4, no. 4, pp. 457–467, 2011.

[126] Y. Hua, K. Sahashi, F. Rigo, G. Hung, G. Horev, C. F. Bennett, and A. R. Krainer, "Peripheral SMN restoration is essential for long-term rescue of a severe spinal muscular atrophy mouse model," *Nature*, vol. 478, no. 7367, pp. 123–126, 2011.

[127] M. Shababi, C. L. Lorson, and S. S. Rudnik-Schöneborn, "Spinal muscular atrophy: A motor neuron disorder or a multi-organ disease?," *J. Anat.*, vol. 224, no. 1, pp. 15–28, 2014.

[128] S. Rudnik-Schöneborn, H. H. Goebel, W. Schlote, S. Molaian, H. Omran, U. Ketelsen, R. Korinthenberg, D. Wenzel, H. Lauffer, M. Kreiss-Nachtsheim, B. Wirth, and K. Zerres, "Classical infantile spinal muscular atrophy with SMN deficiency causes sensory neuronopathy.," *Neurology*, vol. 60, no. 6, pp. 983–987, 2003.

[129] D. Q. Campos, M. Araujo, and K. J. Swoboda, "Vascular Perfusion Abnormalities in Infants with Spinal Muscular Atrophy," *J. Pediatr.*, vol. 155, no. 2, pp. 292–294, 2009.

[130] S. Rudnik-Schöneborn, S. Vogelgesang, S. Armbrust, L. Graul-Neumann, C. Fusch, and K. Zerres, "Digital necroses and vascular thrombosis in severe spinal muscular atrophy," *Muscle and Nerve*, vol. 42, no. 1, pp. 144–147, 2010.

[131] M. Shababi, J. Habibi, H. T. Yang, S. M. Vale, W. A. Sewell, and C. L. Lorson, "Cardiac defects contribute to the pathology of spinal muscular atrophy models," *Hum. Mol. Genet.*, vol. 19, no. 20, pp. 4059–4071, 2010.

[132] J. M. Vitte, B. Davoult, N. Roblot, M. Mayer, V. Joshi, S. Courageot, F. Tronche, J. Vadrot, M. H. Moreau, F. Kemeny, and J. Melki, "Deletion of murine Smn exon 7 directed to liver leads to severe defect of liver development associated with iron overload.," *Am. J. Pathol.*, vol. 165, no. 5, pp. 1731–41, 2004.

[133] S. E. Gombash, C. J. Cowley, J. A. Fitzgerald, C. C. Iyer, D. Fried, V. L. McGovern, K. C. Williams, A. H. M. Burghes, F. L. Christofi, B. D. Gulbransen, and K. D. Foust, "SMN deficiency disrupts gastrointestinal and enteric nervous system function in mice," *Hum. Mol. Genet.*, vol. 24, no. 13, pp. 3847–3860, 2015.

[134] C. Simone, A. Ramirez, M. Bucchia, P. Rinchetti, H. Rideout, D. Papadimitriou, D. B. Re, and S. Corti, "Is spinal muscular atrophy a disease of the motor neurons only: Pathogenesis and therapeutic implications?," *Cell. Mol. Life Sci.*, vol. 73, no. 5, pp. 1003–1020, 2016.

[135] L. Pellizzoni, N. Kataoka, B. Charroux, and G. Dreyfuss, "A novel function for SMN, the spinal muscular atrophy disease gene product, in pre-mRNA splicing,"

Cell, vol. 95, no. 5, pp. 615–624, 1998.

[136] Z. Zhang, F. Lotti, K. Dittmar, I. Younis, L. Wan, M. Kasim, and G. Dreyfuss, "SMN Deficiency Causes Tissue-Specific Perturbations in the Repertoire of snRNAs and Widespread Defects in Splicing," *Cell*, vol. 133, no. 4, pp. 585–600, 2008.

[137] L. Pellizzoni, B. Charroux, and G. Dreyfuss, "SMN mutants of spinal muscular atrophy patients are defective in binding to snRNP proteins.," *Proc. Natl. Acad. Sci. U. S. A.*, vol. 96, no. 20, pp. 11167–72, 1999.

[138] Z. Zhang, A. M. Pinto, L. Wan, W. Wang, M. G. Berg, I. Oliva, L. N. Singh, C. Dengler, Z. Wei, and G. Dreyfuss, "Dysregulation of synaptogenesis genes antecedes motor neuron pathology in spinal muscular atrophy.," *Proc. Natl. Acad. Sci. U. S. A.*, vol. 110, no. 48, pp. 19348–53, 2013.

[139] H. L. Zhang, F. Pan, D. Hong, S. M. Shenoy, R. H. Singer, and G. J. Bassell, "Active transport of the survival motor neuron protein and the role of exon-7 in cytoplasmic localization," *J. Neurosci.*, vol. 23, no. 16, pp. 6627–6637, 2003.

[140] S. K. Custer, A. G. Todd, N. N. Singh, and E. J. Androphy, "Dilysine motifs in exon 2b of SMN protein mediate binding to the COPI vesicle proteina ??-COP and neurite outgrowth in a cell culture model of spinal muscular atrophy," *Hum. Mol. Genet.*, vol. 22, no. 20, pp. 4043–4052, 2013.

[141] M. J. eong Kye, E. D. Niederst, M. H. Wertz, I. do C. G. Gon??alves, B. Akten, K. Z. Dover, M. Peters, M. Riessland, P. Neveu, B. Wirth, K. S. Kosik, S. P. Sardi, U. R. Monani, M. A. Passini, and M. Sahin, "SMN regulates axonal local translation via miR-183/mTOR pathway," *Hum. Mol. Genet.*, vol. 23, no. 23, pp. 6318–6331, 2014.

[142] G. Hamilton and T. H. Gillingwater, "Spinal muscular atrophy: Going beyond the motor neuron," *Trends Mol. Med.*, vol. 19, no. 1, pp. 40–50, 2013.

[143] H. L. Narver, L. Kong, B. G. Burnett, D. W. Choe, M. Bosch-Marcé, A. A. Taye, M. A. Eckhaus, and C. J. Sumner, "Sustained improvement of spinal muscular atrophy mice treated with trichostatin A plus nutrition," *Ann. Neurol.*, vol. 64, no. 4, pp. 465–470, 2008.

[144] K. K. Y. Ling, R. M. Gibbs, Z. Feng, and C. P. Ko, "Severe neuromuscular denervation of clinically relevant muscles in a mouse model of spinal muscular atrophy," *Hum. Mol. Genet.*, vol. 21, no. 1, pp. 185–195, 2012.

[145] C. R. Heier, R. Satta, C. Lutz, and C. J. Didonato, "Arrhythmia and cardiac defects are a feature of spinal muscular atrophy model mice," *Hum. Mol. Genet.*, vol. 19,

no. 20, pp. 3906–3918, 2010.

[146] Y. Hua, K. Sahashi, G. Hung, F. Rigo, M. a. Passini, C. F. Bennett, and A. R. Krainer, "Antisense correction of SMN2 splicing in the CNS rescues necrosis in a type III SMA mouse model," *Genes Dev.*, vol. 24, no. 15, pp. 1634–1644, 2010.

[147] E. Y. Osman, P.-F. Yen, and C. L. Lorson, "Bifunctional RNAs Targeting the Intronic Splicing Silencer N1 Increase SMN Levels and Reduce Disease Severity in an Animal Model of Spinal Muscular Atrophy," *Mol. Ther.*, vol. 20, no. 1, pp. 119–126, 2012.

[148] P. N. Porensky and A. H. M. Burghes, "Antisense oligonucleotides for the treatment of spinal muscular atrophy.," *Hum. Gene Ther.*, vol. 24, no. 5, pp. 489–98, 2013.

[149] N. a. Naryshkin, M. Weetall, a. Dakka, J. Narasimhan, X. Zhao, Z. Feng, K. K. Y. Ling, G. M. Karp, H. Qi, M. G. Woll, G. Chen, N. Zhang, V. Gabbeta, P. Vazirani, a. Bhattacharyya, B. Furia, N. Risher, J. Sheedy, R. Kong, J. Ma, a. Turpoff, C.-S. Lee, X. Zhang, Y.-C. Moon, P. Trifillis, E. M. Welch, J. M. Colacino, J. Babiak, N. G. Almstead, S. W. Peltz, L. a. Eng, K. S. Chen, J. L. Mull, M. S. Lynes, L. L. Rubin, P. Fontoura, L. Santarelli, D. Haehnke, K. D. McCarthy, R. Schmucki, M. Ebeling, M. Sivaramakrishnan, C.-P. Ko, S. V. Paushkin, H. Ratni, I. Gerlach, a. Ghosh, and F. Metzger, "SMN2 splicing modifiers improve motor function and longevity in mice with spinal muscular atrophy," *Science (80-.).*, vol. 345, no. 6197, pp. 688–693, 2014.

[150] A. Dal Mas, M. E. Rogalska, E. Bussani, and F. Pagani, "Improvement of SMN2 Pre-mRNA Processing Mediated by Exon-Specific U1 Small Nuclear RNA," *Am. J. Hum. Genet.*, vol. 96, no. 1, pp. 93–103, 2015.

[151] K. D. Foust, A. M. Y. Poirier, C. A. Pacak, R. J. Mandel, and T. R. Flotte, "Neonatal Intraperitoneal or Intravenous Injections of Recombinant Adeno-Associated Virus Type 8 Transduce Dorsal Root Ganglia and Lower Motor Neurons," vol. 69, no. January, pp. 61–69, 2008.

[152] J. J. Glascock, E. Y. Osman, M. J. Wetz, M. M. Krogman, M. Shababi, and C. L. Lorson, ", Spinal Muscular Atrophy Mice Following scAAV9-SMN Delivery," *Hum. Gene Ther.*, vol. 23, no. 3, pp. 330–335, 2012.

[153] M. A. Passini, J. Bu, E. M. Roskelley, A. M. Richards, S. P. Sardi, C. R. O'Riordan, K. W. Klinger, L. S. Shihabuddin, and S. H. Cheng, "CNS-targeted gene therapy improves survival and motor function in a mouse model of spinal muscular atrophy.," *J. Clin. Invest.*, vol. 120, no. 4, pp. 1253–64, 2010.

[154] E. Dominguez, T. Marais, N. Chatauret, S. Benkhelifa-ziyyat, S. Duque, P.

Ravassard, R. Carcenac, P. De Moura, T. Voit, M. Barkats, M. Curie, U. U. M. R. S, U. Inserm, C. Umr, I. De Myologie, P. Marie, U. Inserm, and C. H. U. De Poitiers, "Intravenous scAAV9 delivery of a codon-optimized SMN1 sequence rescues SMA mice," vol. 20, no. 4, pp. 681–693, 2011.

[155] S. Tisdale and L. Pellizzoni, "Disease mechanisms and therapeutic approaches in spinal muscular atrophy.," *J. Neurosci.*, vol. 35, no. 23, pp. 8691–700, 2015.

[156] Y. Hua, Y. H. Liu, K. Sahashi, F. Rigo, C. F. Bennett, and A. R. Krainer, "Motor neuron cell-nonautonomous rescue of spinal muscular atrophy phenotypes in mild and severe transgenic mouse models.," *Genes Dev.*, vol. 29, no. 3, pp. 288–97, 2015.

[157] J. J. Glascock, E. Y. Osman, M. J. Wetz, M. M. Krogman, M. Shababi, and C. L. Lorson, "Decreasing disease severity in symptomatic, Smn(-/-);SMN2(+/+), spinal muscular atrophy mice following scAAV9-SMN delivery.," *Hum. Gene Ther.*, vol. 23, no. 3, pp. 330–5, 2012.

[158] K. D. Foust, D. L. Salazar, S. Likhite, L. Ferraiuolo, D. Ditsworth, H. Ilieva, K. Meyer, L. Schmelzer, L. Braun, D. W. Cleveland, and B. K. Kaspar, "Therapeutic AAV9-mediated suppression of mutant SOD1 slows disease progression and extends survival in models of inherited ALS.," *Mol. Ther.*, vol. 21, no. 12, pp. 2148–59, 2013.

[159] K. Meyer, L. Ferraiuolo, L. Schmelzer, L. Braun, V. McGovern, S. Likhite, O. Michels, A. Govoni, J. Fitzgerald, P. Morales, K. D. Foust, J. R. Mendell, A. H. M. Burghes, and B. K. Kaspar, "Improving single injection CSF delivery of AAV9-mediated gene therapy for SMA: a dose-response study in mice and nonhuman primates.," *Mol. Ther.*, vol. 23, no. 3, pp. 477–87, 2015.

[160] A. Dal Mas, M. E. Rogalska, E. Bussani, and F. Pagani, "Improvement of SMN2 pre-mRNA processing mediated by exon-specific U1 small nuclear RNA," *Am. J. Hum. Genet.*, vol. 96, no. 1, pp. 93–103, 2015.

[161] D. Balestra, D. Scalet, F. Pagani, M. E. Rogalska, R. Mari, F. Bernardi, and M. Pinotti, "An Exon-Specific U1snRNA Induces a Robust Factor IX Activity in Mice Expressing Multiple Human FIX Splicing Mutants," *Mol. Ther. Acids*, vol. 5, no. 10, p. e370, 2016.

[162] A. Dal Mas, P. Fortugno, I. Donadon, L. Levati, D. Castiglia, and F. Pagani, "Exon-specific U1s correct SPINK5 exon 11 skipping caused by a synonymous substitution that affects a bifunctional splicing regulatory element," *Hum. Mutat.*, vol. 36, no. 5, pp. 504–512, 2015.

[163] N. Ward, S. Buckley, S. Waddington, T. Vandendriessche, M. Chuah, A. Nathwani, J. McIntosh, E. Tuddenham, C. Kinnon, A. Thrasher, and J. McVey, "Codon optimisation of human factor VIII cDNAs leads to high level expression," *Blood*, vol. 117, no. 3, pp. 798–808, 2010.

[164] L. Cartegni, J. Wang, Z. Zhu, M. Q. Zhang, and A. R. Krainer, "ESEfinder: A web resource to identify exonic splicing enhancers," *Nucleic Acids Res.*, vol. 31, no. 13, pp. 3568–3571, 2003.

[165] A. Machida, H. Kuwahara, A. Mayra, T. Kubodera, T. Hirai, F. Sunaga, M. Tajiri, Y. Hirai, T. Shimada, H. Mizusawa, and T. Yokota, "Intraperitoneal administration of AAV9-shRNA inhibits target gene expression in the dorsal root ganglia of neonatal mice.," *Mol. Pain*, vol. 9, no. 1, p. 36, 2013.

[166] M. Pinotti, F. Bernardi, a. Dal Mas, and F. Pagani, "RNA-based therapeutic approaches for coagulation factor deficiencies," *J. Thromb. Haemost.*, vol. 9, no. 11, pp. 2143–2152, 2011.

[167] I. Carmel, S. Tal, I. Vig, and G. Ast, "Comparative analysis detects dependencies among the 5' splice-site positions.," *RNA*, vol. 10, no. 5, pp. 828–840, 2004.

[168] H. Zhou, N. Janghra, C. Mitrpant, R. L. Dickinson, K. Anthony, L. Price, I. C. Eperon, S. D. Wilton, J. Morgan, and F. Muntoni, "A novel morpholino oligomer targeting ISS-N1 improves rescue of severe spinal muscular atrophy transgenic mice.," *Hum. Gene Ther.*, vol. 24, no. 3, pp. 331–42, 2013.

ACKNOWLEDGMENTS

Firstly, I'd like to thank my supervisors Prof. Mirko Pinotti, Prof. Franco Pagani and my tutor Prof. Francesco Bernardi for all their support and encouragement over the last 3 years. Secondly, I'd like to thank Prof. John McVey for his special advices and for making me experiencing a good science in the fascinating Surrey. Thirdly, I'd like to thank all my colleagues in Ferrara, in Trieste and in Guildford for all their help and suggestions. In particular, a special thank goes to Erica and Giulia, who taught me many of my lab skills to date and who is nice to spend time with during the hard times in lab.
The last but not least, I want to thank my families for their support in all its forms over the year, especially to Monika and the new entry Isabelle, who made our Christmas an unforgettable wonderful holiday.